UNIVERSIDAD DE EXTREMADURA

TESIS DOCTORAL

“Funciones de los nanodominios asociados a las balsas lipídicas de la membrana plasmática de neuronas en la regulación y coordinación de la señalización por calcio y por especies reactivas del oxígeno y sus implicaciones para la excitabilidad y supervivencia neuronal.”

Sofia Isabel Almeida Fortalezas

Doctorado en Biomarcadores de Salud y Estados Patológicos
(R012)

2020

UNIVERSIDAD DE EXTREMADURA

TESIS DOCTORAL

“Funciones de los nanodominios asociados a las balsas lipídicas de la membrana plasmática de neuronas en la regulación y coordinación de la señalización por calcio y por especies reactivas del oxígeno y sus implicaciones para la excitabilidad y supervivencia neuronal.”

Sofia Isabel Almeida Fortalezas (Máster)

La conformidad del director de la tesis consta en el original en papel de esta Tesis Doctoral

Fdo: Carlos Gutiérrez-Merino (PhD)

Doctorado en Biomarcadores de Salud y Estados Patológicos (R012)

2020

This work is dedicated to the mans of my life:

My little stars in the heaven Ed and José.

My lovely husband Pedro.

My sweet kids Pedro and Francisco.

Index

Acknowledgements

The greatest thanks go to the director of these thesis Professor Carlos Gutiérrez-Merino. For all the diary teaching, for all the patience and dedication.

I also would like to thank Professor Cecília Rodrigues and Joana Amaral (Ph.D.) for receiving me so well in Lisbon and for all the help and teaching in the gene silencing procedure.

Thanks to Joana Poejo, for receiving me in her house while I was in Lisbon, for helping in the performance of the latest results and for being always there in my life, thank you sister!

A big thanks to all my lab mates, for teaching me something or for let me explain something by learning as well: Dorinda, Alex, María, Isaac, María Isabel, Nerea, Nerea, Jairo, Javier and Ricardo.

A huge thank to my family, for being so proud, supportive and lovely; for the ones that I have lost for the heaven in this period: my brother Ed, my Grandma Cremilde, "Father" Francisco, the proudest Daddy José and my little friend Bimba; For those whose always have been there: Mom Rita, My love Pedro, "Mom" Celeste; And for the most strength donors which life gave me while performing this work, my sons Pedro and Francisco!

This work has been supported by Grants BFU2014-53641-P and BFU2017-85723-P of the Spanish Plan Nacional de I+D+I, and by Grant GR15139 of the Junta de Extremadura to the Research Group BBB008, all with European Funds for Structural Development (FEDER) co-financing. The author, Sofia Fortalezas, has been supported by predoctoral fellowship number SFRH/BD/84543/2012 of the Portuguese Fundação para a Ciência e a Tecnologia (FCT).

Resumen

Una alteración sostenida de la homeostasis intracelular del calcio y un incremento sostenido del estrés oxidativo celular son puntos convergentes en los

procesos neurodegenerativos prevalentes en la actualidad, tales como las enfermedades de Alzheimer y de Parkinson. Los "rafts" o balsas lipídicas de la membrana plasmática definen unos nanodominios de una extensión entre 10 y 200 nm, algo heterogéneos entre diferentes tipos celulares, estructuralmente dinámicos y enriquecidos en colesterol y glicoesfingolípidos. Los sistemas de transporte del calcio de la membrana plasmática neuronal más relevantes para el control de la homeostasis del calcio citosólico dentro del intervalo de concentración que permite la supervivencia y excitabilidad normal de las neuronas glutamatérgicas colocalizan en estos nanodominios. Asociados a estos se encuentran sistemas redox que producen óxido nítrico (oxido nítrico sintasa neuronal) y anión superóxido/H_2O_2 (citocromo b_5 reductasa), que son las principales especies reactivas del oxígeno y del nitrógeno (ROS/RNS) que generan el estrés oxidativo detectado en los procesos neurodegenerativos. Además, los sistemas de transporte del calcio mencionados previamente son dianas moleculares para estas ROS/RNS primarias y de las especies reactivas más neurotóxicas, como el peroxinitrito y el radical hidroxilo, que son producidas por la rápida reacción entre ellas.

Partiendo de estas consideraciones, ampliamente avaladas por publicaciones en revistas de prestigio científico internacional, en este trabajo de tesis doctoral hemos puesto de manifiesto la relevancia para el control de la homeostasis del calcio citosólico de los sistemas de transporte del calcio asociados a los "rafts" lipídicos utilizando metil-β-ciclodextrina (MβCD), un compuesto secuestrante del colesterol que provoca la disrupción de estos nanodominios. Un hallazgo experimental inicial relevante fue observar que el tratamiento con MβCD produjo una fuerte disminución de los niveles de fosforilación de la subunidad β de los canales de calcio de tipo L (LTCC) y la inactivación de estos canales de calcio. El tratamiento con inhibidores de dos proteínas quinasas asociadas con los "rafts" lipídicos, proteína quinasa A y proteína quinasa dependiente de calcio y calmodulina, produce una disminución similar del nivel de fosforilación de la subunidad β e inhibición de la actividad de los LTCC, permitiendo concluir que la disrupción de los "rafts" genera LTCC disfuncionales. Tanto la depleción del colesterol provocada por el tratamiento con MβCD como el tratamiento con inhibidores de las proteínas quinasas precitadas provocan la disminución sostenida de la concentración citosólica del calcio por debajo del umbral mínimo de supervivencia neuronal, hasta valores similares a los medidos en condiciones que inducen la apoptosis neuronal.

Adicionalmente, en este trabajo se han investigado las principales fuentes generadoras de ROS/RNS en estos nanodominios de tipo "raft". Los resultados obtenidos han demostrado que estos nanodominios realizan una importante contribución a la producción total de ROS/RNS en los cultivos primarios de neuronas granulares del cerebelo de rata (CGN) *in vitro* en las condiciones óptimas para la supervivencia neuronal de las CGN, es decir, en condiciones de despolarización parcial de la membrana plasmática. Puesto que la expresión de las proteínas sufre cambios significativos durante la maduración neuronal, se ha estudiado la evolución/desarrollo de la red de nanodominios asociados a los "raft" de la membrana plasmática utilizando CGN a diferentes días *in vitro* tras la siembra en placa y hasta alcanzar el estado de neuronas maduras. Este estudio ha mostrado un notable incremento de los "rafts" lipídicos durante la maduración de las CGN y la relevante contribución de la isoforma 3

de la citocromo b_5 reductasa (Cb_5R3) al control de la producción total de ROS en las CGN maduras.

Finalmente, se ha estudiado la relevancia relativa de la producción de ROS/RNS y de la desregulación de la homeostasis del calcio citosólico en la neurotoxicidad causada por rotenona, una neurotoxina que ha sido mostrado que produce alteraciones neurológicas de tipo Parkinsonismo. Los resultados obtenidos en este trabajo han mostrado que la elevación sostenida de la concentración del calcio citosólico inducida por concentraciones neurotóxicas de la rotenona precede a la despolarización mitocondrial y a la elevación de la producción de ROS que genera el estrés oxidativo asociado a este proceso neurotóxico. Los resultados muestran también que alteraciones de la actividad de los sistemas de transporte de calcio asociados a los "rafts" lipídicos de la membrana plasmática median la elevación sostenida del calcio citosólico producida por exposición aguda de las CGN a concentraciones neurotóxicas de la rotenona. Además, en este trabajo se ha encontrado que la creatina, un compuesto de potencial uso farmacológico o terapéutico, protege contra la neurotoxicidad de la rotenona. La creatina, a dosis protectoras contra la neurotoxicidad producida por exposición de las CGN a rotenona, protege contra la desregulación de la homeostasis del calcio citosólico y contra la despolarización mitocondrial, y atenúa el estrés oxidativo intracelular.

Abstract

A sustained alteration of intracellular calcium homeostasis and a sustained increase in cellular oxidative stress are convergent points in the neurodegenerative processes prevalent nowadays, such as Alzheimer´s and Parkinson´s disease. Plasma membrane lipid rafts define nanodomains of small amplitude (10-200 nm), somewhat heterogeneous between different types of cells, structurally dynamic and enriched in cholesterol and glycosphingolipids. The calcium transport systems of the neuronal plasma membrane most relevant for the control of cytosolic calcium homeostasis within the concentration range that enables the survival and normal excitability of glutamatergic neurons co-localize in these nanodomains. Associated with them are redox systems that produce nitric oxide (neuronal nitric oxide synthase) and superoxide anion / H_2O_2 (cytochrome b_5 reductase), that are the primary reactive oxygen and nitrogen species (ROS/RNS) that generate the oxidative stress detected in neurodegenerative processes. In addition, the calcium transport systems mentioned above are molecular targets for these primary ROS/RNS and the more neurotoxic reactive species, such as peroxynitrite or hydroxyl radical, which are derived by the rapid reaction between them.

Bearing this in mind, in this Ph.D. work we look forward to revealing the calcium transport systems more relevant in the control of cytosolic calcium homeostasis associated with the mentioned lipid rafts using methyl-β-cyclodextrin (MβCD), a compound that produce cellular cholesterol depletion and subsequently lipid raft disruption. A major initial finding was that the levels of phosphorylation of the β-subunit of LTCC were lowered by MβCD-induced rafts disruption and the inactivation of these calcium channels. Treatment with inhibitors of two protein kinases associated with these rafts, protein kinase A and calcium/calmodulin-dependent protein kinase, produced a similar decrease of the β-subunit phosphorylation level and inhibition of LTCC activity, allowing to conclude that lipid rafts disruption leads to functional impairment of the LTCC. Both, cholesterol depletion induced by treatment with MβCD and the treatment with inhibitors of the above mentioned protein kinases elicit a sustained decrease of the cytosolic calcium concentration below the minimum level needed for neuronal survival, and close to the level measured under neuronal proapoptotic conditions.

Additionally, in this work we have studied the main sources of ROS/RNS in these lipid “rafts” nanodomais. The results of this work have demonstrated that these nanodomains make an important contribution to the overall ROS/RNS production in primary cultures of rat cerebellar granule neurons (CGN) *in vitro*, under conditions that favor neuronal survival, i.e. under conditions of partial plasma membrane depolarization. Because the expression of proteins can suffer significant changes during neuronal maturation, we have studied the evolution/development of the nanodomains network associated with the plasma membrane lipid rafts using CGN primary cultures at different days *in vitro* until the neurons are mature. This study has shown a large increase of lipid ‘rafts’ during the maturation of CGN and also a relevant contribution of the isoform 3 of cytochrome b_5 reductase (Cb_5R3) in the control of the overall ROS production in mature CGN.

Finally, this work also addresses the relative relevance of ROS/RNS production and dysregulation of cytosolic calcium homeostasis in the neurotoxicity caused by rotenone, a neurotoxin that it has been shown to produce Parkinsonism’s neurological alterations. The results show that the sustained raise of cytosolic calcium concentration

elicited by neurotoxic concentrations of rotenone precedes the mitochondrial membrane depolarization and also the raise of ROS that generates the oxidative stress in this neurotoxic process. The results also show that the sustained raise of cytosolic calcium induced by CGN acute exposure to neurotoxic concentrations of rotenone is largely due to dysregulation of calcium transport systems associated with lipid rafts. Moreover, in this work it has been found that creatine, a compound of potential pharmacological or therapeutic use, affords a large protection against rotenone neurotoxicity. Indeed, at doses that protect CGN against the neurotoxicity of rotenone creatine also protects against dysregulation of cytosolic calcium homeostasis and against mitochondrial depolarization, and attenuates the intracellular oxidative stress.

Abbreviations

$[Ca^{2+}]i$: intracellular free calcium concentration

AMPA: α-amino-3-hydroxy-5-methylisoxazole-4-propionic acid
BAPTA: 1,2-bis(2-aminophenoxy)ethane-N,N,N0,N0-tetraacetic acid
CaMK-II: calcium/calmodulin-dependent protein kinase II
C*b*$_5$R: cytochrome b_5 reductase
CGN: cerebellar granule neurons
CK: creatine kinase
CPA: cyclopiazonic acid
Cyt c: Cytochrome c
DMEM: Dulbecco's modified Eagle medium
ER: Endoplasmic Reticulum
FCCP: Carbonyl cyanide-4-(trifluoromethoxy)phenylhydrazone
Fura-2 AM: Fura-2-acetoxymethyl ester
LTCC: L-type calcium channels
LTP: long-term potentiation
MCB: monochlorobimane
MβCD: methyl-β-cyclodextrin
NCX: Na^+/Ca^{2+}-exchanger
NMDAr: N-methyl D-aspartate receptor
nNOS: neuronal nitric oxide synthase
PD: Parkinson disease
PKA: protein kinase A
PKC: protein kinase C
PM: Plasma Membrane
PMCA: plasma membrane calcium pump
ROS/RNS: reactive oxygen and nitrogen species
SERCA: endoplasmic reticulum calcium pump
SOCE: store-operated calcium entry
SOD: superoxide dismutase
SPMV: synaptic plasma membrane vesicles
TMRE: Tetramethylrhodamine, ethyl ester
TRPC1: transient receptor potential C1

List of Figures

1. Introduction

1.1. Cytosolic Calcium homeostasis in Neurons

Cytosolic calcium is of extremely importance for the activity of the brain and also for the peripheral nervous system, therefore alterations in their homeostasis are responsible to activate the apoptotic cascade and are also involved in the mechanisms of necrotic cell death (the two most relevant death pathways in cells) [1]. Many authors demonstrated, experimentally using cell cultures, that a sustained rise in the neuronal cytosolic calcium concentration within the range 0.5-1 µM leads to rapid necrotic neuronal death, mediated by calcium-dependent proteases activation, like calpains. Otherwise, a long-term sustained cytosolic calcium concentration below 60-70 nM in the neuronal soma trigger the slow development of apoptotic neuronal death [2, 3]. Therefore, it is not surprising that a sustained alteration of the neuronal intracellular calcium homeostasis is a point of convergence of the cellular mechanisms in the base of many neurodegenerative processes. Pointed out this relevance of cytosolic calcium homeostasis, subsequently there will be presented the major calcium transport systems that control the cytosolic calcium homeostasis in the neuronal soma and also, for a better understanding of the large subcellular regionalization of neuronal processes essential for the normal activity of neurons and especially in neuronal signal transduction pathways, we shall highlight the subcellular compartmentation of these calcium transport systems.

1.1.1. The different types of calcium transport systems involved in neuronal calcium homeostasis

To establish most functional synapses and to maintain and rapidly restore the cytosolic calcium in the neuronal soma within concentrations that allows for neuron survival, neurons must sustain a competent spatial and temporal connection between the activity of transport systems that leads to calcium entry to the cytosol and those that extrudes calcium out of the cytosol. During the last three decades varied experimental studies have established the major molecular actors that allow neurons to achieve this goal [4-7], which are schematically presented in Figure 1.

Therefore, the group of actors of the cytosolic calcium homeostasis in neurons are the transport systems at the plasma membrane with the help of calcium transport systems located in intracellular stores, such as endoplasmic reticulum and mitochondria. And is extremely important to mention that the major responsible for the neuronal excitability are calcium ions (much more than other concentration gradients ions such as potassium, sodium and chloride). Moreover, cytosolic calcium binding proteins afford the neurons with a buffering capacity to attenuate the peak height of free cytosolic calcium concentration ($[Ca^{2+}]_i$) spikes after focal neuronal stimulation by some neurotransmitters or after high frequency repetitive neuronal stimulation [9].

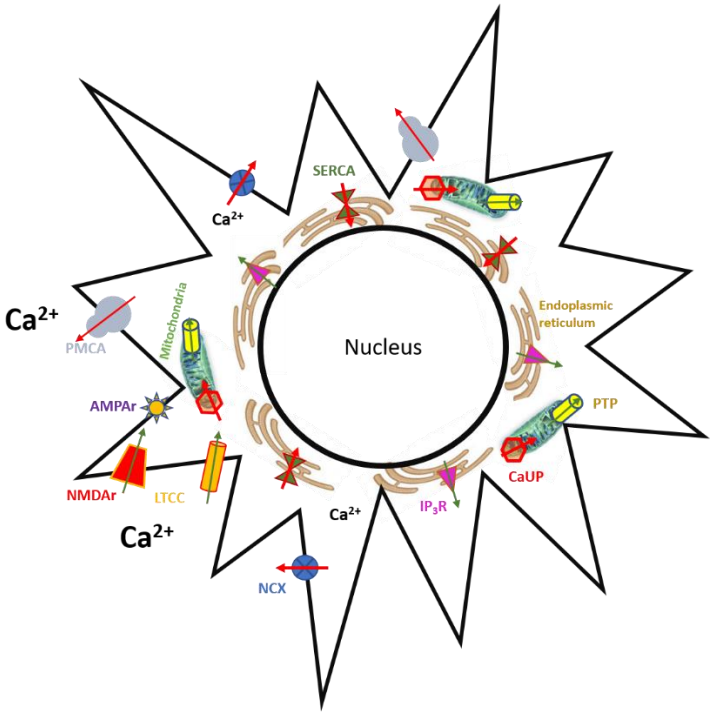

Figure 1: Diagrammatic representation of the major calcium transport systems responsible for the maintenance of neuronal cytosolic calcium homeostasis. Green and red arrows indicate cytosolic calcium entry and extrusion transport systems, respectively. Abbreviations: NMDAr (N-methyl-D-aspartate receptor); AMPAr (α-amino-3-hydroxy-5-methyl-4-isoxazolepropionic acid receptor); LTCC (L-type calcium channel); PMCA (plasma membrane calcium pump); NCX (sodium-calcium exchanger); IP3R (Inositol trisphosphate receptor); SERCA (endoplasmic reticulum calcium pump); PTP (mitochondrial transition pore); CaUP (mitochondrial calcium uniporter). (adapted from Gutierrez-Merino *et al*, 2014 [8])

1.1.1.1. The calcium entry systems of the neuronal plasma membrane.

The main intruders of calcium in neurons are the Calcium Channels and all neurons express different types such as L-, N-, P/Q- and R-type. Nevertheless, based on their unitary conductance, on their rate of inactivation and their subcellular location the most relevant for neuronal calcium homeostasis are the L-type Calcium Channels (LTCC) [10-16]. This family of calcium channels is also known as Ca_V1, and has four subtypes: $Ca_V1.1$, $Ca_V1.2$, $Ca_V1.3$ and $Ca_V1.4$ [17]. $Ca_V1.2$ and $Ca_V1.3$ are expressed in neurons, cardiac and endocrine cells, while $Ca_V1.1$ and $Ca_V1.4$ are specific of skeletal muscle and retina, respectively [18]. In what to concern to the brain, near 80% of LTCC are $Ca_V1.2$ subtype and 10-25% belong to the subtype $Ca_V1.3$ [19].

Even though the activity of these calcium channels is also modulated through their phosphorylation by protein kinases. It has been reported that the activation of different isoforms of protein kinase C (PKC) produce stimulation or inhibition of LTCC activity in different cellular types [20], and the activation of protein kinase A (PKA) and also of

calcium/calmodulin-dependent protein kinase II (CaMKII) have been revealed as increasers of the activity of LTCC.

Additionally, both kinases (PKA and CaMKII) have been described to form complexes with LTCC subunits. In brain, PKA associates with LTCC subunit α1c [21]. LTCC subunits α1c and β2 are phosphorylated by PKA [22-25], and this leads to an increase of LTCC activity. It has been shown that this increase of LTCC activity is mediated by the phosphorylation of Ser478 and Ser479 of the β-subunit and also by phosphorylation of Ser1928 of the α1c-subunit, as their mutations led to complete elimination of the PKA-induced increase of calcium currents catalyzed by LTCC [20,26]. Concerning to CaMKII, it´s self-inhibitory domain as well as the binding domain of this kinase in the NR2B subunit of N-methyl-D-aspartate receptors (NMDAr) have shown high homology with the amino acids sequence near Thr498 of the LTCC subunit β2a [27]. In fact, it has been shown the co-localization within neurons of the LTCC ($Ca_V1.2$ type) and CaMKII [28] and also of the LTCC subunit β2a with CaMKII, and this has led to the suggestion that the LTCC subunit β2a can act as an associated protein of CaMKII *in vivo* [27].

Furthermore, the phosphorylation of LTCC by CaMKII takes place also in Ser1512 and Ser1570 of the α1 subunit (not only in Thr498 of the β2a subunit) leading to an increase of the intensity of calcium currents through these channels [27, 29-31]. And, it has been proposed that the modulation of LTCC by CaMKII can be relevant to potentiate the raise of cytosolic calcium concentration in response to hormones and growth factors [32,33]. On the other hand, an excessive activation of the LTCC ($Ca_V1.3$ type) by CaMKII has been observed in animal models of parkinsonism correlating with the loss of dendritic spines in the striatum after dopamine depletion [34].

Concerning the most potent calcium ionotropic receptors present in the neurons of the mammalian brain (L-glutamate receptors of the NMDA and α-amino-3-hydroxy-5-methyl-4-isoxazolepropionic acid (AMPA)) [35], they have been reported to be present in the major structures of mammalian brain (neocortex, striatum, hippocampus and cerebellum). These receptors are oligomeric integral membrane proteins and their calcium channel structure is mainly formed by a combination of different subunits [36]. Between them, the NMDA receptors have to be highlighted due to their key role in neurosciences, which is supported by many experimental evidences not only in studies of brain development [37], but also in long term post-synaptic potentiation [4] or brain damage after ischemia-reperfusion [38,39].

This relevance of the NMDAr could be explained by three main reasons: (1) conductance: the NMDA single channel conductance is higher than AMPA single channel conductance, 40-50 pS versus ~20 pS [16,50]; (2) affinity: their higher affinity for the endogenous agonist L-glutamate, e.g. the EC50 for L-glutamate is ~10 μM for NMDA receptors and ~200 μM for AMPA receptors, and (3) desensitization rate: the slower desensitization rate of NMDA receptors, e.g. several hundreds of milliseconds for NMDA receptors while it is ~10 milliseconds for AMPA receptors [36].

However, NMDA receptors need not only the presence of L-glutamate for this maximal activation but also need a co-stimulation by glycine or D-serine in the brain and the relief of Mg^{2+} inhibition [36,40].

This potentiation of activation of NMDA receptor in the brain could be promoted by AMPA and P2x receptors. Since AMPA receptors and NMDA receptors co-localizes plasma membrane depolarization induced by activation of AMPA receptors leads to a relief of Mg^{2+} inhibition of NMDA receptors. The channel conductance of this receptor is also enhanced by the phosphorylation promoted by PKC and CaMKII which lead to a synaptic incorporation of AMPA receptors during long-term post-synaptic potentiation (LTP) [41-43]. Concerning to P2x, it has been demonstrated that it´s activation could facilitate the L-glutamate release leading to a stronger NMDA receptor activation. The structure of the calcium channel in the NMDA-receptor can be composed by some different combinations of the of subunit 1 (NR1) and one of the isoforms of subunit 2 (NR2A, NR2B, NR2C and NR2D) [44]. And the expression of the functional NMDA receptors is a process which takes some time in the neuron´s maturation [45], thus, in molecular terms there are different isoforms of functional NMDA receptors whose level of expression varies from one type of neurons to another, and also during neuronal maturation. Furthermore, NMDA receptors are found in synaptic and in extra-synaptic locations [45-47]. The extra-synaptic NMDA receptors seems to be more relevant in the control of cytosolic calcium homeostasis in the neuronal soma since the activation of these receptors can generate a less focalized increase of cytosolic calcium. Additionally, the phosphorylation of the NMDA receptors by PKA and PKC have been shown (*in vitro*) to increase their activity [48]. A stimulation by both kinases at the same time lead to the activation of the NMDA receptor promoted by the phosphorylation of Ser896 and Ser897, on the other hand a phosphorylation of Ser890 only by PKC is capable to re-localize subcellularly the NR1 subunit of NMDA receptors, which is reverted upon dephosphorylation [49].

1.1.1.2. Transport systems that release calcium from intracellular stores.

Several major calcium transport systems of the subcellular organelles are also extremely important to the control of the neuronal calcium homeostasis, among these neuronal intracellular stores two should be highlighted: endoplasmic reticulum and mitochondria.

Concerning to endoplasmic reticulum, it´s Ca^{2+}-ATPase, SERCA, is responsible to pump calcium out from the cytosol to the endoplasmic reticulum internal space [5], while calcium release from the endoplasmic reticulum involves the activation of IP_3 receptors and/or ryanodine receptors in different neuronal responses and in synaptic plasticity [5,50-52].

Despite the neuronal endoplasmic reticulum has a lower capacity to accumulate calcium when compared to sarcoplasmic reticulum of muscle cells it is still significant for hippocampal neurons [4,53]. Neuronal endoplasmic reticulum lead to calcium release

which is capable to sustain a moderate increase of cytosolic calcium and this is extremely important in the process of LTP in hippocampal neurons [4,53]. This capacity of calcium filling of the endoplasmic reticulum has been reported as an important feature for the neuronal survive, since is capable to ensure the correct protein folding of several protein, especially those of the plasma membrane. But not only, it could be also secreted to the extracellular space leading to a correct activity of some endoplasmic reticulum protein-chaperones since they are dependent on the calcium concentration in the internal space of the endoplasmic reticulum [54].

On the other hand, calcium depletion in these intracellular stores has been shown to promote the opening of a specific calcium channels, the store-operated calcium entry (SOCE) [5,55,56]. The opening of SOCE, which have been documented in the last years to be present in neurons, leads to a transient increase of the cytosolic calcium under neuronal stress conditions to restore the calcium levels of intracellular stores [4,57]. Furthermore, in order to induce the large calcium depletion in the endoplasmic reticulum required for SOCE in experiments with cells in culture a inhibition of SERCA by selective inhibitors (thapsigargin or cyclopiazonic acid), is needed, therefore this could be seen has a "rescue call" when the energetic depletion of the neurons is severe. Actually, these channels (specifically isoforms TRPC-3 and -6) have been also involved in the neuronal survival of cerebellar granule neurons (CGN) [58]. And more recently, Selvaraj et al. [59] have demonstrated in a model of Parkinson´s disease, that a reduction of Ca^{2+} influx through transient receptor potential C1 (TRPC1) channels in the plasma membrane of dopaminergic neurons leads to a cell death-inducing endoplasmic reticulum-stress response. Highlighting the relevance of calcium homeostasis in Parkinson's disease.

In is turn, neuronal mitochondria represented by a large population, can store larger amounts of calcium, leading to a large increase of cytosolic calcium [60,61]. However, the rate of calcium fluxes across the mitochondrial membrane transporters in normal cells is much slower than that measured for the major endoplasmic reticulum calcium transport systems mentioned before. Despite this higher calcium release from mitochondria, in neurons it was only observed during the development of neuronal cell death, as one consequence of the steady opening of the high permeability mitochondrial transition pore [62]. Therefore, the large calcium mitochondrial release was associated to a neuronal cell death pathway, being part of a molecular mechanism mediated by calpains activation. Whereas, the uptake of calcium by mitochondria takes place through a calcium uniporter [60,62], having a submicromolar rate of uptake which is extremely lower than the major cytosolic calcium extrusion pathways, namely, plasma membrane calcium pump (PMCA) and SERCA in neurons [4,6].

1.1.1.3. The transport systems involved in calcium extrusion from the cytosol.

Concerning to the transport systems involved in the extrusion of calcium in neurons, we must highlight PMCA and Na^+/Ca^{2+}-exchanger (NCX) which are expressed in all neuronal types. PMCA is the responsible for the major extrusion of cytosolic calcium, maintaining the concentration below the neurotoxic calcium range, i.e. <0.4 μM of cytosolic calcium [6,63,64]. Because, PMCA is active at cytosolic calcium concentrations under 0.4 μM [6,63], neurons need to employ a significant amount of metabolic energy (ATP) to maintain cytosolic calcium within the small concentration range required for neuronal survival. Bearing this in mid, cytosolic calcium concentration can be considered as a key bioenergetics marker of neuronal activity and survival. On the other hand, NCX is more potent than the PMCA at cytosolic calcium concentrations ≥0.5 μM [6,65]. Therefore, this transport system can be considered as a "safety system" which is capable to minimise neuronal damage associated with cytosolic calcium ≥0.4 μM, because the activation of NCX when cytosolic calcium reaches this range lets neurons to rapidly reset cytosolic calcium to the concentration window that allows neuronal survival. The expression levels of different neuronal isoforms of both PMCA and NCX suffer significant changes during neuronal maturation [66, 67]. This could be a neuronal adaptative response to the to the fine set of $[Ca^{2+}]_i$ and control of cytosolic calcium homeostasis, since it has been demonstrated that different PMCA isoforms show different affinity for calcium [68].

Nevertheless, despite PMCA as well as NCX are found in the plasma membrane of the neural soma and dendrites, some studies cast doubt on the current hypothesis that both transport systems are almost homogeneously distributed in the plasma membrane. For example, regulatory effects of actin cytoskeleton have been recently associated to NCX activity [69], and actin filaments are components of caveolin-rich structures associated with 'lipid rafts' [70].

SERCA, by is way, plays a secondary role as a system for calcium extrusion from the cytosol because in neurons PMCA is a calcium pump more potent [4].

Regarding to the uptake of calcium mediated by mitochondria it is occupied by the Ca^{2+} uniporter which is carry out by the large mitochondrial inner membrane potential [62], in spite of the contribution of an alternate transport system yet ill-defined in molecular terms cannot be excluded under conditions of high frequency of cytosolic calcium peaks [71]. However, in neurons the calcium uptake mediated by mitochondria is much slower than the extrusion from the cytosol via the plasma membrane systems, such as PMCA and NCX, and via the SERCA.

1.2. Lipid Rafts

Lipid rafts (Figure 2) of the plasma membrane are dynamic nanodomains of a dimension between 10 and 200 nm [72], which define cellular sub-microdomains of the mentioned plasma membrane, these nanodomains are enriched in cholesterol and sphingolipids [72], particularly gangliosides [73], in which anchor caveolins, flotillin, actin

microfilaments and also an increasingly higher number of palmitoylated or farnesylated proteins [70].

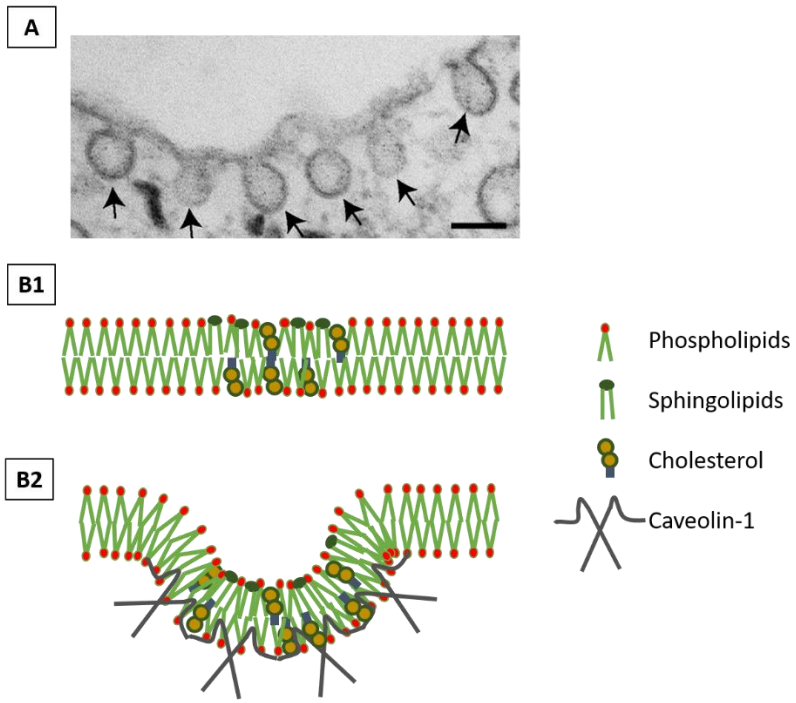

Figure 2: Membrane Organization of Lipid Rafts and Caveolae. (A) Electron micrograph of caveolae in an adipocyte cell line. (Scale bar, 100 nm). Caveolae are signalized by the arrows. **(B)** Diagram summarizing membrane organization of Lipid Rafts and Caveolae. **(B1)** Representation of the structure of Lipid rafts. Is observed at the center a region enriched in sphingolipids and cholesterol; **(B2)** Caveolae representation. Caveolin-1 oligomerizes to generate the proteinaceous coat of caveolae, small invaginations (50-100 nm) of the plasma membrane. Adapted from [74, 75]**.**

Some years ago, lipid rafts were defined as small, but discrete platforms within the plane of the membrane, in which they function as signalling organizers [70,76-79]. In spite of, nowadays, membrane rafts are known to play a significant role in many biological processes, such as signal transduction pathways, apoptosis, viral infections, cell adhesion and migration, synaptic transmission, organization of the cytoskeleton, and plasma membrane protein sorting (exocytosis and endocytosis) [80-82]. Most of the above physiological processes are also known to require Ca^{2+}, therefore it was hypothesized that lipid rafts were capable to regulate these processes by manipulating Ca^{2+} signalling. In fact, the putative implication of lipid rafts in the regulation of intracellular calcium homeostasis and calcium signalling pathways was already proposed in the 1970´s [83,84], nevertheless only during the last decade this theory has been experimentally demonstrated [85,86].

It has been suggested that “caveola invaginations” can assist to focalize signal transduction in neurons [87]. Caveolae (Figure 2) are plasma membrane invaginations of 50–100 nm in diameter, first identified in the 1950s by electron microscopy [88], which are expressed in various tissues and cell types [89]. These invaginations have the advantage to facilitate the interaction between proteins that are localized in separate

organelles such as ER and mitochondria [90], so they are capable to mediate a communication between separate membrane compartments (e.g. PM with ER), that would otherwise be several microns apart. The major constituent of caveolae is the protein Caveolin-1 [91].

1.2.1. Compartmentation of calcium transport systems relevant for the control of cytosolic calcium homeostasis in lipid rafts

The association between lipid rafts and the muscle type of LTCC in cardiomyocytes was recognised almost a decade ago [70,92]. More recently, it was demonstrated using FRET microscopy imaging the association of LTCC with lipid rafts nanodomains in mature primary cultures of CGN [93]. The mentioned association has a major functional relevance for the regulation by protein kinases of the calcium influx through these channels in neurons. Within the brain the α1c subunit of LTCC forms a complex with PKA [21] and Razani *et al*. [94] have demonstrated the co-localization and direct interaction between the scaffolding domain of caveolin-1 and the catalytic subunit of PKA *in vivo* and *in vitro*, respectively. Furthermore, there was also suggested the possibility of direct association of CaMKII with lipid rafts [95], and this agrees with the reported co-localization of $Ca_V1.2$, the predominant LTCC subtype in the brain, and CaMKII [28]. Functional regulation of LTCC by lipid rafts was also described in cardiomyocytes [96]. Because many proteins having the PDZ binding domain which also bind to the NMDA receptor [97], directly interact with the two major subtypes of LTCC present in the brain ($Ca_V1.2$ and $Ca_V1.3$) [98, 99], the association of these receptors with lipid rafts nanodomains is not an unexpected finding. In fact, the presence of NMDA receptors in lipid rafts has been shown in a variety of studies [100-103]. It has been suggested that the clustering of NMDA receptors in lipid rafts-associated sub-microdomains can potentiate the activation of these receptors serving as a molecular mechanism for potentiation of the synaptic efficiency in neuronal connections [102,103]. Due to the key role played by AMPA receptor clustering near NMDA receptor for the last mentioned receptor activation as well as for LTP induction is extremely important to note that the association of AMPA receptors with molecular components of the lipid rafts of neuronal plasma membranes has also been experimentally demonstrated [100,104,105].

Concerning to the major systems of the neuronal plasma membrane for extrusion of calcium from the cytosol, PMCA and NCX; it´s association with lipid rafts was also described, nevertheless only PMCA seems to be in neuronal plasma membrane. This association of PMCA with lipid rafts has been shown using preparations of synaptic plasma membranes [106], in primary cultures of rat cortical and in hippocampal neurons [107]. Moreover, Jiang *et al.* [107] showed that disruption of lipid rafts domains by chronic depletion of cholesterol lead to accentuated decrease of PMCA activity, suggesting that PMCA associated with lipid rafts is more active than PMCA bound to non-raft domains. NCX has been shown to be associated with lipid rafts in the smooth muscle of coronary arteries [108], it has also been shown to be present in membrane fractions of vascular endothelial cells enriched in the lipid rafts markers caveolin-1 and

e-NOS [109] and the direct interaction of cardiac NCX with caveolin-3 has been demonstrated by co-precipitation [110].

1.2.2. Compartmentation of ROS/RNS producers in lipid rafts

Since that is extremely documented the relevance of oxidative stress in neurodegenerative disorders is important to highlight that two enzymatic sources of reactive oxygen and nitrogen species (ROS/RNS), neuronal nitric oxide synthase (nNOS) and cytochrome b5 reductase (Cb5R), have been shown to be also associated with these lipid rafts nanodomains in the neuronal plasma membrane. Sato et al. [111] showed that the oxygenase and the reductase domains of the nNOS, interact with the caveolin-1 scaffolding domain. Furthermore, it was also demonstrated that nNOS is associated with lipid rafts nanodomains enriched in NMDA receptors and LTCC in mature cultures of primary CGN using FRET microscopy imaging [103]. As soon as nitric oxide plays a very important role in neuromodulation, this association reveal a special bearing as protein/protein interactions regulate the enzyme activity of nNOS as well as anchoring points for the subcellular location of this protein [111,112]. It has been shown that the interaction of nNOS with caveolin-3 in skeletal muscle modulates the catalytic activity of NOS [112]. Additionally, Cb5R was demonstrated to generates a burst of superoxide anion that stimulates the entry in the irreversible phase characterized by caspases activation at the onset of neuronal apoptosis [113-116], furthermore Cb5R was also associated with lipid rafts nanodomains enriched in LTCC and NMDA receptors in mature cultures of primary CGN [115-93]. Indeed, this association of lipid rafts with the main producer of nitric oxide (nNOS) and the source of superoxide anion (Cb5R) could reveal these nanodomains as high producers of focalized generators of the oxidant peroxynitrite in the plasma membrane. In table I are summarized the main proteins associated with lipid rafts, including proteins of the cytoskeleton typically associated with this nanodomains. Remarkably it has to be mentioned that because ROS significantly alter the actin polymerisation/depolymerisation dynamics [117], and this proteins are part of the structural protein network associated with lipid rafts nanodomains, ROS are expected to lead to an important distortion of this protein network, as well as nNOS which has been shown to associate with the neuronal cytoskeleton in synaptic terminals [118]. In fact, regulatory effects of actin cytoskeleton have been reported on NMDA receptors activation [119], on the distribution of LTCC in myocytes [120], and on the activity of NCX [69].

Table I: Main proteins associated to lipid rafts relevant to ROS/RNS and Calcium signalling cross-talk. (adapted from [8])

Structural elements	*Calcium transport systems*	*ROS/RNS sources*	*Regulatory kinases*
Cholesterol, Caveolins, Sphingolipids, Flotillin, Actin microfilaments, PDZ-binding proteins	L-VOCC, NMDA and AMPA receptors, PMCA and NCX	nNOS and Cb_5R	PKA and CaMKII

Concluding, this close spatial location of the calcium transport systems in the neuronal plasma membrane could lead to a fast and fine regulation of the cytosolic calcium homeostasis. Furthermore, the presence of redox centers, producers of ROS, in lipid rafts point out the cross-talk between ROS and calcium signalling in neurons, as well as between oxidative stress and sustained cytosolic calcium deregulation, reviewed in [121,122].

1.3. Oxidative stress

An imbalance between oxidants and antioxidants in favor of the oxidants, potentially leading to damage, is termed 'oxidative stress'. Oxidants (Figure 3) are formed as a normal product of aerobic metabolism but can be produced at elevated rates under pathophysiological conditions. Antioxidant defense involves several strategies, both enzymatic and non-enzymatic [123].

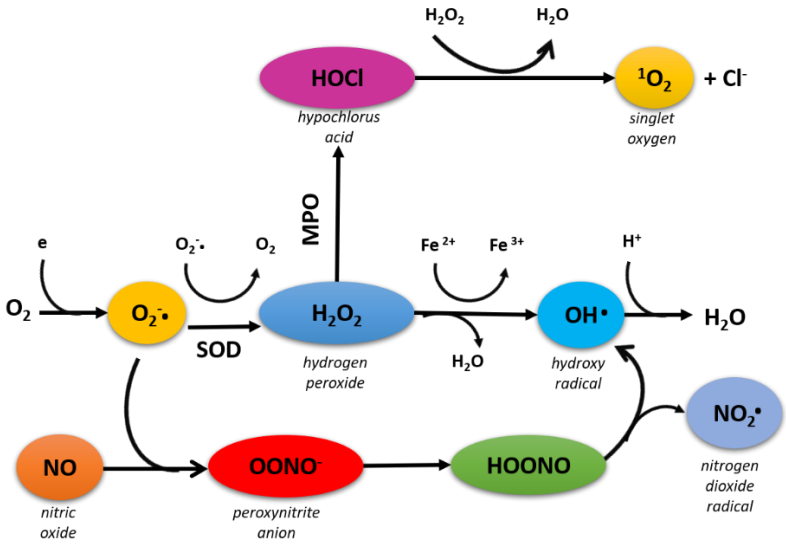

Figure 3: Generation of reactive oxygen/nitrogen species; where MPO is myeloperoxidase and SOD is superoxide dismutase (adapted from [123]).

ROS and RNS producing oxidative stress to neurons can be generated by neuronal and by non-neuronal cells, like microglia or endothelial cells of the brain blood vessels. Excessive production of reactive oxygen and nitrogen species can promote a neuronal cell death leading to brain neurodegeneration. This has been shown during last 20 years with neuronal cultures *in vitro* [39, 124, 125], with animal models of neurodegenerative diseases [126, 127] and brain insults like transient ischemia [128, 129], and also in human brains after brain stroke [130] or affected by major neurodegenerative diseases [124, 131-134]. These "victory" of oxidants is at least in part due to the fact that the cerebrospinal fluid is poorer in antioxidants than the blood, because of the low permeability and high selectivity of the blood-brain barrier.

The major ROS/RNS reported to have a significant importance in the enhanced brain oxidative stress associated with neurodegenerative diseases and insults like ischemia-reperfusion and inflammation can be divided into three major groups: (i) primary biochemical ROS/RNS: chemical species directly generated by some enzymes or proteins during brain activity in normal or pathophysiological conditions, (ii) secondary biochemical ROS/RNS: chemical species derived by rapid reaction between the primary biochemical ROS/RNS or by systems involved in their detoxification, and (iii) radicalic chain ROSRNS: chemical radicals involved in the initiation of radical reaction chains or that are largely generated within radical reaction chains, reviewed in [8]

An example of primary biochemical ROS is superoxide anion which can be produced by neuronal and non-neuronal cells within the brain, this anion plays a key role in the generation of many of the more harmful ROS and RNS detected in the oxidative stress-induced neurodegeneration. Because of the relatively low permeability to superoxide anion of lipid bilayers [135], extracellular superoxide anion should be mainly generated by redox centres of the plasma membrane cells. In the plasma membrane of neurons, the NADH-dependent production of superoxide anion associated with their NADH oxidase activity was nearly ten-fold higher than their NADPH activity [136,137]. Undeniably, an overshot of superoxide anion production at the plasma membrane have been seen as an early event in the apoptosis of CGN induced by the deprivation of extracellular K^+ [113,116], which is catalysed by deregulation of Cb5R associated with plasma membrane lipid rafts sub-microdomains [115,116]. Presently the most accepted source of intracellular superoxide anion is mitochondria in oxidative stress-induced neuronal death in cultures in vitro, particularly that generates by complexes I and III of the mitochondrial respiratory chain [138]. Furthermore and what to concern to non-mitochondrial enzymes that use oxygen as substrate, they can also become a source of intracellular superoxide anion in neurons, such as the conversion of xanthine dehydrogenase into xanthine oxidase either by direct oxidation and/or by proteolytic activation during oxidative stress-induced neuronal death [139].

Nitric oxide is the major primary biochemical RNS produced in oxidative stress-induced brain degeneration, is not harmful by itself, nevertheless its, very fast, reaction with superoxide anion yields peroxynitrite (a secondary biochemical ROS/RNS), probably the most neurotoxic ROS/RNS generated during oxidative stress-mediated brain neurodegeneration, see e.g. [130,140]. Although peroxynitrite has a short lifetime within the cells [140], is very harmful ROS/RNS and have been involved in the brain damage produced by ischemia-reperfusion [130], by inflammation and spinal cord injury [141,142] and also in neurodegenerative diseases and aging [124,131]. The damage promoted by peroxynitrite could be mediated by oxidation of proteins, such as cysteines and methionines; acids, such as sulfenic and sulfinic acid; Lipid peroxidation; DNA and RNA oxidation as well as nitration of protein tyrosines and lipids. There was also observed that the activation of nNOS requires an increase of cytosolic calcium, therefore peroxynitrite is extremely harmful when accompanied by a sustain alteration of calcium homeostasis. Indeed, there has been shown an excitotoxic neuronal death elicited by L-glutamate through activation of NMDA receptors [124,143].

1.3.1. ROS and RNS producers in brain

Some studies with primary cultures of CGN revealed that an overshot of ROS production plays a critical role for the entry in the irreversible stage of low potassium-induced apoptosis [113, 144, 145]. Remarkably, the peak of this ROS overshot occurred at approximately 3 h after changing CGN to low potassium medium, faster than the drop of mitochondrial membrane potential and before a significant release of cytochrome c from mitochondria to the cytosol [116]. Additionally, this ROS overshot accumulation is quenched more than 90% by the superoxide dismutase (SOD) released to the extracellular medium of CGN cultures, blocking the apoptotic process as well [113, 144]. Since superoxide anion has a low permeability across lipid bilayers [135], this ROS overshot must have a large component of superoxide anion released to the extracellular medium. Consequently, even though mitochondria is widely accepted as the major source of intracellular superoxide anion in oxidative stress-induced neuronal death in cultures *in vitro* [124, 125, 138], extramitochondrial ROS production seems to play a major role in the superoxide anion overshot at the onset of CGN apoptosis induced by potassium deprivation of the extracellular medium. Therefore, the possibility that redox systems of the plasma membrane may be a major subcellular source of superoxide anion deserves to be studied.

1.3.1.1. C*b*$_5$R family in ROS/RNS production

The production of superoxide anion has been reported to be mostly due to plasma membrane NADPH oxidases of the NOX family whether in glial or in macrophages and endothelial cells [146]. Nevertheless, using brain synaptic membranes derived from rat synaptosomes and CGN cultures there has been shown that the NADPH-dependent superoxide anion production is nearly ten-fold lower than the NADH-dependent superoxide anion production [113, 136, 137]. In another works there was also reported that the overshot of superoxide anion observed at the onset of CGN apoptosis induced by 5 mM potassium concentration in the extracellular medium is prompted by the dysregulation of C*b*$_5$R associated with plasma membrane lipid rafts sub-microdomains [115,116]. These results showed that the mRNA levels of both C*b*$_5$R and cytochrome *b*$_5$ increases nearly three-fold and an enhanced translocation of C*b*$_5$R to the neuronal plasma membrane within 1-3 hours after switching CGN to a 5 mM K^+ medium [116].

The increase of the level of cytochrome *b*$_5$ can account for the stimulation of the NADH activity of the plasma membrane of CGN in this time window [113], because cellular cytochrome *b*$_5$ concentration is not saturating for C*b*$_5$R. It is to be noted that this correlated with the three to four-fold increase of superoxide anion production measured three hours after the change of CGN to a pro-apoptotic low potassium medium [116]. There was shown that C*b*$_5$R3 and cytochrome *b*$_5$ are highly expressed not only in the CGN of the adult rat brain, but also in cerebellar Purkinje cells and pyramidal neurons of the brain neocortex and neuronal motor nuclei of the brain stem [147]. Therefore, dysregulation of C*b*$_5$R3 is also likely to play a widespread role in brain

neuronal degeneration in oxidative stress-mediated apoptosis and not only in CGN apoptosis. It is to be recalled here that over 40 mutations of Cb_5R3 have been linked to recessive congenital type II methemoglobinemia [148, 149]. In persons affected by this rare disease mild cyanosis is accompanied by generalized dystonia, movement disorders, failure to thrive, and cortical and subcortical atrophy [148, 149], including cerebellar atrophy [150].

1.3.1.2. nNOS in ROS/RNS production

nNOS is another redox system that is tightly associated with plasma membrane lipid rafts in neurons [103, 111, 151], and was shown that nNOS and Cb_5R3 co-localize within caveolin-1-rich lipid rafts of mature CGN in culture [111, 151]. Nitric oxide overproduction has been widely noticed in oxidative stress-induced brain degeneration, see e.g. [130]. Nitric oxide reaction with superoxide anion yields peroxynitrite [140], one of the most neurotoxic ROS generated during oxidative stress-induced brain neurodegeneration as excitotoxic neuronal death elicited by L-glutamate through activation of NMDAr [124, 143], brain ischemia-reperfusion [130], inflammation and spinal cord injury [141, 142], neurodegenerative disease and aging [124,131].

1.4. Rotenone

Rotenone (Figure 4) is a natural compound, used as an insecticide and a herbicide and is a naturally occurring complex ketone, derived from the roots of *Lonchocarpus* species.

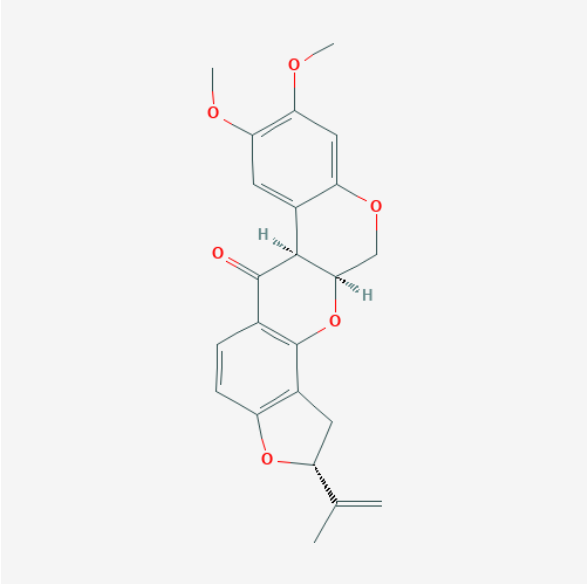

Figure 4: 2D chemical structure of rotenone, adapted from Pubchem.

Rotenone inhibit complex I, which induces dopaminergic cell loss in cell culture [152] and in animal models [153, 154]. An inhibition of mitochondrial complex I by rotenone may not only enhance ROS production but also lead to mitochondrial dysfunction, such as a decrease in ATP production and mitochondrial membrane depolarization [155-157]. Besides complex I inhibition, nitrosative stress, increased nitric oxide and malondialdehyde levels, aggregation of α-synuclein and polyubiquitin, activation of astrocytes and microglial cells, inflammatory reaction, glutamate excitotoxicity, and neuronal apoptosis are involved in the mechanisms of rotenone-evoked parkinsonism [reviewed *in* 158].

However, during last years the relevance of neuronal neurotoxicity of rotenone *in vivo* has been questioned by studies with mixed neuronal/glia co-cultures showing that in these model systems most of the neuronal death induced by low nanomolar concentrations was mediated by microglial activation, while direct neurotoxicity required much higher concentrations of rotenone [159]. On these grounds, it has been proposed that rotenone-induced autophagy dominate over neuronal neurotoxicity in vivo [159]. However, these studies were not performed in serum-free cell culture media and, thus, the putative modulation of rotenone neurotoxicity by serum proteins which can bind the highly lipophilic molecule rotenone, like albumin, was not taken into account. Let us recall here that the cerebrospinal fluid content of serum albumin is more than 150-fold lower than in the blood [160, 161].

1.4.1. Rotenone/CGN as a Parkinson Disease's neuronal model

The application during the last years of medical techniques, such as transcranial magnetic stimulation, single-photon emission computed tomography, positron emission tomography and functional magnetic resonance imaging has revealed functional anomalies of the cerebellum in Parkinson disease (PD) and Parkinsonism patients [162-166]. Despite that this disorder is characterized, in part, by rest tremor, initially (in the 1960's) associated to loss of dopaminergic neurons of the substantia nigra *pars compacta* [167], more recent studies have pointed out that PD pathology is not restricted only to dopaminergic neurons degeneration. Noteworthy, degeneration of other brain areas involving cholinergic, serotinergic and noradrenergic neuronal pathways has also been implicated in disease´s pathology (reviewed in [168]). Anatomical studies have identified reciprocal connections between the basal ganglia and cerebellum [169].

Moreover, no single cellular and animal model to date has been able to recapitulate all the pathological features of PD, although the neurotoxic animal models of PD have contributed much to our understanding on human PD [170].

Bearing this in mind, we will use a CGN/rotenone model, considering also that CGN is a widely used model for the study of cellular and molecular correlates of cell death and neurodegeneration/neuroprotection [171].

1.4.2. Calcium and ROS crosstalk in Rotenone/CGN model

On the other hand and although the etiology of PD remains unknown, there are several significant pathological features, such as mitochondrial dysfunction, oxidative

stress [172-174], altered protein handling, and inflammatory response [175], which are considered to lead to cell dysfunction and death mainly by apoptosis or autophagy [159, 176].

The possible involvement of oxidative stress/mitochondrial dysfunction as an etiological factor of PD is further supported by studies with specific neurotoxins that are extremely potent inducers of Parkinsonism in humans and animals [177]. An example is the rotenone model [152]. Because mitochondria play a central role in energy production, bioenergetics alterations have also been associated with PD. The shortage of mitochondrial supply of ATP and other energy-rich metabolites could be counterbalanced by cellular enzymes such as creatine kinase (CK), especially in locations of high energy consumption like the cytosol.CK is an enzyme that rapidly catalyses the conversion of creatine and consumes ATP to produce phosphocreatine and ADP, being an important enzyme in producing and buffering energy stores in excitable cells [178]. Moreover, CK isoenzymes are highly susceptible to oxidative stress, an important pathophysiological condition associated with the progress of neurodegeneration in PD [178] and it has been demonstrated that CK activity is compromised in common neurodegenerative diseases [179, 180]. Indeed, creatine has been increasingly pointed out as a beneficial compound in neurodegenerative diseases with impaired bioenergetics [181-183]. However, contrary to the positive results obtained with creatine-rich diet in model experimental animals, extensive clinical trials with creatine oral supplementation performed in humans affected with PD has failed to show significant improvement in the score of neurological impairments, reviewed in [184]. It is to be noted, though, that at difference to model experimental animals where the treatment with creatine supplementation has been performed at the onset of the induction of Parkinsonism by toxins, clinical trials are performed with PD patients with a brain neurodegeneration which had begun earlier at an undefined time. Therefore, a better knowledge of the temporal events associated to an impaired neuronal bioenergetics in Parkinsonism is a need to develop more successful combination therapies against PD.

In neurons cytosolic calcium can be considered as a bioenergetics marker of neuronal activity, as many neuronal functions are extremely dependent on cytosolic Ca^{2+} concentration, such as secretion of neurotransmitters and synaptic plasticity [185] intracellular signalling pathways that mediate the metabolic extracellular neuronal stimuli [186] and development of neuritis [187]. The sustained impairment of intracellular Ca^{2+} homeostasis in neurons associated with the oxidative stress induced by an elevated production of ROS is a common metabolic feature in brain neurodegenerative diseases [8, 121]. Indeed, alterations of intracellular Ca^{2+} homeostasis in neurons have been implicated in PD [188]. Furthermore, it has been shown that 1-methyl-4-phenylpyridinium (MPP+), which is the active metabolic product of the neurotoxin MTPT that mimics PD upon administration to mice, alters intracellular Ca^{2+} homeostasis and cause endoplasmic reticulum stress in a human neuroblastoma cell line [189]. Therefore, the putative impairment of intracellular Ca^{2+} homeostasis as an early event in rotenone neurotoxicity deserved to be studied.

2. Aims of this work

This Ph.D. work aims to study the function of the nanodomains associated with the lipid rafts as integrators of the calcium and ROS / RNS signaling pathways, their formation during neuronal maturation and the implications for excitability and neuronal survival of its structural or functional disruption.

To achieve the major objective, the following minor objectives should be accomplished:

1. Study of the regulation by components of lipid rafts nanodomains of the calcium transport systems more relevant to the control of neuronal cytosolic calcium homeostasis.
2. Study of the neuronal plasma membrane lipid rafts nanodomains contribution to the overall ROS/RNS production in neurons.
3. Study of the cross-talk between ROS/RNS production and the activity of calcium-transport and calcium-dependent proteins associated with these nanodomains: implications on excitotoxicity and in the neurotoxicity promoted by rotenone.
4. Study of the evolution/development of the nanodomains network associated to the plasma membrane lipid rafts during CGN *in vitro* maturation.

3. Results

3.1. Study of the calcium transport systems regulation, more relevant to the control of neuronal cytosolic calcium homeostasis, by components of lipid rafts nanodomains.

3.1.1. Treatment of CGNs with MβCD Decreases the Phosphorylation Level of the *b*2 Subunit of LTCC

The experimental conditions for significant cholesterol sequestration by MβCD were fixed in this work while considering the average duration of the CGN treatments with protein kinase inhibitors (15 min) more the time for the acquisition of 340/380 ratio images (5 min). Thus, CGNs were incubated with different concentrations of MβCD at 37 °C for 20 min, followed by removal of the medium to analyze the neurons cholesterol content. The results shown in Table II demonstrate that a 20 min exposure of CGNs to 10 mM MβCD at 37 °C is enough to reduce their cholesterol content from 22.8 ± 2.1 to 4.6 ± 0.4 nmol cholesterol/mg of CGN protein, i.e., more than an 80% reduction in the cholesterol content of CGNs.

Table II: A short-term incubation of Cerebellar Granule Neurons (CGN) with methyl-β-cyclodextrin (MβCD) efficiently extracts it´s content of cholesterol even though preserving cell viability.

[MβCD] (mM)	Cholesterol Content (nmol/mg of CGN Protein)	Cell Viability
0	22.8 ± 2.1	100 ± 5%
5	8.4 ± 0.9	100 ± 5%
10	4.6 ± 0.4	100 ± 6%
20	4.7 ± 0.4	95 ± 5%

These results also displayed that the maximum sequestration of cholesterol from these cells is obtained with 10 mM MβCD under experimental conditions that do not produce a significant loss of cell viability after 20 min (Table II). Concentrations of MβCD higher than 20 mM were needed to observe a significant loss of cell viability within this time period. Indeed, the experimental conditions used are like those used in a previous work, where we showed that a large impairment of the NMDAr response to L-glutamate is induced by MβCD treatment in mature CGNs [151].

In the present work we observed that the treatment with MβCD largely alters the phosphorylation levels of LTCCs in CGNs (Figure 5). Treatment with 1 and 5 mM MβCD decreases the phosphorylation level of the β2 subunit of LTCCs by 60–70%, comparing to control conditions (K25).

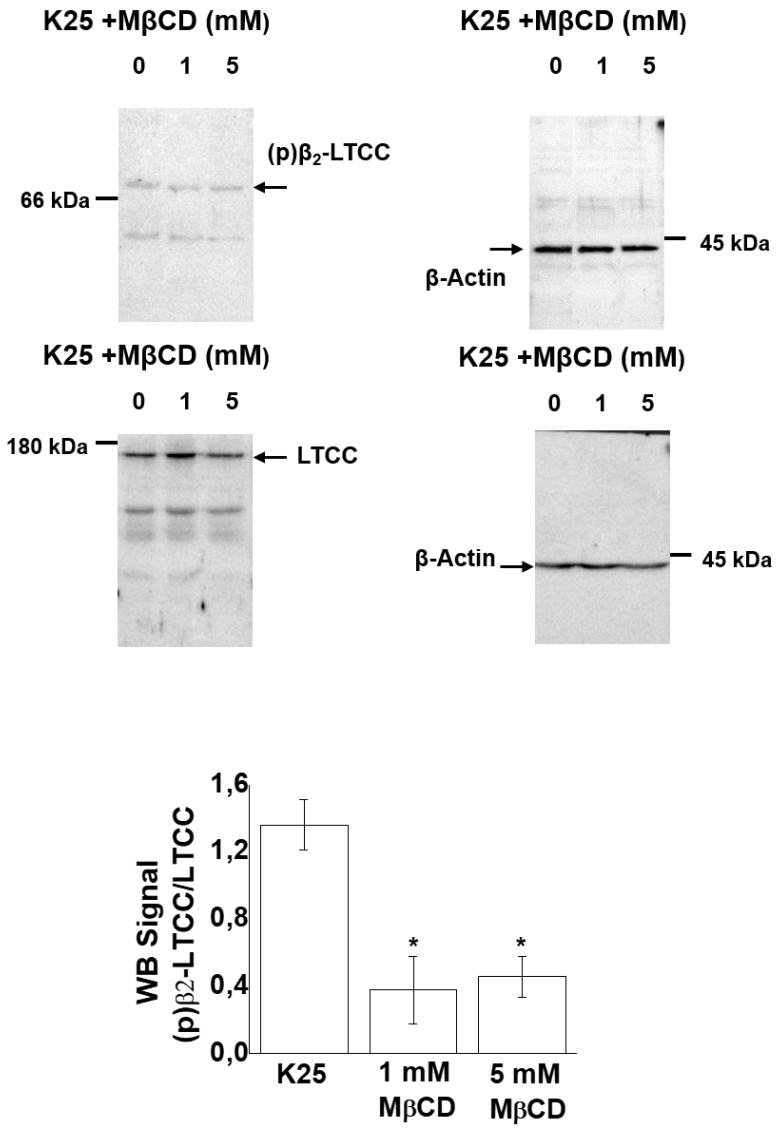

Figure 5: MβCD decreases the phosphorylation level of the β2 subunit of L-type calcium channels (LTCCs). Phosphorylation level of the LTCCs β2 subunit was measured by Western blotting. After the incubation of CGNs in MLocke's K25 with 1 or 5 mM of MβCD for 15 min at 37 °C in a 5% CO_2 culture chamber, cell lysates were performed. Subsequently, and after SDS-PAGE (7.5% acrylamide), the proteins were transferred to PVDF membranes for Western blotting. The positions of the molecular weight marker bands closest to the target proteins of the primary antibodies, i.e., β2 subunit of LTCCs, LTCC β1C subunit, and α-actin, are shown at the left or right side of the corresponding PVDF membrane images. The phosphorylation levels of the β2 subunit of LTCCs, (p)β2LTCC/LTCC, are the measure of the ratio between the intensities of the ~73 and ~174 kDa bands obtained with rabbit antibodies: PCCb2-140AP (FabGennix Inc., Frisco, TX, USA)—dilution 1:100 [(p)β2LTCC]—and anti-LTCC-β1C-subunit (Santa Cruz Biotechnology, Heidelberg, Germany, sc-25686)—dilution 1:100 [LTCC], respectively. For quantification of the ratio (p)β2LTCC/LTCC, the intensities of the bands were normalized first to the intensities of their corresponding ~42 kDa anti-β-actin bands (mouse anti-β-actin A1978, 0.75 µg/mL) as internal control of protein loading. Images shown are representative of the results obtained in experiments done with at least three different CGN preparations. The average results ± S.E. of triplicate experiments are presented as a bar plot. (*) $p < 0.05$.

3.1.2. PKA and CaMK-II Are Associated with Caveolin-1-Rich Lipid Rafts in the Plasma Membrane of CGNs

To evaluate the relative distribution of proteins between lipid raft and non-lipid raft membrane fractions, we experimentally assessed: (1) the presence of PKA and CaMK-II in caveolin-1-rich lipid rafts prepared from of mature CGNs in culture and (2) the percentage of immunoprecipitation of PKA and CaMK-II with caveolin-1 in cell lysates treated with 1% Triton X-100. Lipid rafts were isolated running sucrose gradients as in previous works [103, 151], from mature CGNs in MLocke's K5 (proapoptotic conditions) and also in partially depolarizing plasma membrane media K25 (survival conditions).

To perform the characterization of lipid raft fractions we used as protein markers: H-Ras, caveolin-1, and flotillin, as in previous works [103, 93, 151]. Western blots of lipid raft fractions show that PKA and CaMK-II are present in lipid rafts prepared from CGNs in MLocke's K5 and K25 (Figure 6A). Nevertheless, we must note that these protein kinases are not only present in the lipid raft fractions, since PKA and CaMK-II are also present in other membrane fractions. Cell lysates were also submitted to immunoprecipitation with caveolin-1 as described previously [103, 151]. Briefly, complexes between matrix and antibodies were prepared in an Eppendorf tube, 5 µg of the antibody selected for immunoprecipitation were mixed with 50 µl of the appropriate matrix and 500 µl of TBS. After 1 h incubation in a tube-rotor with continuous shaking, the matrix was precipitated, and the supernatant was removed. The precipitated matrix was subjected to three washes with 500 µl of TBS, namely, by 30 s centrifugation at 4°C. Cell lysates of CGN with 2 mg of protein (previously prepared) were mixed with 40 µl of the matrix. After 30 min incubation in a tube-rotor with continuous shaking, matrix was precipitated by 30 s. The supernatant was deposited in a separate tube and treated with 25 mM MβCD and homogenized under mild stirring. Thereafter, the treated supernatant was added to the tube containing the precipitate of matrix/antibody complex prepared as indicated above and incubated during 1 h at room temperature under continuous shaking in a tube-rotor. Then, the matrix was precipitated, and the supernatant was carefully removed. The precipitated matrix was washed four times in TBS. The washed matrix precipitate was mixed with standard sample buffer for SDS-electrophoresis supplemented with 125 mM urea and 0.3% saponin, boiled during 5 min and loaded onto an SDS-PAGE gel. The results presented in image and table format in Figure 6B, show that both PKA and CaMK-II coimmunoprecipitate with anti-caveolin-1.

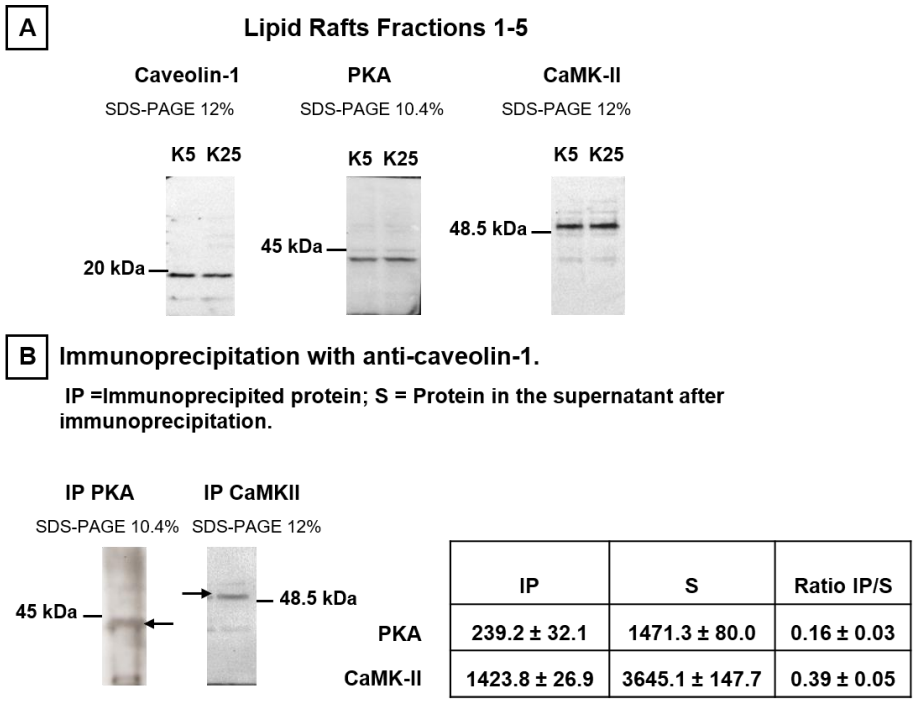

	IP	S	Ratio IP/S
PKA	239.2 ± 32.1	1471.3 ± 80.0	0.16 ± 0.03
CaMK-II	1423.8 ± 26.9	3645.1 ± 147.7	0.39 ± 0.05

Figure 6: Protein kinase A (PKA) and calmodulin-dependent protein kinase II (CaMK-II) are associated with lipid rafts isolated from mature CGNs in culture. The presence of PKA and CaMK-II in lipid raft membrane fractions was determined by Western blotting using rabbit anti-PKA (sc-28892) and rabbit anti-CaMK-II (sc-9035), with rabbit anti-caveolin-1 (sc-894) for the lipid raft protein marker caveolin-1. (**A**) PKA and CaMK-II are present in fractions 1–5 which are enriched in lipid raft markers, both in CGN survival medium MLocke's K25 and after 1 h incubation at 37 °C in a 5% CO_2 culture chamber in proapoptotic MLocke's K5 medium. Western blot images shown are representative of the results obtained in experiments done with at least three different preparations of lipid rafts. The same amount of lipid raft protein, 5 µg, was loaded into each lane in these experiments. The position of the molecular weight marker bands closest to the target proteins of the primary antibodies, i.e., caveolin-1 (~20 kDa), CaMK-II (~50 kDa), and PKA (~40 kDa), are shown at the left or right side of the corresponding PVDF membrane images. (**B**) Results of immunoprecipitation of cell lysates with caveolin-1, were performed. The fraction of PKA and CaMK-II immunoprecipitated with caveolin-1 was calculated from a densitometry analysis of their bands in the Western blots and revealed using the primary and secondary antibodies indicated above, taking into account that while all precipitated samples were loaded into the corresponding lanes of the SDS-PAGE gels (IP), only a fraction of the total supernatant volume (S) was loaded into the gel lanes. The results shown in the table inserted in this panel are the average ± S.E. of triplicate experiments.

The intensity of Western blot bands was calculated for the whole immunoprecipitate and supernatant fractions to analyze the percentage of PKA and CaMK-II present in the total cell lysate that is bound to caveolin-1 or to proteins associated with caveolin-1. The results also highlight that CaMK-II has a higher percentage of coimmunoprecipitation with caveolin-1 (39 ± 5%) than PKA (16 ± 2%).

3.1.3. PKA and CAMK-II Inhibitors Decrease the Phosphorylation Level of the β2 Subunit of LTCCs to the Phosphorylation Levels Measured after CGN Treatment with MβCD and Also in Proapoptotic K5 Medium

The effects of pre-incubating CGNs with the PKA inhibitor H-89, the CaMKII inhibitor KN 93, and the KN-93 analogue KN-92 (noninhibitor) for 15 min on the steady-

state level of the phosphorylation of the LTCC β2 subunit were measured by Western blotting using the antibody PCCb2-140AP (FabGennix Inc.). The results presented in Figure 7A demonstrate that the phosphorylation level of the β2 subunit of LTCCs of mature CGNs in MLocke's K25 is high, suggesting that LTCCs are largely phosphorylated in these experimental conditions.

The results also show that the ratio (p)LTCC/LTCC decreases 30 ± 5% when CGNs are treated with the PKA inhibitor H-89 and 45 ± 5% when CGNs are treated with the CaMK-II inhibitor KN-93 (Figure 7A). Notably, the analogue of KN-93, KN-92, though not an inhibitor of CaMK-II, affords a decrease of 30 ± 3% in the (p)LTCC/LTCC ratio, which is about 2/3 of the decrease produced by KN-93 (Figure 7B). Considering the major role of LTCCs in controlling the steady-state concentration of cytosolic calcium in CGNs [190-192] and that both KN-92 and KN-93 are potent inhibitors of calcium entry through LTCCs [193], we hypothesized that at the concentrations of KN-93 and KN-92 used, these compounds can produce a large drop in CGN cytosolic calcium concentration, and this would elicit CaMK-II inhibition. This hypothesis was confirmed by measuring the cytosolic calcium concentration of Fura-2-loaded CGNs after the addition of KN-92 and KN-93 (Figure 7C). The results display that (a) both compounds produce a large decrease in the (340/380) ratio, from 1.0 ± 0.1 to 0.55 ± 0.05 for KN-93 and to 0.65 ± 0.05 for KN-92, values similar to those attained after the addition of the LTCC blocker nifedipine, 0.55 ± 0.05, and (b) there is a slower rate $[Ca^{2+}]_i$ decrease in CGN somas for KN-92 than for KN-93. It is worthy to note that low (340/380) ratio values (close to 0.5) are also attained upon lowering the concentration of K^+ in the extracellular medium to 5 mM [114, 190]. As early as 1 h after changing these neurons to a K5 medium the proapoptotic conditioning events appear [113, 114, 116, 192]. Notably, the phosphorylation level of the β2 subunit of LTCCs after 1 h of proapoptotic conditioning in MLocke's K5 decreases by 65 ± 5% (Figure 7A). This decrease is higher than that observed after incubation of CGNs in MLocke's K25 for 15 min with the CaMK-II inhibitor KN-93. However, the sum of the contributions of CaMK II and PKA to the steady phosphorylation level in MLocke's K25 is 80 ± 10% (see above), a value that can fully account for the decrease in phosphorylation of the β2 subunit of LTCCs observed after CGN treatment with MβCD or after 1 h in MLocke´s K5.

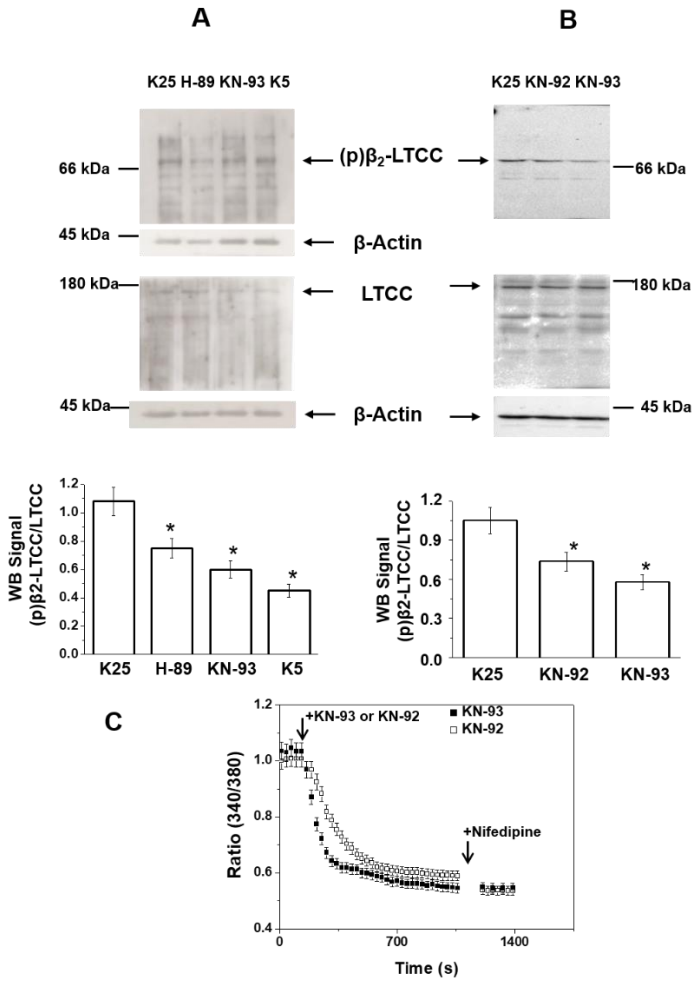

Figure 7: H-89 and KN-93 decrease the phosphorylation of the β2 subunit of LTCCs to values measured in proapoptotic MLocke's K5. (A) CGNs in MLocke's K25 were incubated for 15 min at 37 °C in a 5% CO2 culture chamber with 20 µM H-89, 30 µM KN-93, or in the absence of these inhibitors (K25 control), or after CGN incubation for 1 h at 37 °C in the 5% CO2 culture chamber in the proapoptosis MLocke's K5 condition (K5). **(B)** CGNs in MLocke's K25 were incubated for 15 min at 37 °C in the 5% CO2 culture chamber with 30 µM KN-92, 30 µM KN-93, or in the absence of these inhibitors (K25 control). After SDS-PAGE (7.5% acrylamide), the proteins were transferred to PVDF membranes for Western blotting. For panel B, the PVDF membrane was stripped twice to remove primary antibodies—anti-β2 subunit of LTCCs and anti-LTCC α1C subunit—and used afterward for β-actin detection. The results shown in these panels are representative of the results obtained in triplicate experiments with different CGN preparations. The position of the molecular weight marker bands closest to the target proteins of the primary antibodies, i.e., β2 subunit of LTCC, LTCC α1C subunit, and β-actin, are shown at the left or right side of the corresponding PVDF membrane images. Western blots were revealed by exposure to autoradiography films for (A) and with ChemiDocTM XRS+ from Bio-Rad for (B). The phosphorylation levels of the β2 subunit of LTCCs, (p)β2LTCC/LTCC, shown in the bar graphs of panels A and B, were measured as indicated in the legend for Figure 5 and are average results ± S.E. of triplicate experiments. (*) $p < 0.05$. **(C)** Time dependence of population averages of the 340/380 ratio in neuronal somas before and after the addition of 30 µM KN-93 (black-filled squares) or 30 µM KN-92 (white-filled squares) at the point indicated by the first arrow. At the point indicated by the second arrow, 10 µM nifedipine was added. Mature CGNs in culture were loaded with Fura-2, by the addition of 5 µM Fura-2-acetoxymethyl ester (Fura-2 AM) and 0.025% Pluronic-F127 at 37 °C during 60 min, and then changed to MLocke's K25 buffer (37 °C) to start serial 340 and 380 image acquisition. Data acquisition was done with exposure times lower than 0.4 s at time intervals of 30 s. The 340/380 ratio of neuronal somas was measured using the region of interest (ROI) tool of the HCImage software. The 340/380 ratio values shown are the average ± S.E. of experiments done with three different preparations of CGNs ($n > 300$ neuronal somas of fields taken from six plates for each experimental condition).

3.1.4. Treatment of CGNs with MβCD or with the PKA Inhibitor H-89 Lowers Steady-State $[Ca^{2+}]_i$ to Values Close to Those Attained in Proapoptotic K5 Medium

To experimentally evaluate the effect of CGN treatment with MβCD on calcium entry through LTCCs, neurons were incubated with 5 mM MβCD for 1 h in serum-free DMEM:F12 medium (1:1). Afterwards the medium was replaced to remove MβCD–cholesterol complexes, and CGNs were loaded with 5 µM Fura-2 AM for 30 to 35 min (times shorter than usual because we noticed that treatment with MβCD enhances the loading of this probe) at 37 °C in the 5% CO2 culture chamber.

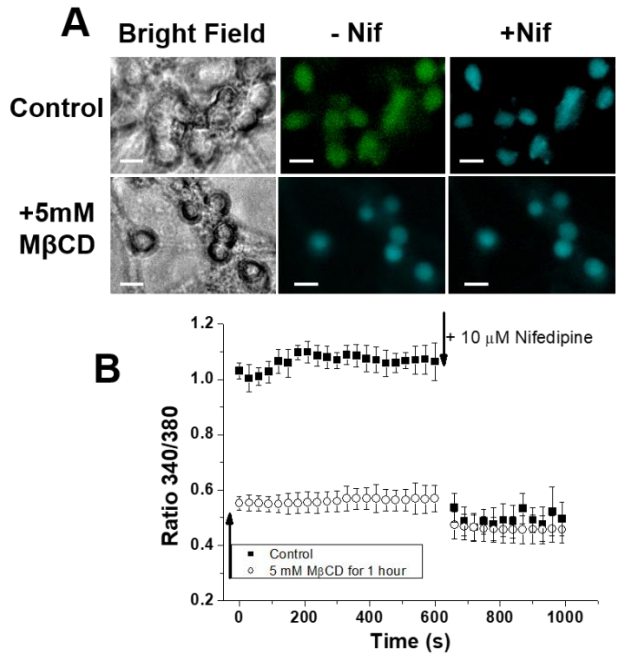

Figure 8: CGN treatment with MβCD decreases the steady-state $[Ca^{2+}]_i$ to values close to those measured after the addition of nifedipine. (A) Pre-incubation and removal of MβCD–cholesterol complexes decrease the 340/380 ratio of CGNs in MLocke's K25 to values close to those measured after blocking LTCCs by nifedipine. Representative images of mature CGNs in culture (controls) and treated with 5 mM MβCD for 1 h at 37 °C in a 5% CO2 culture chamber in the maturation medium DMEM/F12 followed by a change of the DMEM/F12 medium to efficiently remove MβCD–cholesterol complexes (+5 mM MβCD). Thereafter, CGNs were loaded with Fura-2, by the addition of 5 µM Fura-2-acetoxymethyl ester (Fura-2 AM) and 0.025% Pluronic-F127 at 37 °C during 60 min, and then changed to MLocke's K25 buffer at 37 °C, and 340/380 ratio images were captured at different times before (-Nif) and 1 min after the addition of 10 µM nifedipine (+Nif). Pseudocolor scale for 340/380 ratio values: light blue, 0.5–0.6; green, 1.0–1.1. Scale bar = 10 µm. **(B)** Time dependence of population averages of the 340/380 ratio in neuronal somas before and after the addition of 10 µM nifedipine at the time indicated by an arrow for CGNs treated with 5 mM MβCD in Panel A (open circles) and for controls (untreated CGN, solid black squares). The sequential 340/380 ratio images acquired at different times after the addition of nifedipine show that a new steady-state $[Ca^{2+}]_i$ is already reached at 1 min. Data acquisition and analysis were done after the selection of neuronal somas using the region of interest (ROI) tool of the HCImage software, with exposure times lower than 0.4 s at time intervals of 30 s. The 340/380 ratio values are the average ± S.E. of experiments done with three different preparations of CGNs (n > 300 neuronal somas of fields taken from six plates for each experimental condition).

After CGN loading with Fura-2 AM, we measured the cell viability by the MTT assay [194] and found that this treatment produces less than a 10% loss of cell viability,

i.e., a statistically nonsignificant loss of cell viability. The 340/380 ratio measurements show that the treatment with MβCD lowers the steady-state $[Ca^{2+}]_i$ to those obtained after the addition of nifedipine (Figure 8A,B). Control experiments show that the 340/380 ratio of Fura-2-loaded CGNs in MLocke's K25 is steady for at least 30 min, yielding an average 340/380 ratio of 1.0 ± 0.1 (Figure 9B), as also exposed in previous works [114, 151, 190]. To understand the contribution of calcium entry through LTCCs to steady-state $[Ca^{2+}]_i$, we used the specific blockers nifedipine and nimodipine. The addition of both dihydropyridines produces a drop in the 340/380 ratio to a value of 0.55 ± 0.05 in less than 1 min after adding these LTCC blockers (Figure 9). The values observed are very close to the steady-state 340/380 ratio measured after changing CGNs to the proapoptotic K5 medium, 0.50 ± 0.05 (see below), and this is consistent with the inactivation of LTCCs upon CGN plasma membrane polarization noticed in earlier works. PKA and PKC have been reported as possible modulators of LTCC activity, as they can affect Ca^{2+} influx through LTCCs [20, 31]. As also shown in Figure 9, the addition of the PKA inhibitor H-89 decreases the 340/380 ratio to 0.55 ± 0.05. Remarkably, after 15 min of the addition of the PKA inhibitor H-89, the 340/380 ratio reaches the steady-state value attained after the addition of the LTCC blockers nifedipine and nimodipine (Figure 9). These results show that the inhibition of PKA produces a potent inhibition of calcium entry through LTCCs in mature CGNs in MLocke's K25 medium. On the other hand, the addition of 2 μM of the PKC inhibitor calphostin C does not have a statistically significant effect on the steady 340/380 ratio, revealing that PKC activity does not seem to be relevant to the control of the steady-state $[Ca^{2+}]_i$ in CGN soma (in the mentioned experimental conditions).

Thereafter we can conclude that the effects of H-89, KN-93, and KN-92 on the steady-state $[Ca^{2+}]_i$ in the somas of CGN in MLocke's K25 are largely dominated by the inhibition of calcium entry through LTCC.

3.1.5. Inhibition of PKA Alters the LTCC Response to Partial Depolarization of the Plasma Membrane in CGNs

When incubated with MLocke's K5 (5 mM of KCl), fluorescence imaging of CGNs loaded with Fura-2 yields a low steady 340/380 ratio in the neuronal somas of 0.50 ± 0.05, i.e., $[Ca^{2+}]_i$ ~40–50 nM (Figure 10A,B). Thereafter to understand the effect of PKA inhibition on the LTCC response of partial depolarization (promoted by K5 medium) we performed the same 340/380 ratio readings in the presence or absence of H-89 (PKA inhibitor) added to the plate 10 min before starting the measurements of cytosolic calcium concentration (Figure 10A,B). Nevertheless, H-89 largely impairs the kinetics of the $[Ca^{2+}]_i$ response to the addition of 20 mM KCl to the extracellular medium, which increases the extracellular KCl up to 25 mM. In the controls for CGNs loaded with Fura-2, the addition of 20 mM KCl elicits biphasic kinetics with a strong and fast rise in the 340/380 ratio until reaching values higher than 1.0—between 1.2 and 1.5 for most neuronal somas in the plates—followed by slower kinetics for the decay in the 340/380 ratio (t1/2± 2 min) until reaching values of approximately 0.95 ± 0.05 (Figure 10A,B), i.e., $[Ca^{2+}]_i$ ~150 ± 30 nM, which is within the range obtained for the somas of CGNs loaded with Fura-2 several minutes after changing the cells to MLocke's K25 [190].

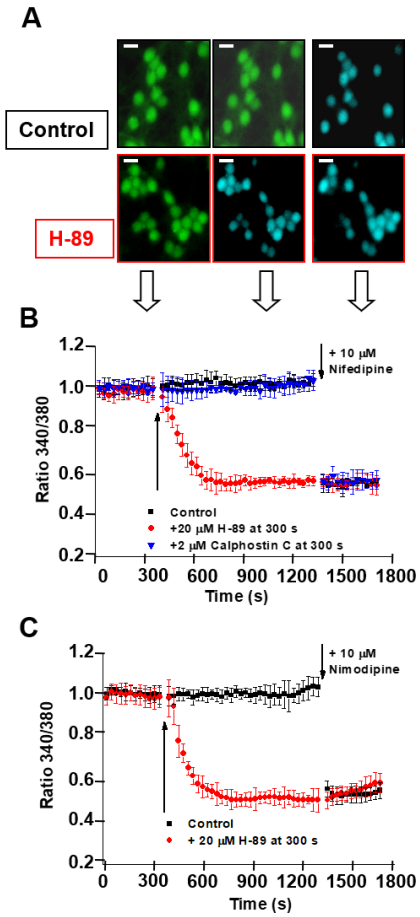

Figure 9: H-89 decreases CGN steady-state $[Ca^{2+}]_i$ to values obtained upon the blockade of LTCCs by nifedipine and nimodipine, while calphostin C has no effect. Mature CGNs in culture were loaded with Fura-2, by the addition of 5 µM Fura-2-acetoxymethyl ester (Fura-2 AM) and 0.025% Pluronic-F127 at 37 °C during 60 min, and then changed to MLocke's K25 buffer (37 °C) and treated with the indicated protein kinase inhibitors. **(A)** Representative pseudocolor images of the same fields of selected CGN plates before (left-most column of images) and after 15 min incubation (middle column of images) with 20 µM of the PKA inhibitor (H-89) or in the absence of inhibitor (control) and 2 min after the addition of 10 µM nifedipine post-H-89 (images in the right-most column). Pseudocolor scale for 340/380 ratio values: light blue, 0.5–0.6; green, 1.0–1.1. Scale bar = 10 µm. The white-filled arrows pointing toward Panel B indicate the approximate times at which these images were captured. **(B,C)** Time dependence of population averages of the 340/380 ratio in neuronal somas before and after the addition of the indicated protein kinase inhibitors after 350 s (at the point indicated by the first arrow). The kinetic analysis of the 340/380 ratio of the somas of CGNs was done for controls (vehicle DMSO addition, solid black squares) and for the addition of 20 µM H-89 (red solid circles) and 2 µM calphostin C (blue down-triangles), inhibitors of PKA and PKC, respectively. Each inhibitor was added to a different culture plate. At approximately 1350 s (at the point indicated by the second arrow), 10 µM nifedipine (B) or 10 µM nimodipine (C) was added to the culture plates in all conditions. Data acquisition and analysis were done after the selection of neuronal somas using the region of interest (ROI) tool of the HCImage software, with exposure times lower than 0.4 s at time intervals of 30 s. The 340/380 ratio values shown are the average ± S.E. of experiments done with three different preparations of CGNs (n > 300 neuronal somas of fields taken from six plates for each experimental condition).

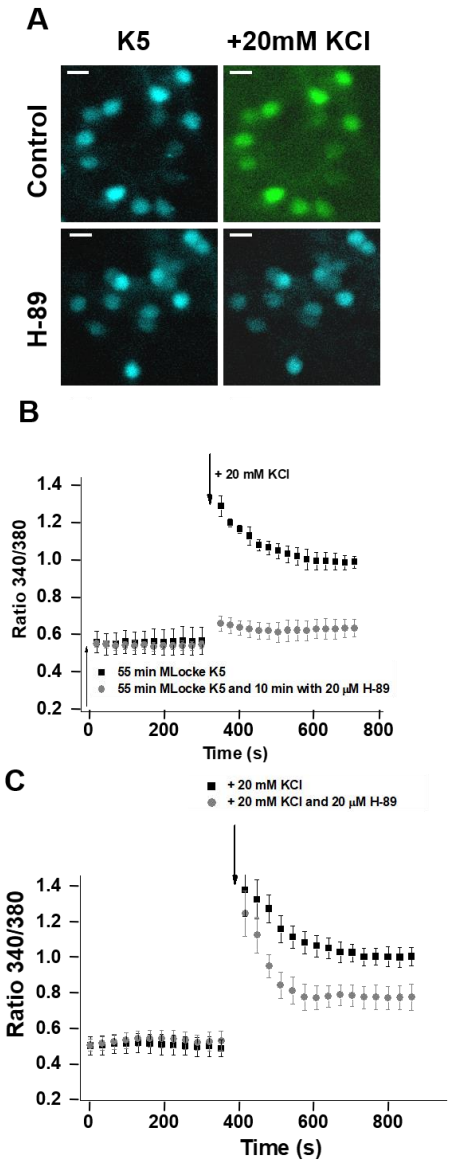

Figure 10: H-89 blocks the rise in $[Ca^{2+}]_i$ of CGNs in response to the increase in extracellular potassium. Mature CGNs in culture were loaded with Fura-2, by the addition of 5 µM Fura-2-acetoxymethyl ester (Fura-2 AM) and 0.025% Pluronic-F127 at 37 °C during 60 min, and then changed to MLocke's K5 buffer (37 °C) and incubated for 1 h in a 5% CO2 culture chamber and thereafter treated as indicated below. **(A)** Representative pseudocolor images of the same fields of selected CGN plates after 1 h in low-potassium MLocke's K5 before (left) and 10 min after the addition of a pulse of 20 mM KCl to the extracellular medium (right) for a control and after a 15 min incubation with 20 µM of the PKA inhibitor H-89. Pseudocolor scale for 340/380 ratio values: light blue, 0.5–0.6; green, 1.0–1.1. Scale bar = 10 µm. **(B)** Population averages of 340/380 ratio measurements in neuronal somas before and after the addition of 20 mM KCl at the time indicated with a black arrow. Before starting the measurements of 340/380 ratios, cell plates were incubated for 10 min with 20 µM of the PKA inhibitor (H-89, gray-filled circles). The results obtained for controls in the absence of these inhibitors (addition of the solvent DMSO used to solubilize H-89) are shown with solid black squares. **(C)** Population averages of 340/380 ratio measurements in neuronal somas before and after the addition of 20 mM KCl (control, solid black squares) or 20 mM KCl plus 20 µM H-89 (gray-filled circles) at the time indicated with a black arrow. For all the panels, each inhibitor was added to a different culture plate. Data acquisition and analysis were done after the selection of neuronal somas using the region of interest (ROI) tool of the HCImage software, with exposure times lower than 0.4 s at time intervals of 30 s. The 340/380 ratio values shown are the average ± S.E. of experiments done with three different preparations of CGNs (n > 300 neuronal somas of fields taken from six cell plates for each experimental condition).

The pre-incubation of CGNs with H-89 for only 15 min largely attenuates the rise in the 340/380 ratio after the addition of 20 mM KCl to the extracellular medium (Figure 10A,B). Noteworthy is that the steady-state 340/380 ratio attained after several minutes reaches a value of 0.60 ± 0.05, which is very close to the (340/380) ratio measured for the somas of control CGN plates before the addition of 20 mM KCl to the extracellular MLocke's medium. The blockade of the $[Ca^{2+}]_i$ response by the inhibitor of PKA requires several minutes of CGN pre-incubation, since only a slight attenuation of the strong and fast rise in the 340/380 ratio is observed when the PKA inhibitor is added simultaneously with 20 mM KCl to the extracellular MLocke's medium (Figure 10C). This correlates with the change in the phosphorylation level of LTCCs elicited by the PKA inhibitor H89 after only a 15 min pre-incubation (Figure 7). It is to be noted that a 15 min pre-incubation of Fura-2-loaded CGNs with 2 µM of the PKC inhibitor calphostin C before the addition of 20 mM KCl has, at most, a weak effect that is statistically nonsignificant on the kinetics of the $[Ca^{2+}]_i$ response to the addition of 20 mM KCl to the extracellular medium.

3.2. Study of ROS/RNS production into the neuronal plasma membrane lipid rafts nanodomains.

3.2.1. Treatment of CGN with millimolar concentrations of methyl-β-cyclodextrin for 5-15 min led to more than 90% attenuation of the kinetics of ROS production monitored by the ROS-sensitive fluorescent dyes dihydrodichlorofluorescein diacetate and dihydroethidium.

To understand the ROS/RNS levels and distribution in mature CGN, neurons in MLocke's K25 were stained with H_2DCF-DA and DHE. Selected representative images of fluorescence microscopy of mature CGN showed that the intensity of fluorescence of these dyes (Figure 11) is clearly higher in the neuronal somas. In addition, the long dendritic extensions connecting distant neuronal somas are more intensely stained with H_2DCF-DA than with DHE. Indeed, these extensions are hardly seen with the red fluorescence of DHE staining. A priori, this could be since the red fluorescence of DHE is enhanced by DNA- and RNA-DHE complexes formation [195, 196] and likewise by superoxide anion-DHE chemical adducts [195, 197]. To experimentally assess this hypothesis, we have acquired images of DHE staining after preincubation for 1.5 hours with the superoxide anion scavenger Tiron (Figure 11C). As we can observe in Figure 11 the fluorescence of DHE mainly in neuronal somas (as mentioned before) was basically quenched (nearly 70 % quenching) by 20 mM Tiron. This result reveals that the DHE staining CGN soma was largely due to the formation of superoxide anion-DHE chemical adducts.

Therefore, the analysis of these images led to the conclusion that the neuronal somas produced most of superoxide anion generated by mature CGN in culture, and that its production along the large dendritic extensions it is rather low compared with the production of another ROS.

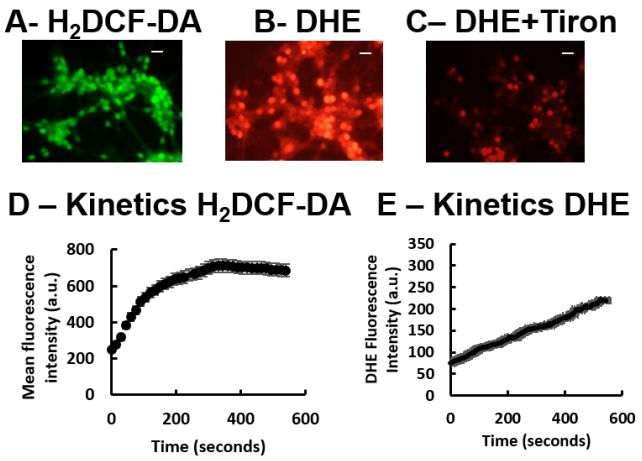

Figure 11: H_2DCF-DA and DHE monitors ROS production upon incorporation to CGN. Representative fluorescence microscopy images of mature CGN showed that they accumulated a significant amount of DCF **(A)** and oxidized DHE **(B)** only after 10 min of addition of 10 µM H_2DCF-DA and DHE to MLocke's K25. Addition of 20 mM Tiron to the extracellular medium 1 hour before the addition of DHE largely attenuated the increase of DHE fluorescence **(C)**. The kinetics of increase of the average fluorescence intensity per pixel in the soma of mature CGN after the addition of H_2DCF-DA and DHE to MLocke's K25 medium is shown in Panels **D** and **E**, respectively. Images of DCF and oxidized DHE fluorescence were acquired using exposure times of 0.5 s for DCF fluorescence and 0.05 s for DHE fluorescence. Scale bar inserted in fluorescence microscopy images = 10 µm. The mean ± s.e. intensity reading of fluorescence per pixel within CGN somas were obtained using the ROI tool of the Hamamatsu HCImage software to select somas as areas of interest in experiments performed by triplicate (n>100 CGN somas in each case).

As observed in Figure 11D-E , were are represented the kinetics of increase of fluorescence intensity upon addition of these dyes to the extracellular medium of mature CGN in culture, the addition of H_2DCF-DA to the extracellular medium of CGN is complex, with three defined phases: (1) an initial short delay phase, (2) an almost linear rise phase, and (3) a delayed fluorescence decrease phase, likely due to release of the de-esterified dye to the extracellular medium. Therefore, as an index of the relative rate of ROS production by CGN using H_2DCF-DA we have obtained the maximum slope of the second phase of the increase of fluorescence or the increase of fluorescence intensity after 5 minutes. On the other hand, and what concerns to the kinetics of the increase of fluorescence obtained with DHE we observed a sustained linear increase of fluorescence in the minutes scale range; so, the slope of this linear increase were utilized as an index of the relative rate of superoxide anion production by CGN.

As mentioned above in section 3.1.1. a short-term incubation of CGN during 20 min with MβCD did not produce a significant decrease of cell viability, nevertheless, efficiently extracts cholesterol from neurons. The results also pointed out that treatment of CGN during 20 min with millimolar MβCD concentrations were highly effective in cholesterol removal from these neurons, as 5 mM MβCD already elicited approximately 80% of the maximum extraction of cholesterol. Therefore, as the shorter the incubation time with MβCD, the cholesterol removal should be more restricted to the CGN plasma membrane, in the next experiments we have fixed 5 min the incubation time for MβCD titrations.

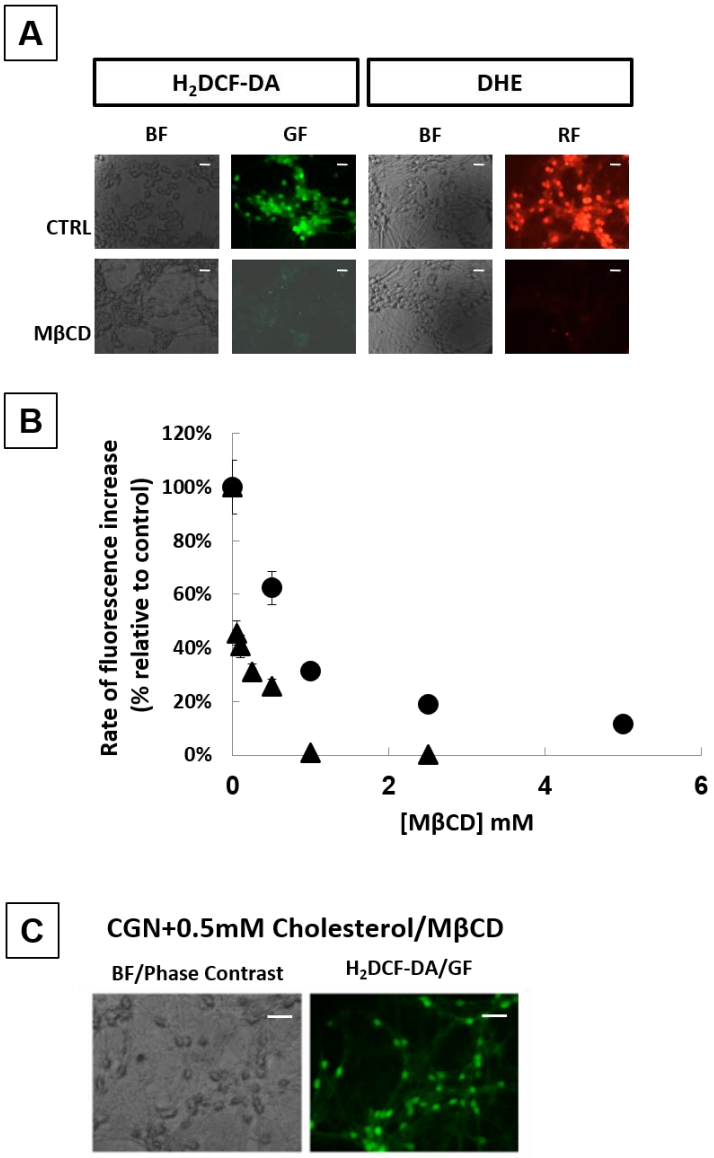

Figure 12: The production of ROS detected by H_2DCF-DA and DHE in mature CGN is more than 90% inhibited by MβCD. (A) Representative fluorescence microscopy images acquired as indicated in the legend for the Figures 3.7.A and 3.7.B show that treatment of CGN with 0.5-1 mM MβCD during 5 min almost completely blocks the increase of fluorescence associated with production of ROS detected by H_2DCF-DA or DHE addition to the medium. Bright field (BF), green fluorescence (GF) and red fluorescence (RF) images are shown for each one of the selected fields. **(B)** Dependence of the rate of ROS production upon MβCD concentration by 5 min treatment of CGN with MβCD. The rate of ROS production (means ± s.e.) has been determined from the maximum slope of the kinetics of increase of the average fluorescence intensity per pixel in CGN somas of DCF (solid triangles) or of oxidized DHE (solid circles). **(C)** The increase of fluorescence intensity per pixel in CGN somas of DCF after 5 min (mean ± s.e.) was approximately 60% of the increase recorded for controls when CGN were preincubated with 0.5 mM cholesterol-MβCD complexes instead of only MβCD. Phase contrast or bright field (BF) and green fluorescence (GF) images are shown for a representative selected field. Scale bar inserted in fluorescence microscopy images = 10 µm.

As we can see in Figure 12, this incubation with MβCD for 5 min, produced a dose-dependent reduction of the rise of fluorescence after addition of the fluorescent dyes H_2DCF-DA and DHE, with IC_{50} of submillimolar MβCD. And we also observed that

this reduction is not due to quenching since we perform titration of the fluorescence of the mentioned dyes with MβCD in buffer MLocke's K25 and it produced less than 10% quenching. Noteworthy, the IC_{50} value of MβCD obtained for H_2DCF-DA was nearly 10-fold lower than the IC_{50} value obtained for DHE. The results showed that 5-15 min incubation of CGN with millimolar concentrations of MβCD before addition of H_2DCF-DA and DHE led to more than 90% attenuation of the increase of fluorescence of these dyes. In addition, as shown with H_2DCF-DA the extent of attenuation of the increase of fluorescence was clearly lowered when CGN where preincubated with cholesterol-MβCD complexes instead of only MβCD (Figure 12C).

3.2.2. Mitochondrial and extramitochondrial contribution to ROS production of mature CGN in MLocke's K25.

To accurate the mitochondrial contribution to the production of ROS by CGN in MLocke's K25 we have analyzed the effects of Carbonyl cyanide-4-(trifluoromethoxy)phenylhydrazone (FCCP) and 2,4-dinitrophenol (DNP) added to the extracellular medium 10 minutes before the addition of H2DCF-DA or DHE. The results obtained are shown in the Figure 13 These results led to the conclusion that 2,4-dinitrophenol or FCCP only produced a decrease of 38±5% and 42±5% of the rate of ROS production monitored by H_2DCF-DA and DHE, respectively.

On the other hand, the extracellularly addition of cell impermeable superoxide anion scavenger, SOD, lead to more than 90% decrease of the production of ROS monitored by H_2DCF-DA or DHE (Figure 13). This result adding the strong inhibition of ROS production by MβCD (Figure 12) revealed that plasma membrane lipid rafts are a major source of ROS production in mature CGN in culture in a chemically defined survival medium.

Flavoproteins redox systems have been involved in ROS/RNS production in mammalian cells [116, 198, 199]. Likewise, was demonstrated that two flavoprotein redox systems are associated with lipid rafts of the plasma membrane of mature CGN, namely, Cb_5R and nNOS isoform [103, 115, 116, 151]. Due to this substantiated relevance of flavoproteins in superoxide anion, hydrogen peroxide and related ROS generation, we have experimentally assessed the effect of the generic flavoproteins inhibitor diphenyleneiodonium (DPI) on the kinetics of fluorescence increase after addition of H_2DCF-DA. As observed in Figure 13C micromolar concentrations of DPI elicited a potent and complete blockade of the ROS production by CGN detected by H_2DCF-DA.

3.2.3. $O_2^{\cdot-}$ production by synaptic plasma membrane vesicles NADH oxidase activity is stimulated by Cytochrome c.

We also looked forward to monitoring the effect of oxidized Cytochrome c (Cyt c) (Fe^{3+}) on the NADH-dependent $O_2^{\cdot-}$ production by synaptic plasma membrane vesicles (SPMV) using DHE.

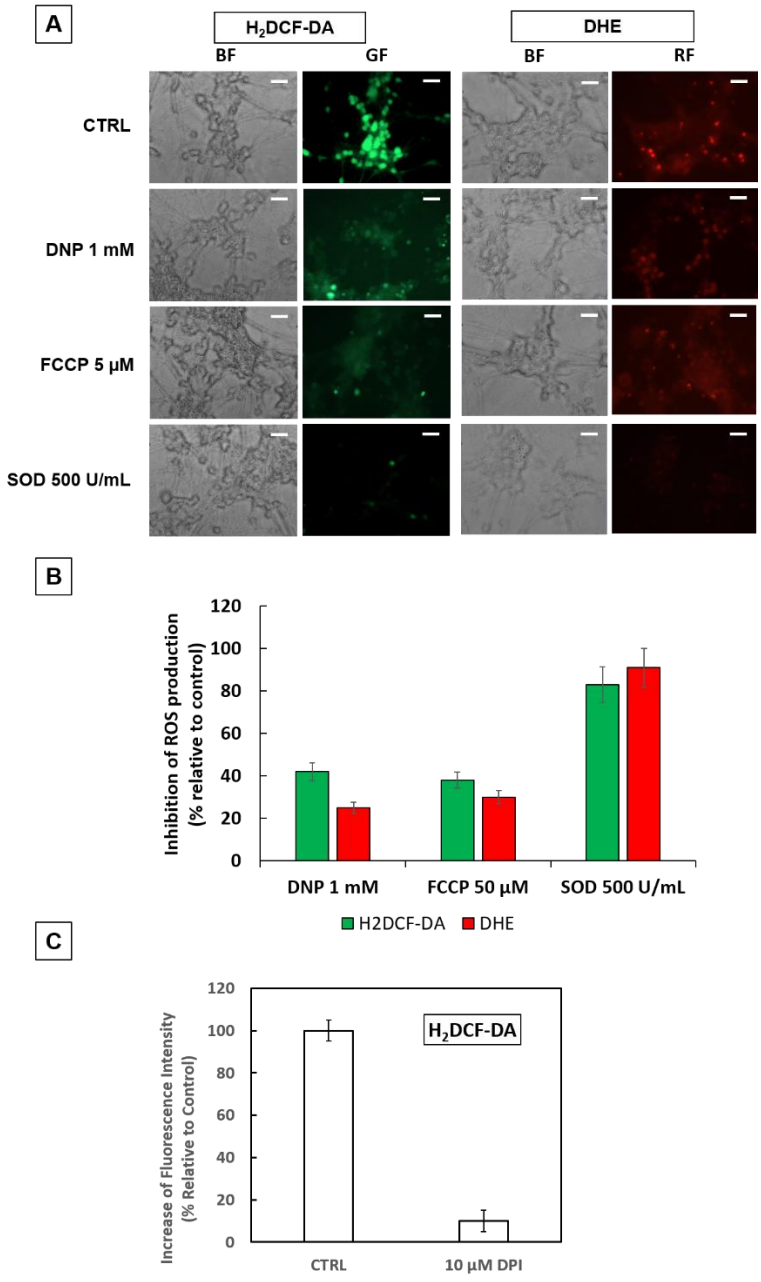

Figure 13: The production of ROS detected by H_2DCF-DA and DHE in mature CGN is almost completely inhibited by SOD and DPI, but it is only partially inhibited by DNP or FCCP. (A) Representative fluorescence microscopy images acquired as indicated in the legend for the Figures 3.7.A and 3.7.B show that 10 min before treatment of CGN between 8 and 10 DIV with 1 mM DNP or 5 µM FCCP inhibits ≤40% of ROS production of CGN detected by H_2DCF-DA or DHE 5 min after their addition to the medium, while it is almost completely inhibited by addition of 500 U/mL SOD only 5 min before of H2DCF-DA or DHE addition **(A)**. Bright field (BF), green fluorescence (GF) and red fluorescence (RF) images are shown for

each one of the selected fields. Scale bar inserted in fluorescence microscopy images = 10 µm. **(B)** Percentage of inhibition of ROS production by 1 mM DNP, 5 µM FCCP and 500 U/mL SOD relative to controls, calculated from the increase of the average ± s.e. fluorescence intensity per pixel in CGN somas 5 min after addition of H_2DCF-DA or DHE to MLocke's K25 medium. **(C)** The inhibition of ROS production after 5 min preincubation with 10 µM DPI relative to controls is also shown by the large attenuation produced by DPI on the increase of the average fluorescence intensity per pixel in CGN somas 5 min after addition of H_2DCF-DA to MLocke's K25 medium. The average ± s.e. intensity reading of fluorescence per pixel within CGN somas were obtained using the ROI tool of the Hamamatsu HCImage software to select somas as areas of interest in experiments performed by triplicate (n>100 CGN somas in each case).

As observed in Figure 14A (continuous line and B), the addition of Cyt c (2.5 µM) to the assay lead to more than 3-fold increase in the oxidation of DHE, in the presence of SPMV (7.5 µg/mL) and NADH (50 µM). Furthermore, SOD added to the assay blocked the Cyt c stimulated DHE oxidation rate by SPMV (Figure 14A, dotted line and B), pointing out that the increased DHE oxidation rate was due to production of O2 ·-, as expected for a $O2^{\cdot-}$ responsive dye [195]. Likewise, we tested the effect of a specific antibody against Cb_5R (ProteinTech, Cat #4668234) (Figure 14A, dashed line and B). The results revealed an almost complete inhibition ($\geq$ 90 %) of the $O2^{\cdot-}$ production by SPMV in the presence of the specific antibody against Cb_5R. The DHE oxidation rate dependence upon Cyt c (Fe^{3+}) concentration, in the absence (filled squares) and presence of SOD (1 U/mL) (open squares) (Figure 14C) was also measured. We verified that addition of increasing concentrations of Cyt c to the assay produced a Cyt c dependent increase of the DHE oxidation rate. Thereafter, we calculated that Cyt c was stimulating the NADH-dependent $O2^{\cdot-}$ production by SPMV almost 20-fold, reaching a maximum value of 192±41 nmoles/min/mg protein, in comparison to the activity measured in absence of Cyt c (10 nmoles/min/mg protein) (Figure 14D). The NADH dependent $O2^{\cdot-}$ production dependence upon Cyt c concentration yielded a Km for Cyt c stimulation of 0.2±0.03 µM.

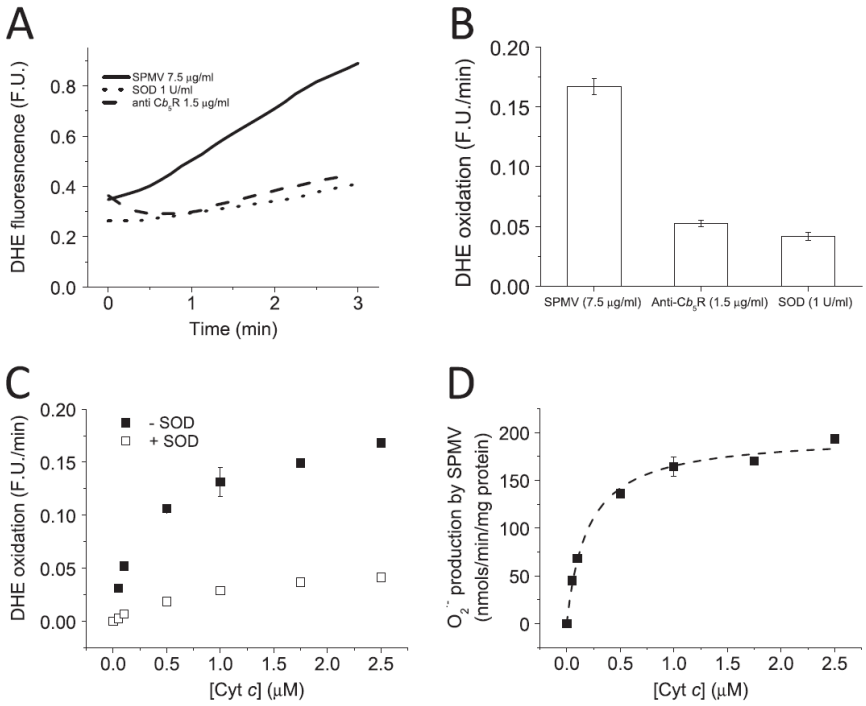

Figure 14: Cyt c stimulated NADH-dependent $O_2^{\cdot-}$ production by SPMV. (A) Kinetics of the NADH dependent DHE oxidation by SPMV measured by fluorescence in the absence and presence of SOD (1 U/mL) and anti-C*b*$_5$R antibody (1.5 µg/mL). DHE oxidation was measured at 37 °C in potassium phosphate 20 mM plus DTPA 0.1 mM (pH 7.0), using a Perkin Elmer spectrofluorimeter with 470 nm and 605 nm excitation and emission wavelengths, respectively, and 10 nm excitation and emission slits. Representative traces of DHE oxidation by SPMV (7.5 µg/mL) in the presence of NADH (50 µM), oxidized Cyt c (Fe^{3+}) (2.5 µM) and DHE (2 µM), in the presence of 1.5 µg/mL anti-Cb_5R (dashed line) or 1 U/mL SOD (dotted line) are shown. **(B)** Quantification of the inhibition induced by anti-C*b*$_5$R (1.5 µg/mL) and SOD (1 U/mL) on the DHE oxidation rate by SPMV (7.5 µg/mL) in the presence of NADH (50 µM) and oxidized Cyt c (Fe^{3+}) (2.5 µM). **(C)** Dependence of the NADH-dependent DHE oxidation rate by SPMV (7.5 µg/mL) upon Cyt c concentration in the absence (filled squares) or in the presence of SOD (1 U/mL) (open squares). **(D)** NADH dependent O2 $^{\cdot-}$ production by SPMV (7.5 µg/mL) dependence upon Cyt c concentration, measured with DHE. All the results shown in this Figure are the average (± s.e) of experiments done by triplicate.

3.2.4. DAF2-DA monitors the rapid propagation between neighbor cells and along dendritic extensions of ROS waves induced by irradiation of CGN cultures with light of 470 nm.

DAF2 is a fluorescent dye that, besides being useful for nitric oxide detection under controlled experimental conditions [200, 201], it has been shown to be largely photoactivated upon the irradiation with the 490nm light of a fluorescence microscope xenon lamp [201]. As we observed, only 5-10 minutes incubation of CGN with DAF2-DA are needed to acquire bright green fluorescence images, (Figure 15). Actually, as can be observe in the videos recordings obtained (data not shown, but can be consulted in the respective publication of this results), acquisition of images every 30 s with exposure times of 0,05 s to the 470 nm xenon lamp blue-light of the epifluorescence microscope, starting approximately 10-15 s after addition of DAF2-DA to mature CGN, elicited a

strong and flash-like increase of the fluorescence intensity at the neurons located close to the center of the light beam.

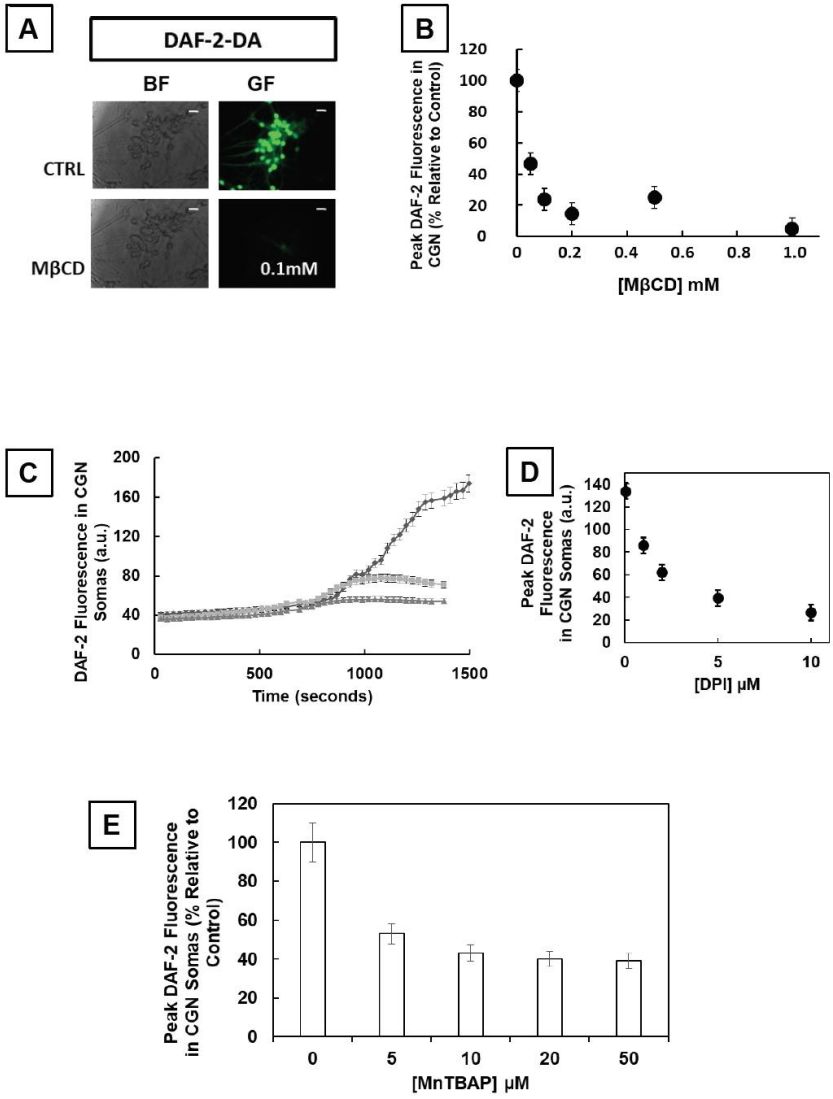

Figure 15: The production of ROS/RNS detected by DAF2-DA in mature CGN is largely inhibited by MβCD, DPI and MnTBAP. (A) Representative fluorescence microscopy images of CGN (8-9 DIV) showing that treatment of CGN with MβCD during 5 min almost completely blocks the increase of fluorescence associated with production of ROS/RNS detected by DAF2-DA at 1200 s after addition of 5 µM DAF2-DA. Bright field (BF) and green fluorescence (GF) images are shown for each one of the selected fields. GF images were obtained with 0.05 s irradiation (exposure) time at time intervals of 30 s. Scale bar inserted in fluorescence microscopy images = 10 µm. **(B)** Dependence of the maximum increase of the DAF2 fluorescence intensity per pixel in CGN somas (peak DAF2 fluorescence) upon treatment of CGN during 5 min with the indicated MβCD concentrations. Y-axis values have been expressed as percent relative to control (0 MβCD). **(C)** Kinetics of the increase of the average DAF2 fluorescence intensity per pixel in CGN somas of CGN at 8-9 DIV in the absence (control, filled circles) and in the presence of 5 µM (filled squares) and 10 µM DPI (filled triangles). **(D)** Dependence upon DPI concentration of the peak DAF2 fluorescence intensity per pixel in CGN somas. **(E)** Dependence of the peak DAF2 fluorescence intensity per pixel in CGN somas upon treatment of CGN during 5 min with the indicated MnTBAP concentrations. Y-axis values have been expressed as percent relative to control (0 MnTBAP). The results shown in panels B, C, D and E are the means of experiments performed by triplicate ± s.e.

Through the analysis of the increase of fluorescence intensity in the neuronal soma we could observed that the fluorescence intensity initially increases slowly and steadily during several minutes and then sharply increases, reaching a peak fluorescence intensity followed by a rapid decay phase only few minutes later (control traces of Figure 15A).

For a constant exposure time, the increase of the time interval of images acquisition between light pulses flash-like delays the time at which the flash-like increase of fluorescence intensity is observed and also its amplitude. In addition, the flash-like increase of fluorescence intensity was largely attenuated by DPI (Figure 15D). Noteworthy, the concentration of 10 µM DPI produced an almost identical decrease of the amplitude of the flash-like increase of fluorescence intensity of CGN plus DAF2-DA and of the increase of the fluorescence intensity of CGN plus H_2DCF-DA, 80±5% (Figure 15A) and 90±5% (Figure 13C), respectively. Therefore, this result strongly suggested flavoproteins as a common source for the ROS involved in the flash-like increase of fluorescence increase of DAF2-DA and those detected by H_2DCF-DA.

The sequential images of the video recordings (data not shown, but can be consulted in the respective publication of this results) also show that the flash-like increase of fluorescence rapidly propagates to neighbor cells through neuronal contact sites and dendritic extensions, mimicking a green light-wiring pattern through the longest dendritic extensions. This raised the possibility of a role of the neuronal plasma membrane as a major source of the ROS producing the flash-like increase of fluorescence intensity of DAF2 upon xenon lamp blue light irradiation. This hypothesis was also supported by the large attenuation of the peak intensity of the fluorescence of CGN plus DAF2-DA produced by submillimolar concentrations of MβCD (Figure 15B). Indeed, the concentration of MβCD that elicited 50% of the maximum attenuation of the increase of CGN/DAF2 fluorescence intensity was the same that yielded 50% attenuation of the increase of CGN/DCF fluorescence, compare Figures 3.11.B and 3.8.B.

3.3. Study of the cross-talk between ROS/RNS production and the activity of calcium-transport and calcium-dependent proteins associated with these nanodomains: implications on excitotoxicity and in the neurotoxicity promoted by rotenone.

3.3.1. Rotenone Nanomolar Concentrations Are Cytotoxic for Mature CGN in Culture in Serum-Free Medium and This Cytotoxicity Is Not Mediated by Glial Contamination

To evaluate the toxic effect of the incubation of rotenone on CGN, cell viability was measured using the MTT assay [194]. As observed in Figure 16A the cell viability of mature CGN in culture decreased in a dose-dependent manner by the treatment with rotenone for 12 h.

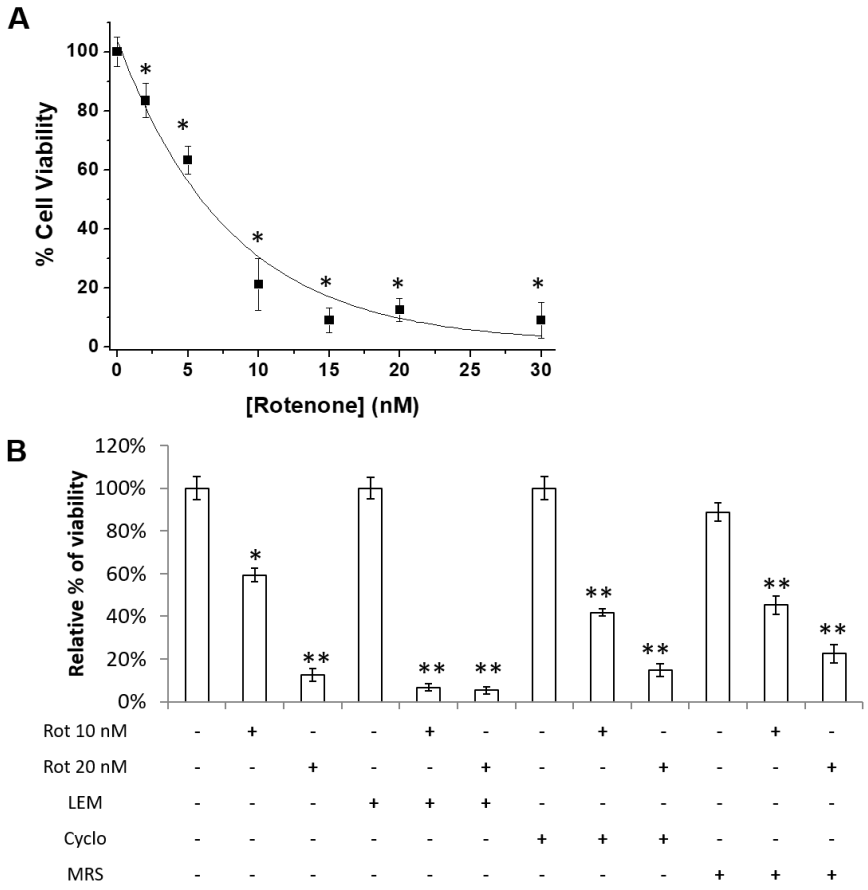

Figure 16: Minor contribution of microglial contamination and serum interference on CGN death induced by nanomolar concentrations of rotenone. (A) Dose-response curve of cell viability measured with the MTT assay after incubation of CGN for 12 h with 2, 5, 10, 15, 20, 30, and 50 nM rotenone. **(B)** The loss of CGN viability induced by 12-h incubation of CGN with 10 or 20 nM rotenone was at most modestly attenuated by preincubation of CGN with 5mM of L-leucine methyl ester (LME) for 4 h or for 1 h with 50 µM cyclo(Arg-Gly-Asp-D-Phe-Val) (Cyclo) or with 5 µM MRS2578. Cell viability values are presented as mean ± s.e. of experiments carried out with more than six different CGN preparations (n ≥ 6). *p < 0.05 and **p < 0.01 compared to non-treated cells

Thereafter the CGN death was also assessed by PI staining (Figure 17), and population averages of n > 500 cells pointed out that PI stained approximately 85% of CGN after 12-h treatment with 10 nM rotenone. Controls (no rotenone added) were run with DMSO, the vehicle added with rotenone, which was always less than 0.1% volume DMSO/volume of cell culture medium, i.e., < 2 µL DMSO/2 mL serum-free medium. The results of Figure 16A pointed out that exposure of CGN to 5.65 ± 0.51 nM of rotenone triggered 50% cell death after 12 h, which are in good agreement with previous studies showing that direct neurotoxicity required rotenone concentrations of 10–50 nM [202, 203].

The addition of serum proteins to the culture medium was found to attenuate rotenone neurotoxicity (Figure 18), likely because this is a highly hydrophobic compound and serum albumin binds efficiently these compounds, and this is likely to underlie the large differences in the neurotoxic concentration range reported for rotenone by different laboratories [159, 202, 203 and this work]. Noteworthy, the cerebrospinal fluid

has a content of serum albumin more than 1 50-fold lower than that of the blood [160, 161] and this may provide a simple explanation for the higher toxicity of rotenone for brain as compared with other tissues.

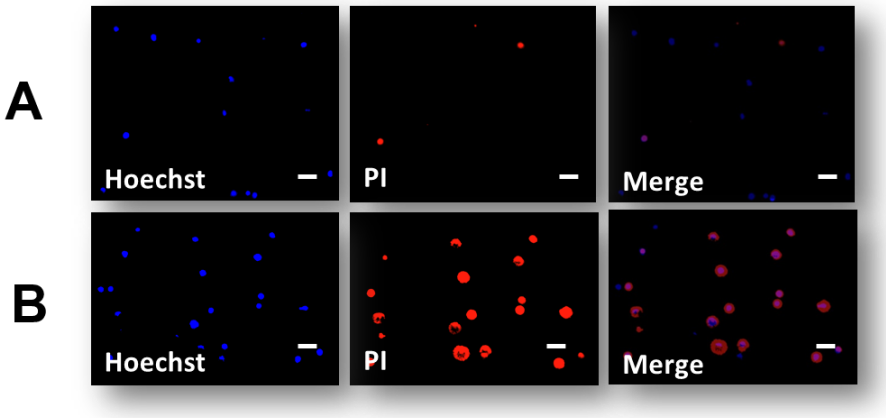

Figure 17: CGN rotenone-mediated death assessed by PI staining. CGN cultures were stained with Hoechst as a nucleus (DNA) dye; and with PI as a membrane disruption indicator which could be consider as a necrotic cell death dye. **A:** Control condition; the cells were incubated with the vehicle DMSO. **B:** PI staining after CGN rotenone incubation. The images shown are representative of the results obtained with three different CGN preparations.

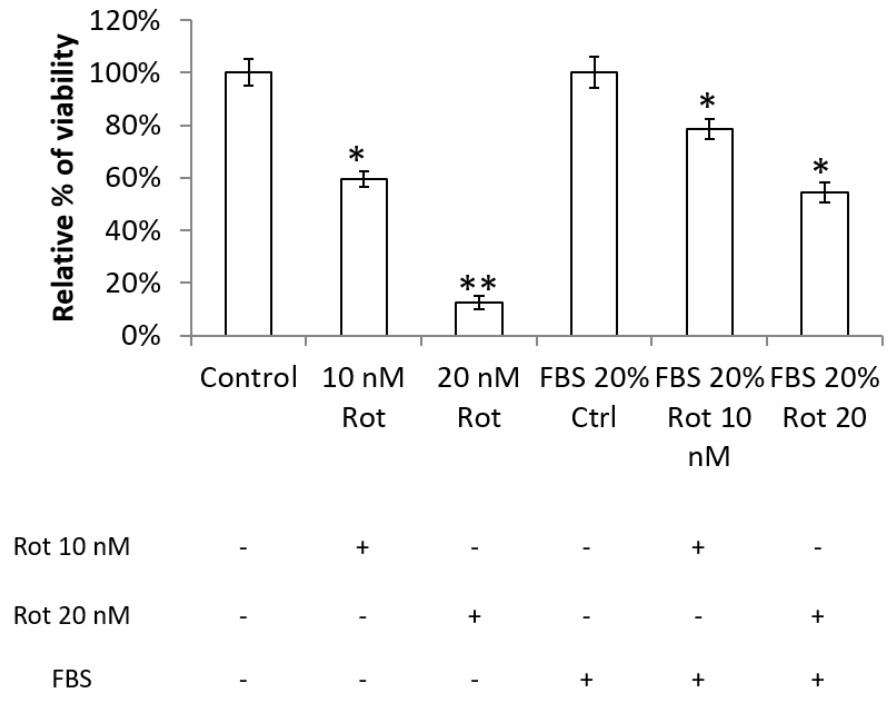

Figure 18: Effect of Fetal Bovine Serum in CGN death mediated by rotenone. Cell viability was measured by the MTT assay after incubation of 10 and 20 nM of rotenone in absence and in presence of 20% FBS supplementation. The results shown are means ± s.e. of triplicate experiments.

On the other hand, some studies have mentioned that the neurotoxic effect of rotenone is mediated by glial cells. Consequently, we assessed this contribution of glial autophagy in rotenone-induced cell death in our CGN cultures as described in [159]: (1) by selective elimination of contaminant microglia adding the lysosomotropic reagent LME; (2) in the presence of cyclo(Arg-Gly-Asp-DPhe- Val) to block the microglial vitronectin receptor; and (3) in the presence of MRS2578 to block the microglial P2Y6 receptor. In Figure 16B is clearly depicted that microglial phagocytosis accounts for less than 20% of the total of the rotenone-induced CGN cell death in our cultures. Taking all this into account we decided to choose a treatment with concentration of 5 nM rotenone during 12 h for subsequent experiments.

3.3.2. Creatine Afforded Protection Against Cell Death, Mitochondrial Membrane Depolarization and Against the Increase of ROS Production Caused by the Treatment of CGN with 5 nM Rotenone During 12 h

In previous studies with different neuronal cultures, direct neurotoxicity of rotenone has been suggested to arise from impairment of neuronal bioenergetics [202, 203]. Our results revealed a strong protection by the ergogenic molecule creatine against CGN death promoted by rotenone, confirming an energetic failure mediated by rotenone in these neurons, since creatine have been widely reported as an energetic compound [181, 183, 204].

As observed in Figure 16A, pre-incubation of 1 h with creatine before the addition of rotenone (5 nM by 12h) significantly inhibited rotenone induced cell death. Creatine (10–30 mM) increased the cell viability, and 30 mM creatine enhanced the cell viability up to the control level (around 100% of viability). Additionally, as shown in the Figure 19B, pre incubation with creatine preserved the morphology of CGN in culture and avoided the massive disruption of neuronal extensions induced by the rotenone treatment. Rotenone is extensively known as a blocker of the electron transport chain complex I, and our results showed that after 30 min of incubation of CGN in MLocke K25 medium with 15 nM rotenone produced 68 ± 4% inhibition of the activity of the complex I (Figure 20A), revealing that rotenone rapidly diffused into the CGN intracellular space. Ours results also showed that the presence of 30 mM creatine in the extracellular medium did not significantly decreased the inhibition of complex I activity by rotenone (Figure 20A), excluding the straightforward possibility of a direct antagonism of rotenone access to the intracellular space by creatine.

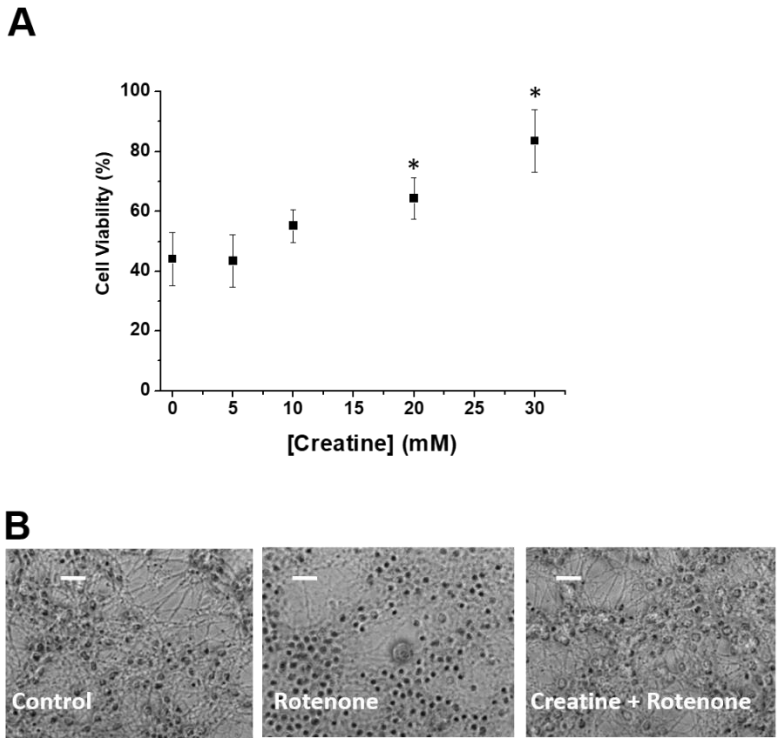

Figure 19: Creatine protected against rotenone-induced CGN death. (A) Creatine largely attenuated rotenone cytotoxicity for CGN. Creatine (5, 10, 20, or 30 mM) was added 1 h before CGN treatment with 5 nM rotenone for 12 h. Cell viability values are presented as mean ± s.e. of experiments carried out with six different CGN preparations (n = 6). All the values statistically different compared to non-treated cells are labeled with (*) $p < 0.05$. **(B)** Representative phase contrast images of CGN after 12-h incubation with the vehicle DMSO (control) or with 5 nM rotenone (rotenone) or with 5 nM rotenone plus 30 mM creatine added 1 h before (creatine + rotenone). Inserted white scale bar = 20 µm

Then, we experimentally assessed the effect of rotenone on mitochondrial membrane potential in the presence or absence of creatine, using tetramethylrhodamine, ethyl ester (TMRE). TMRE is a fluorescent dye that accumulates in non-depolarized mitochondria. We also used FCCP, which is used as a positive control for mitochondrial depolarization. Therefore, CGN were treated with 5 µM FCCP to collapse the proton gradient across the mitochondrial inner membrane, leading to abolition of the mitochondrial potential. Thus, the extent of mitochondria depolarization is proportional to the decrease of the average number of high intensity fluorescence pixels per soma of CGN. FCCP was added at the end of each assay. After FCCP addition, the measured red fluorescence intensity per pixel decreased to a more diffuse background level within the somas (Figure 20, compare panels B1 and B2). As observed, the incubation of CGN with 5 nM rotenone during 12 h lead to a large decrease in the mitochondrial membrane potential, as shown by the decrease of brighter over background pixels of TMRE fluorescence within the CGN somas, i.e., the loss of fluorescence intensity signal in microscopy images and a diffuse fluorescence pattern resembling that of CGN treated with FCCP (Figure 20B).

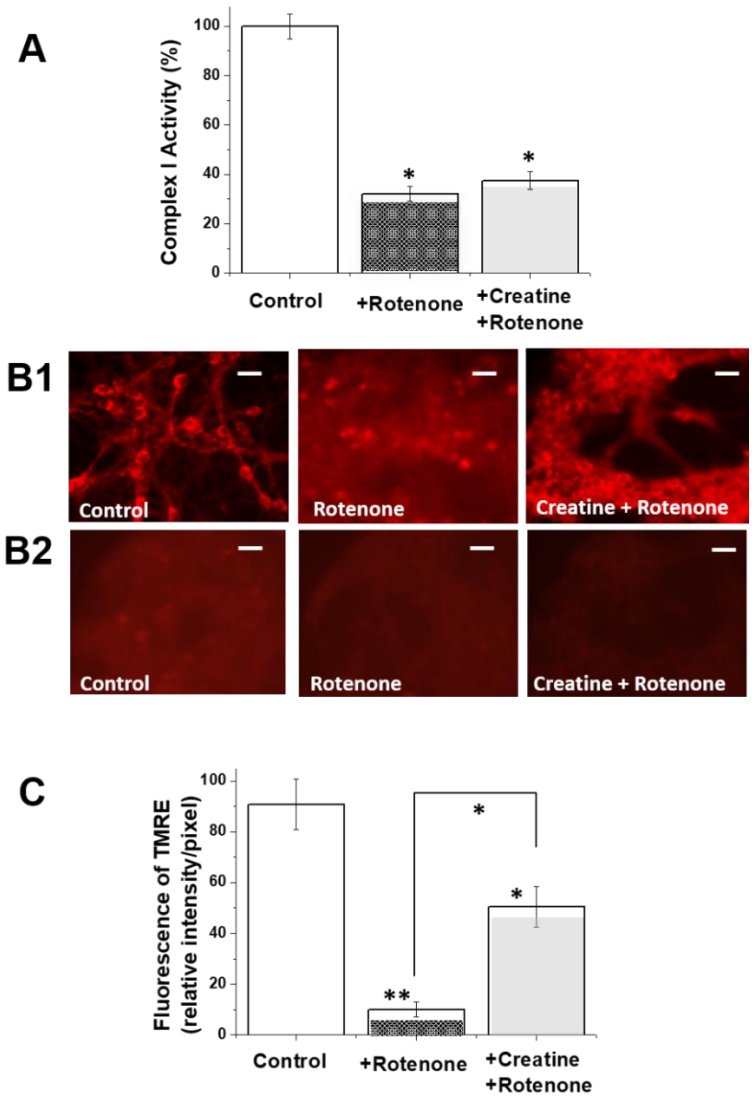

Figure 20: Creatine did not protect against inhibition by rotenone of mitochondrial complex I activity but protected against rotenone induced mitochondrial depolarization. (A) Incubation of CGN with rotenone for only 30 min produced a large inhibition of mitochondrial complex I activity, which was not prevented by creatine. Mitochondrial complex I activity is expressed as percentage of the activity of non-treated CGN (control) for CGN treated during 30 min with 15 nM rotenone (+rotenone) and preincubated during 30 min with 30 mM creatine and then treated during 30 min with 15 nM rotenone (+creatine + rotenone). Mitochondrial complex I activity was measured in CGN lysates with a method using NADH by the monitoring of it´s linear decrease of absorbance at 340 nm at 37 °C. Values are presented as mean ± s.e. of the results obtained in experiments carried out by triplicate with three different preparations of CGN cultures. *p < 0.05 compared to nontreated CGN. **(B, C)** Creatine afforded partial protection against rotenone induced mitochondrial depolarization. Representative images of CGN cultures after treatment with 5 nM rotenone for 12 h (rotenone), or after preincubation with 30 mM of creatine for 1 h before doing the treatment with rotenone (creatine + rotenone), or vehicle-treated CGN (control). Inserted white scale bar = 10 µm. Mitochondrial membrane potential was monitored by fluorescence microscopy using TMRE. Cells were stained by incubation for 15 min with TMRE (0.1 µM) and 0.01% pluronic-F127 at 37 °C. Cell fluorescence images were acquired each 15 s during a period of 30 min using the Hamamatsu Orca R2 CCD camera with an excitation filter of 470 nm and a dichroic mirror DM580 plus an emission filter of 590 nm. **(B)** Images of fluorescence microscopy of TMRE-loaded CGN acquired with a constant exposure time (flash-lamp time) of 0.2 s before (B1) and 5‑10 min after (B2) addition of 5 µM FCCP. The decrease of the intensity of TMRE fluorescence revealed loss of mitochondrial membrane potential (Δψm). Pretreatment with creatine significantly protected neurons against rotenone-induced loss of Δψm, as

demonstrated by the partial maintenance of red fluorescence intensity as well as by the distribution of TMRE fluorescence staining within CGN soma. **(C)** Relative intensity per pixel obtained by subtraction of the values obtained after treating CGN with 5 µM FCCP (n > 100 cells). Rotenone produced a large decrease in TMRE fluorescence intensity (compared to control) indicating an extensive mitochondrial membrane depolarization. Creatine was able to protect partially against the decrease caused by rotenone on the fluorescence intensity within CGN somas. Values are presented as mean ± s.e. of the results obtained in experiments carried out by triplicate with three different preparations of CGN cultures. *p < 0.05 and **p < 0.01 compared to non-treated cells and *p < 0.05 between CGN treated with rotenone only and with creatine + rotenone

On the other hand, creatine significantly protected cells against this loss of mitochondrial potential, as demonstrated by the maintenance of high fluorescence intensity pixels in the somas of CGN treated with 5 nM rotenone in the presence of 30mM creatine (Figure 20C) compared to that obtained for rotenone (averages of n > 100 CGN somas). Thus, these results support the above-mentioned energetic failure, since creatine shown the ability to protect against the mitochondrial depolarization, a target event of a cellular energetic imbalance. Further, we have evaluated the ROS production using the rate of H_2DCF-DA oxidation to DCF as in [114]. The results of measurements of fluorescence intensities in neuronal somas at a fixed time (10 min) after addition of H_2DCF-DA to the CGN culture are presented in Figure 21A. The results pointed out a 6-fold increase in DCF compared to the control (treated with the vehicle DMSO). Moreover, the pre-incubation with 30 mM of Creatine exhibited a strong attenuation of the increase of ROS production induced by rotenone. The GSH levels were also determined, in whole CGN cells, to evaluate whether the increase of ROS elicited by rotenone affected the levels of GSH, the major water-soluble antioxidant present in the neuronal cytosol. These levels were determined using the cell permeable dye monochlorobimane (MCB), after a 12-h incubation of CGN with rotenone. The intensities of the fluorescence of the neuronal soma, at a fixed time after addition of 10 µM MCB to the extracellular medium (10 min), are presented in Figure 21B, revealing that GSH levels were not altered by 12-h incubation of CGN with rotenone.

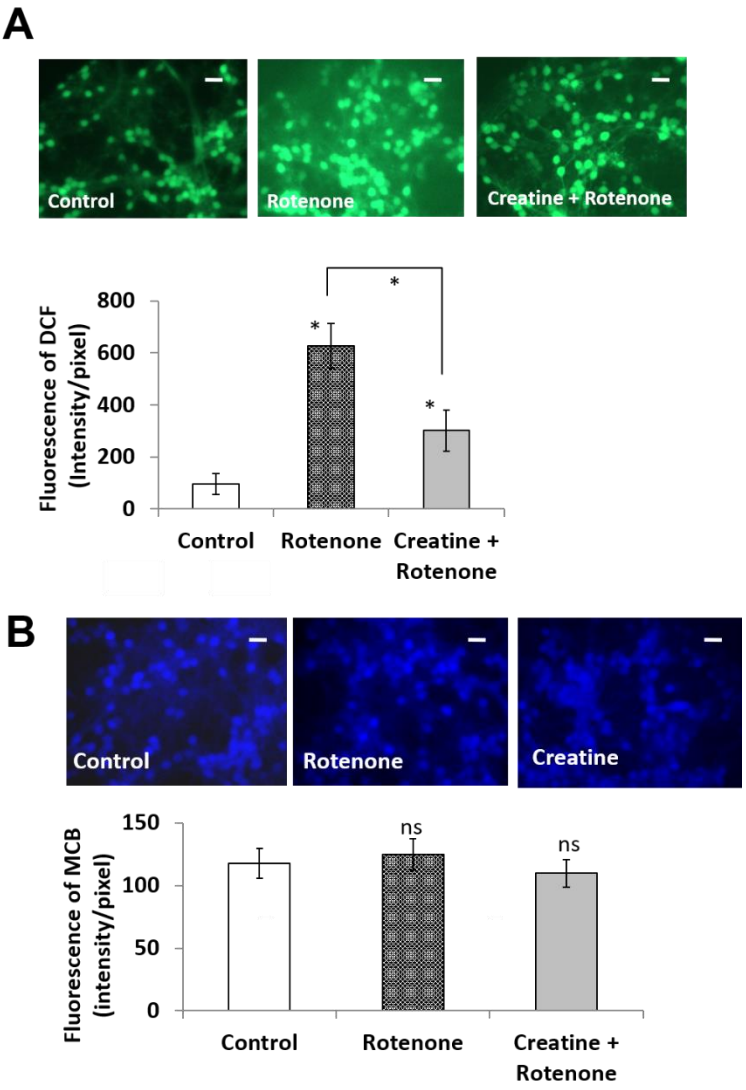

Figure 21: Oxidative stress induced by rotenone in CGN. (A) ROS production was monitored by H2DCF-DA oxidation to DCF after incubation of CGN with 5 nM rotenone for 12 h (rotenone), or after preincubation with 30 mM of creatine for 1 h before doing the treatment with rotenone (creatine + rotenone), or vehicle-treated CGN (control). The extent of H2DCF-DA oxidation to DCF was monitored by the average intensity per pixel in CGN somas 10 min after addition of 10 µMH2DCF-DA (n > 100 cells). **(B)** Representative fluorescence microscopy images of CGN loaded with MCB. CGN were incubated with MCB during 10 min in the culture chamber at 37 °C under a 5% CO2 atmosphere. Afterwards, cell dishes were placed in the thermostatic plate (37 °C) of a Nikon Diaphot 300 epifluorescence microscope, and images were taken each 10 s for 20 min with an excitation filter of 380 nm and a dichroic mirror DM510 plus an emission filter of 510 nm with a constant exposure time (flashlamp time) of 0.77 s. Inserted white scale bar = 10 µm. The average intensity of MCB fluorescence per pixel in CGN somas was not significantly different between CGN treated with 5 nM rotenone for 12 h (rotenone) and CGN treated with the vehicle DMSO for the same time (control) or with 30 mM creatine for 12 h (creatine). Values are presented as mean ± SEM of the results obtained in experiments carried out by triplicate with three different preparations of CGN cultures. *p < 0.05 and **p < 0.01 compared to non-treated cells and *p < 0.05 between CGN treated with rotenone only and with creatine + rotenone; ns: not significant

3.3.3. CK Was Not Impaired by Treatment of CGN with 5 nM Rotenone During 12 h

As our results pointed out that a bioenergetics crisis is at the onset of the CGN death induced by rotenone, and this is on line with the major role of impaired bioenergetics in PD suggested by other authors, we decided to experimentally assess whether the functional state of one of the main bioenergetics compensatory systems CK, is preserved or altered. Besides, the observed creatine protection against rotenone-induced CGN death suggested that ATP-production by CK activity may compensate the energetic failure produced by the partial deficit of respiratory chain elicited by inhibition of mitochondrial complex I of electron transport chain by rotenone. Therefore, we determined the CK levels by Western blotting of CGN lysates. The results presented in the left panel of Figure 22A demonstrate that the levels of CK were not significantly altered after 12-h incubation of CGN with 5 nM rotenone, nor in the absence nor in the presence of 30 mM creatine. Due to an extremely sensitivity of CK to peroxynitrite [205, 206], its activity in the CGN lysates cannot be predicted exclusively by the protein expression levels.

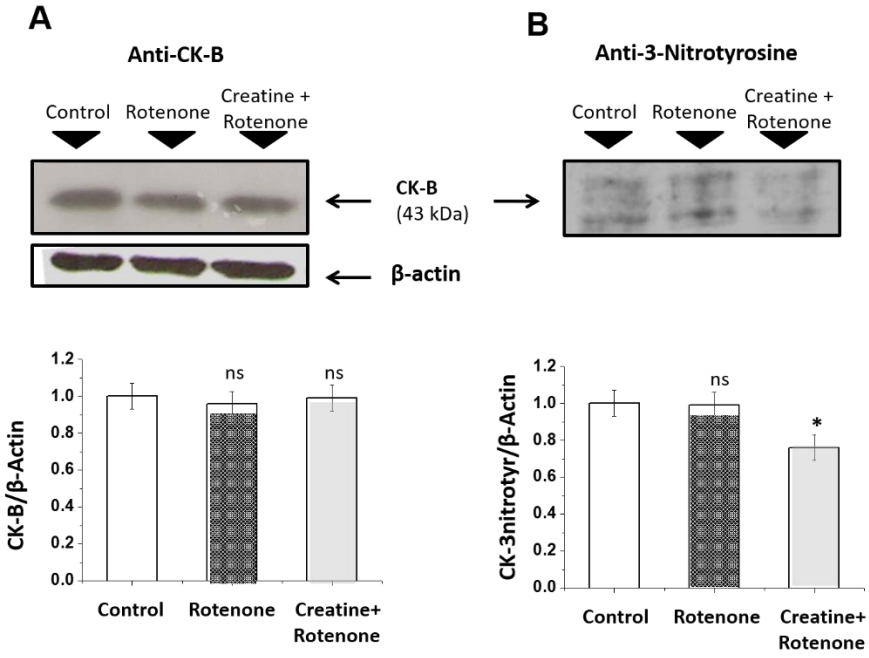

Figure 22: The treatment of CGN with 5 nM rotenone for 12 h did not alter the expression level of CK nor significantly increase protein 3- nitrotyrosines. Western blot analysis of CGN lysates did not show significant differences in the expression level of brain CK isoform, CKB **(A)**, nor in anti-nitrotyrosine labelling of the protein band **(B)** corresponding to the molecular weight of CK in CGN treated with 5 nM rotenone for 12 h (rotenone) compared to CGN treated only with the vehicle DMSO (control). Preincubation with 30 mM of creatine for 1 h before doing the treatment with rotenone (creatine + rotenone) did not alter the expression level of CK-B but significantly reduced antinitrotyrosine labeling at the CK-B band compared to control. After the acquisition of CK-B Western blotting images, membranes were stripped by 10-min incubation in 0.2 M glycine plus 0.5 M NaCl adjusted to pH 2.8 with acetic acid, plus 10-min incubation with 0.5 M acetic acid plus 0.5 M NaCl (pH 2.5), and then 10-min incubation with distilled water and re-used for immunodetection of β-actin. For the sake of clarity, values relative to β-actin were normalized to the value obtained for the control, which was fixed to 1, and are presented as

mean ± SEM of the results obtained in experiments carried out by triplicate with three different preparations of CGN cultures.*p < 0.05 compared to non-treated cells; ns: not significant

Therefore, the CK activity of CGN lysates were also measured and the results point out that 12-h incubation with 5 nM rotenone did not elicit a significant change of the CK activity (Figure 23).

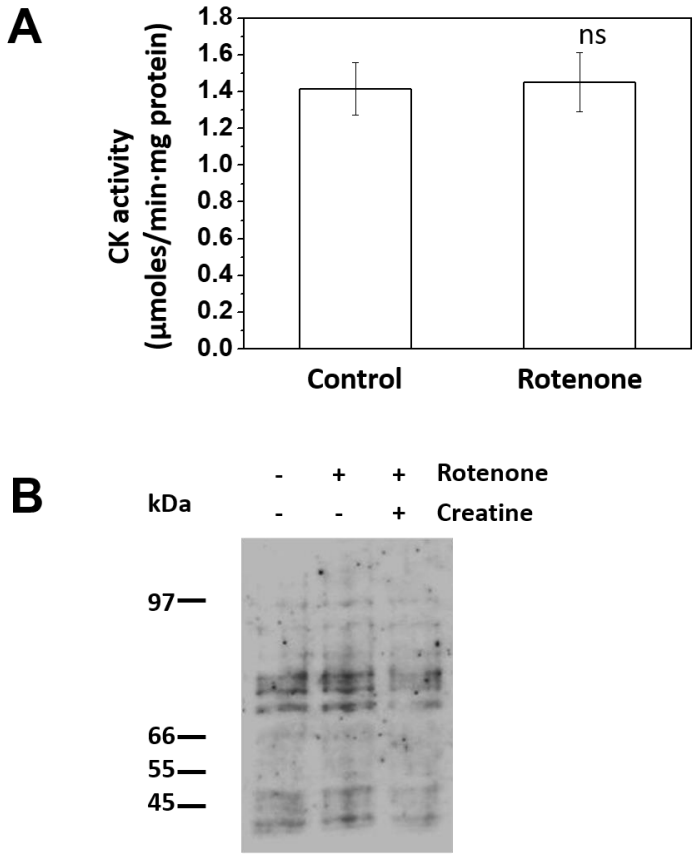

Figure 23: Rotenone did not alter the activity of CK neither elicit nitroxidative stress. A: CK activity was measured in CGN lysates and calculated from the rate of formation of reduced nicotinamide adenine dinucleotide phosphate, monitored spectrophotometrically at 340 nm, at 37°C. Activity was expressed in µmol of phosphocreatine hydrolysed per minute per milligram of protein. **B:** Western blotting showing the specific immunodetection of protein nitrotyrosines in CGN lysates with mouse anti-nitrotyrosine antibody (Calbiochem CC22.8C7.3; 1:1500 dilution). The images shown are representative of the results obtained with three different CGN preparations.

Thus, the maintenance of the activity of CK is fully consistent with other experimental observations done in this work, namely, that rotenone (12h incubation) induced at most a weak nitroxidative environment (non-significant increase of protein 3-nitrotyrosines with respect to control showed in Figure 23B) in CGN. Consistent with

these results, Western blotting of protein 3-nitrotyrosines in lysates of CGN treated with rotenone did not reveal any significant increase of anti-nitrotyrosines labeling of the protein band corresponding to the molecular weight of CK with respect to control lysates prepared from untreated CGN (Figure 22B, right panel).

3.3.4. Rotenone Elicited a Rapid and Sustained Rise of the Steady-State Cytosolic $[Ca^{2+}]_i$ in the Soma of CGN and Creatine Largely Attenuated the Ca^{2+} Homeostasis Alteration Promoted by Rotenone

In this scenario of partial energetic failure, we look forward to understand the effect of rotenone in Ca^{2+} homeostasis, since cytosolic Ca^{2+} concentration can be regarded as a major bioenergetics marker for neuronal activity and survival [8]. Aiming to experimentally assess the possibility that an impairment of intracellular Ca^{2+} homeostasis could be an early event in the neurotoxicity of rotenone, an acute exposure of CGN to rotenone was performed and the concentration of cytosolic Ca^{2+} evaluated. As observed in Figure 24, 10 and 15 nM rotenone elicited a significant sustained increase within 30 min after rotenone addition of the ratio 340/380 of CGN pre-loaded with Fura-2-AM, i.e., a sustained increase of cytosolic Ca^{2+} being steeper and larger at the highest rotenone concentration studied herein. Thereafter, we calculated that 10 or 15 nM rotenone raised cytosolic $[Ca^{2+}]_i$ from 120 ± 30 up to 240 ± 30 nM in less than 30 min.

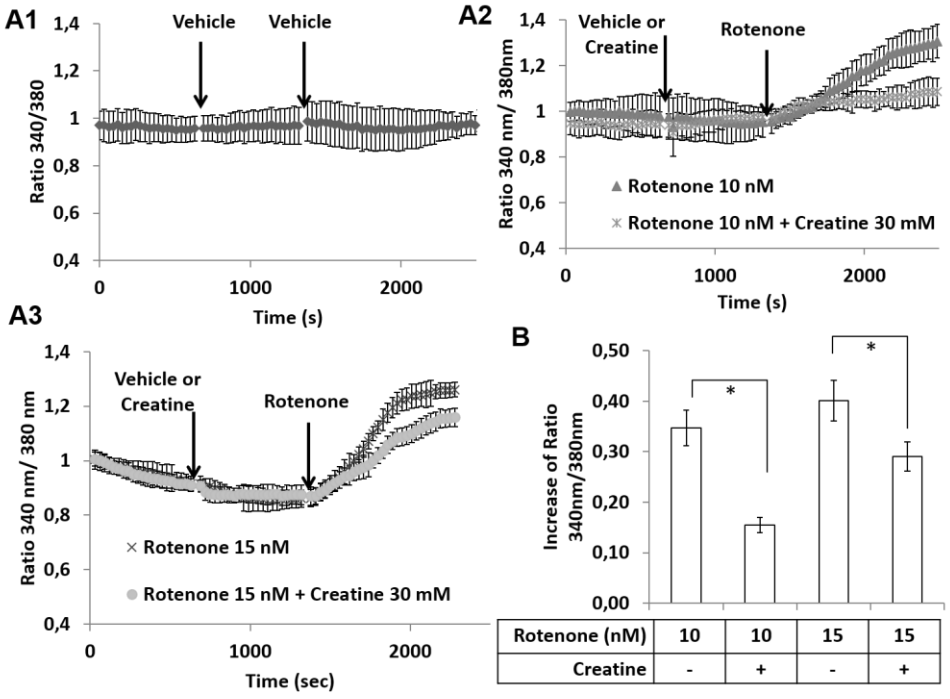

Figure 24: Creatine affords protection against dysregulation of cytosolic Ca^{2+} by rotenone. (A) Kinetic traces of the ratio 340/380 of Fura 2- AM-loaded CGN after the additions indicated in each figure of this panel (A1, A2, and A3). After loading CGN with Fura 2- AM, by the addition of 5 µM Fura-2-acetoxymethyl ester (Fura-2 AM) and 0.025% Pluronic-F127 at 37 °C during 60 min, the medium was changed to MLockeK25 and the ratio 340/ 380 measurements were initiated, 30 mM creatine was added after ≈ 600 s and 10 or 15 nM rotenone after ≈ 1200 s. The results shown are the population averages ± s.e. (averages

of > 100 cell somas in each case) of experiments carried out by triplicate with six different preparations of CGN cultures. **(B)** Ratio (340/380) increase after 800 s post-addition of rotenone (absolute values) obtained from the analysis of the kinetic traces shown in a. *p < 0.05 compared to cells treated only with rotenone

We also evaluated the capacity of Creatine to prevent the mentioned cytosolic Ca^{2+} alterations. As shown in the Figure 24, 30mM creatine pre-incubation were capable of a significantly reduction of the cytosolic Ca^{2+} increase in both cases (10 nM and 15 nM), revealing as predictable higher protective effect against 10 nM (≈ 80%) than against 15 nM of rotenone (≈ 40%).

The confirmed alteration of the steady cytosolic Ca^{2+} concentration, lead us to develop experimental studies in order to identify the putative impairment of the major Ca^{2+} transport systems involved in the control of CGN cytosolic Ca^{2+} homeostasis. To this end, we have used nifedipine (2 µM) as LVOCC blocker, the NMDAr antagonist MK-801 (10 µM), and KBR7943 (5 µM) as inhibitor of the NCX. In addition, we have also experimentally assessed the putative impairment of SERCA using the specific inhibitor cyclopiazonic acid (CPA) (50 µM).

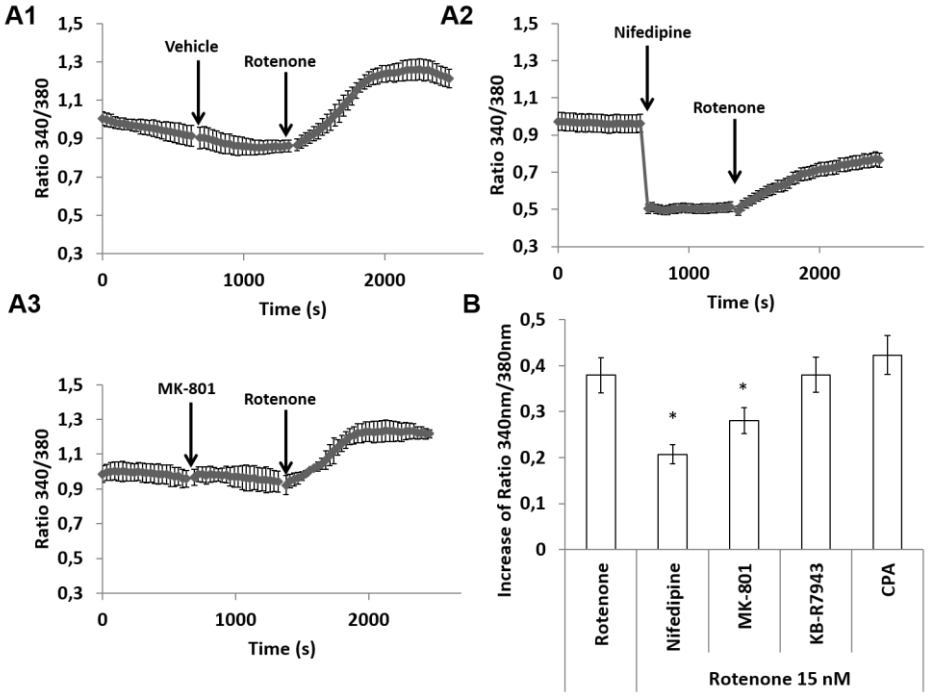

Figure 25: Effects of inhibitors of the major Ca^{2+} transport systems controlling the cytosolic Ca^{2+} homeostasis in CGN on Ca2+ dysregulation caused by rotenone. (A) Kinetic traces of the ratio 340/380 of Fura 2-AM-loaded CGN after the additions indicated in each figure of this panel. After loading CGN with Fura 2-AM, by the addition of 5 µM Fura-2-acetoxymethyl ester (Fura-2 AM) and 0.025% Pluronic-F127 at 37 °C during 60 min, the medium was changed to MLockeK25 and the ratio 340/380 measurements were initiated. Nifedipine (LTCC inhibitor) (2 µM) or MK-801 (NMDAr inhibitor) (10 µM) were added after ≈ 600 s and 15 nM rotenone after ≈ 1200 s (where indicated by the arrows). The kinetic traces obtained in the presence of 50 µM cyclopiazonic acid (CPA, SERCA inhibitor) or 5 µM KB-R7943 (sodium/calcium exchanger inhibitor) were almost identical to the averaged trace obtained for rotenone only. **(B)** Increase of the ratio (340/380) after 800 s post-addition of rotenone (absolute values) obtained from the analysis

of the kinetic traces. The results shown are the population averages ± s.e. (averages of > 100 cell somas in each case) of experiments carried out by triplicate with six different preparations of CGN cultures. *p < 0.05 compared to CGN treated only with rotenone

The results attained demonstrated that only nifedipine and, to a lesser extent, MK-801 elicited a partial and statistically significant attenuation of the rate of alteration of calcium homeostasis caused by rotenone (Figure 25), therefore, indicating functional impairment of LTCCs and NMDA receptors by rotenone, but not of SERCA nor of the NCX.

3.3.5. Short 30-min Exposure of CGN to 15 nM Rotenone Did Not Produce a Large Oxidative Stress or Mitochondrial Membrane Depolarization

In the meantime, we witness that rotenone triggered cell death, oxidative stress and a mitochondrial membrane depolarization in CGN after 12-h incubation, we wanted to ascertain whether these are early or later events than the observed cytosolic Ca^{2+} alteration. Initially we measure the cell viability using the MTT assay and the results showed no significant loss of viability after an incubation of 1 h with 15 nM of rotenone (Figure 26A). As also observed in Figure 26B, the rate of oxidation of H_2DCF-DA only modestly increase after incubation of 30 min with rotenone with respect to that measured for control (untreated) CGN.

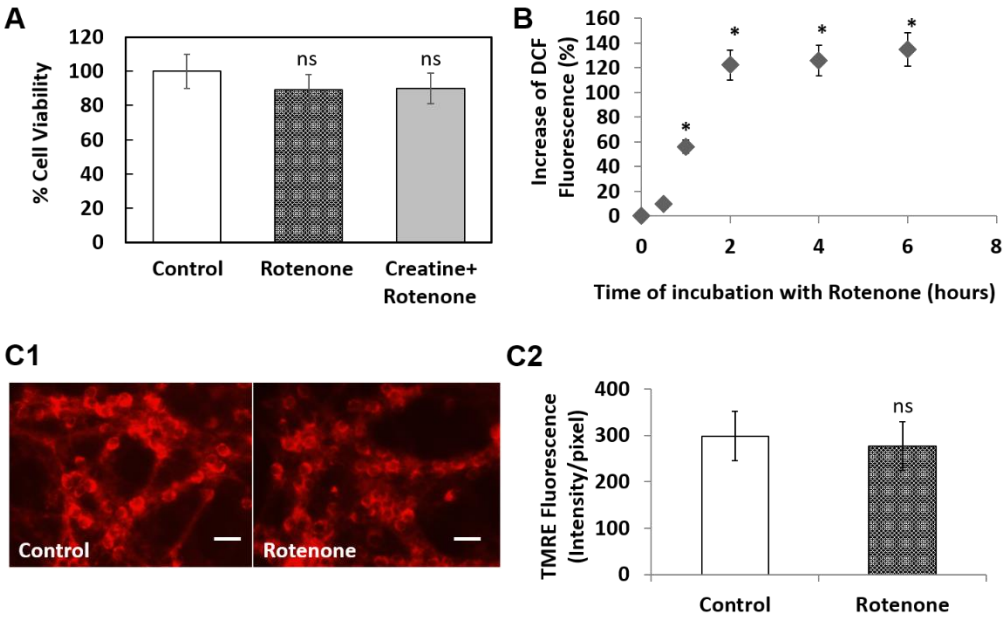

Figure 26: CGN exposure for 30 min to 15 nM rotenone did not produce a significant loss of cell viability, nor significantly increase oxidative stress, nor produce significant mitochondrial membrane depolarization. (A) MTT cell viability assays after exposure of CGN to 15 nM rotenone for 1 h, with or without pre-incubation with 30mM creatine for 30 min indicated a non-significant loss of viability. **(B)** Increase of intracellular oxidative stress induced by rotenone as a function of the time exposure of CGN to this neurotoxin. CGN were treated with 15 nM rotenone for different times in separate Petri dishes. H_2DCF-DA 10 µM was added to separate dishes at the times after addition of rotenone indicated in the abscissae, and the average fluorescence intensity per pixel of CGN soma (n > 100 somas of each experimental condition) was measured 10 min after the addition of H_2DCF-DA. Fluorescence intensity microscopy images were acquired with the Hamamatsu Orca R2 CCD and HCImage software, using the

same lamp-exposure time and fluorescence microscope settings for the acquisition of all images. In the Y-axis, the increase of fluorescence intensity per pixel (%) after exposure to rotenone during the times indicated in the abscissae over the values obtained for vehicle-treated CGN (control condition) is plotted, i.e., [(Ft F0)/F0] × 100. The results pointed out that rotenone-induced increase of oxidative stress reached its maximum after 2 h, while after 30-min incubation of CGN with 15 nM rotenone, it was not statistically significant. **(C1)** Representative images of fluorescence microscopy of CGN stained with TMRE acquired with the Hamamatsu Orca R2 CCD and HCImage software of control (untreated) CGN and of CGN after incubation with 15 nM rotenone during 30min. Inserted white scale bar = 10 µm. Rotenone-treated neurons maintained the bright red fluorescence indicative of active mitochondria. **(C2)** The average intensity of fluorescence per pixel obtained at 10 min after addition of TMRE showed that incubation of CGN with 15 nM rotenone for 30 min did not produce a statistically significant decrease of TMRE fluorescence intensity with respect to control untreated CGN. The results shown are the population averages ± s.e. (averages of > 100 cell somas in each case) of experiments carried out by triplicate with three different preparations of CGN cultures. *$p < 0.05$ and **$p < 0.01$; ns: not significant

Therefore, although 30 min of incubation with rotenone is at the onset of the increase of ROS elicited by 15 nM rotenone, this result pointed out that the highest production of rotenone-induced ROS in CGN is a later event. To understand and accomplish the peak time of ROS production after the exposure to rotenone, we measured the increase of fluorescence of DCF at different times of incubation with 15 nM of rotenone (0, 0.5, 1, 2, 4, and 6 h). The results pointed out 2h as the maximum of intracellular oxidative stress production in the above-mentioned conditions (Figure 26B).

Concerning to nitroxidative stress, results showed no statistically significant differences on protein nitrotyrosine levels between rotenone-treated and control (untreated CGN lysates), Figure 23, indicating that an acute exposure to rotenone does not stimulate reactive nitrogen species production in CGN. The effect of rotenone on the mitochondrial membrane potential was assessed using TMRE as described before. The mitochondria of the cells incubated with 15 nM of rotenone during 30 min maintained the membrane potential, as indicated by the preservation of the pattern of accumulation of TMRE within the cells (red fluorescence, Figure 26C1), and also by an average value of the fluorescence intensity per pixel in the soma of treated CGN not statistically different from those obtained for control untreated CGN (Figure 26C2).

3.4. Study of the evolution/development of the nanodomains network associated to the plasma membrane lipid rafts during cerebellar granule neurons *in vitro* maduration.

3.4.1. CGN maturation in vitro leads to an approximately 2-fold increase of the overall lipid rafts network of these neurons from 4 to 9 days in vitro, and 2 to 3-fold increase of the expression of neuronal nitric oxide synthase and cytochrome b_5 reductase.

Staining with fluorescent cholera toxin B-Alexa 488 demonstrated that lipid rafts are widely present in the plasma membrane of CGN in culture (Figure 27A). Moreover, quantitative fluorescence images acquired with the same exposure time and camera gain showed that they increase about two-fold during the in vitro CGN maturation process (Figure 27A). This point was also confirmed with fluorescence intensity

measurements of cell lysates using a fluorimeter (Figure 27B). The increase is widespread within the neurons, but it is more readily seen at neuronal somas and interdendritic contact sites (Figure 27A).

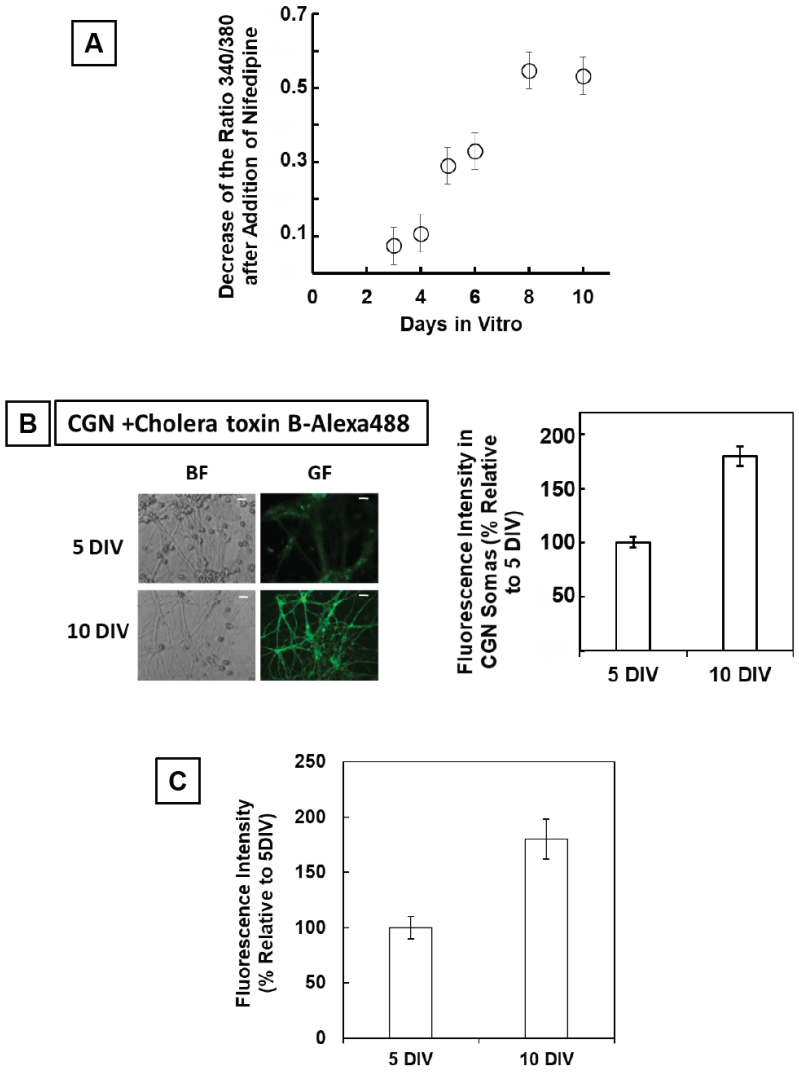

Figure 27: Staining of CGN with cholera toxin B-Alexa 488 monitors lipid rafts increase during CGN maturation *in vitro*. (A) Dependence upon DIV of the decrease of the ratio (340/380) of the fluorescence of Fura2-loaded CGN after addition of 10 µM of the LTCCs blocker nifedipine. Mature CGNs in culture were loaded with Fura-2, by the addition of 5 µM Fura-2-acetoxymethyl ester (Fura-2 AM) and 0.025% Pluronic-F127 at 37 °C during 60 min, and then changed to MLocke's K25 buffer (37 °C). Data acquisition was done with exposure times lower than 0.4 s at time intervals of 30 s. The means ± s.e. intensity reading of fluorescence per pixel within CGN somas were obtained using the ROI tool of the Hamamatsu HCImage software to select somas as areas of interest in experiments performed by triplicate (n>100 CGN somas in each case). **(B)** Representative fluorescence microscopy images of non-mature (5 DIV) and mature CGN (10 DIV) stained by 1 hour incubation at 37ºC and 5% CO2 with 1 µg cholera toxin B-Alexa 488, and washed with 1 mL MLocke's K25 medium immediately before images acquisition. Bright field (BF) and green fluorescence (GF) images are shown for each one of the selected fields. GF images were acquired with an exposure time of 0.1 s, using an excitation filter of 470 nm and 510 nm dichroic mirror/520 nm emission filter. Scale bar inserted in fluorescence microscopy images = 10 µm. The average ± s.e. intensity of fluorescence per pixel within CGN somas were obtained using the ROI tool of the Hamamatsu HCImage software to select somas as areas of interest in experiments performed by triplicate (n>100 CGN somas

in each case). **(C)** Quantitative analysis of cholera toxin B-Alexa 488 bound to CGN was also performed with a fluorimeter Perkin-Elmer 650-40 in a cuvette under mild stirring, after washing the Petri plates with 1mL of MLocke's K25 buffer and careful resuspension of the cells in 2 mL of MLocke's K25 buffer. The results yielded a nearly two-fold increase, 1.8±0.2 (mean of triplicate experiment ± s.e.), of the fluorescence of CGN-bound cholera toxin B-Alexa 488 from 5 to 10 DIV.

Because of the relevance of the increase of lipid rafts during the maturation process of CGN, this point was also experimentally assessed measuring by Western blotting the expression level of H-Ras and of caveolin-1, which in previous works we have shown that are standard protein lipid raft markers of mature CGN lipid rafts [93, 103, 151]. Quantification of the expression level of H-Ras and of caveolin-1 by Western blotting was performed relative to β-actin, to normalize for total protein load per lane. Western blotting results showed that CGN maturation in vitro leads to ≥2-fold increase of H-Ras and 2 to 3-fold increase of caveolin-1 from 4 to 9 days in vitro (Figure 28). Noteworthy, these increases are similar to the increase of Cb_5R during maturation of CGN reported in a previous work of our group [116], and to the increase of nNOS expression level during CGN maturation reported by others [207, 208].

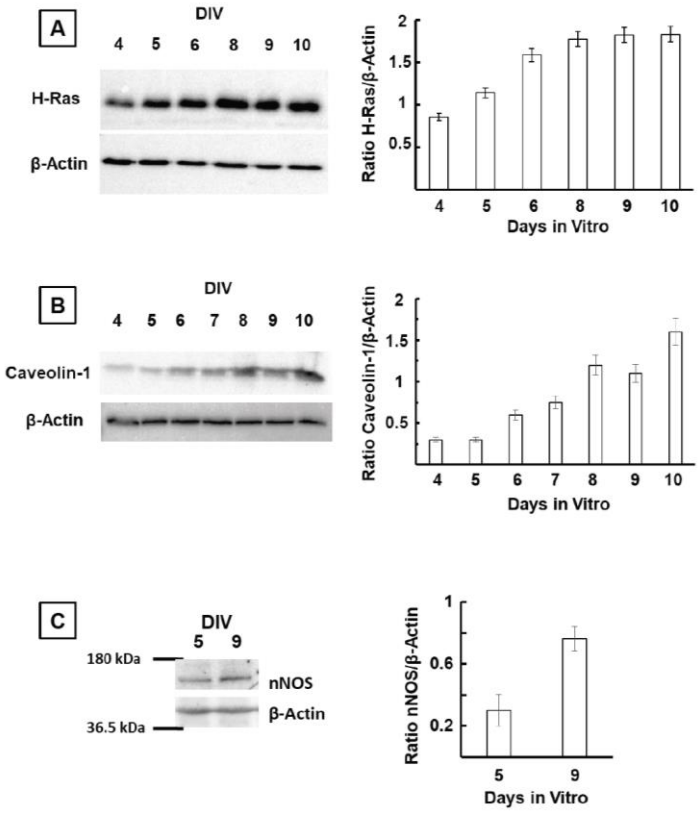

Figure 28: Increase of CGN lipid rafts markers H-Ras and caveolin-1 and of nNOS during CGN maturation *in vitro*. Western blotting of H-Ras **(A)** and caveolin-1 **(B)** in CGN lysates as a function of days in vitro (DIV). After immunodetection of H-Ras with goat anti-H-Ras (Santa Cruz Biotechnology sc-32026, 1:200 dilution) and of caveolin-1 with rabbit anti-caveolin-1 (Santa Cruz Biotechnology sc-894, 1:200 dilution), the PVDF membrane was washed and stripped and used for immunodetection of β-actin with monoclonal mouse anti-β-actin (Sigma-Aldrich A1978, clone AC-15, 1:200 dilution). **(C)** Western blotting of nNOS in CGN lysates at 5 and 9 DIV. After immunodetection of nNOS with goat anti-nNOS (Santa Cruz Biotechnology

sc-5302, 1:200 dilution), the PVDF membrane was washed, stripped and used for immunodetection of β-actin. The images shown in Panels A, B and C are representative of the results obtained with three different CGN preparations. The results have been analyzed with Bio Rad ChemiDocTM XRS+ software and plotted in Panels A, B and C as the averages ± s.e. of the ratio of intensities (H-Ras/ β-actin), (caveolin-1/ β-actin) and (nNOS/ β-actin), respectively, versus days in vitro.

Furthermore, in this work we show by fluorescence microscopy imaging using anti-caveolin-1 stained with IgG-Alexa 488 and anti-H-Ras stained with IgG-Cy3 that caveolin-1 and H-Ras are within FRET distance in fixed mature CGN (Figure 29). Considering that using this experimental FRET approach this means that they are at a distance ≤80 nm, as discussed in previous works of our group [93, 103, 151], this result mean that both are within the same lipid rafts.

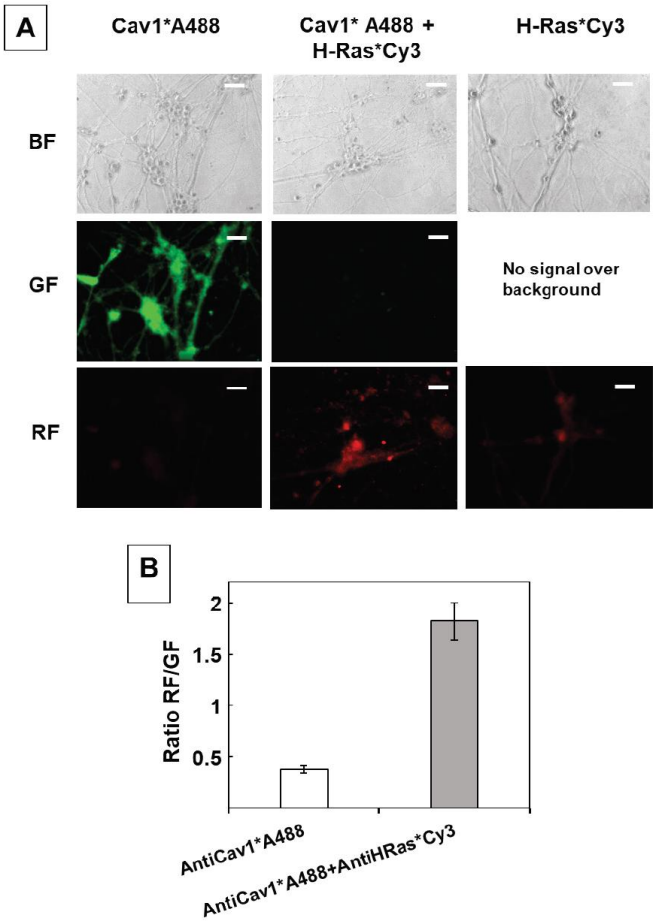

Figure 29: Extensive FRET in CGN from caveolin-1 tagged with IgG-Alexa488 (as FRET donor) to H-Ras tagged with IgG-Cy3 (as FRET acceptor). (A) Representative quantitative fluorescence microscopy images of CGN stained with anti-caveolin-1 (sc-894)/IgG-Alexa488 (cav1*A488), with anti-caveolin-1/IgGAlexa488 and anti-H-Ras (sc-32026)/IgG-Cy3 (cav1*A488/H-Ras*Cy3) and only with anti-H-Ras/IgG-Cy3 (H-Ras*Cy3). Bright field (BF), green fluorescence (GF) and red fluorescence (RF) images are shown for each one of the selected fields. Green and red frames display the donor and acceptor fluorescence, respectively. The exposure time for acquisition of all fluorescence images was 0.3 s. Scale bar inserted in fluorescence microscopy images = 10 µm. **(B)** Ratio of Red/Green fluorescence intensity per pixel (RF/GF) obtained from the analysis of fluorescence intensity data of CGN somas stained with anti-caveolin-1/IgG-Alexa488 only (cav1*A488) and double stained with anti-caveolin-1/IgG-Alexa488//anti-H-Ras/IgG-Cy3

(cav1*A488/H-Ras*Cy3). The average intensity of fluorescence per pixel within CGN somas were taken using the ROI tool of the Hamamatsu HCImage software to select somas as areas of interest in experiments performed by triplicate (n>200 CGN somas in each case). Images of CGN stained only with anti-H-Ras/IgG-Cy3 (H-Ras*Cy3) were acquired to subtract the direct excitation component of the red fluorescence intensity per pixel. The results shown in the panel B are the mean ± s.e. (*) $p<0.05$, i.e. statistically significant with respect to the control (CGN labeled with the Alexa488 FRET donor only).

In the present work, we have experimentally confirmed by FRET microscopy imaging that nNOS is separated by less than 80 nm from H-Ras (Figure 30), i.e. both proteins co-localize within the same lipid rafts. In previous works, we reached the same conclusion for Cb_5R [93, 151].

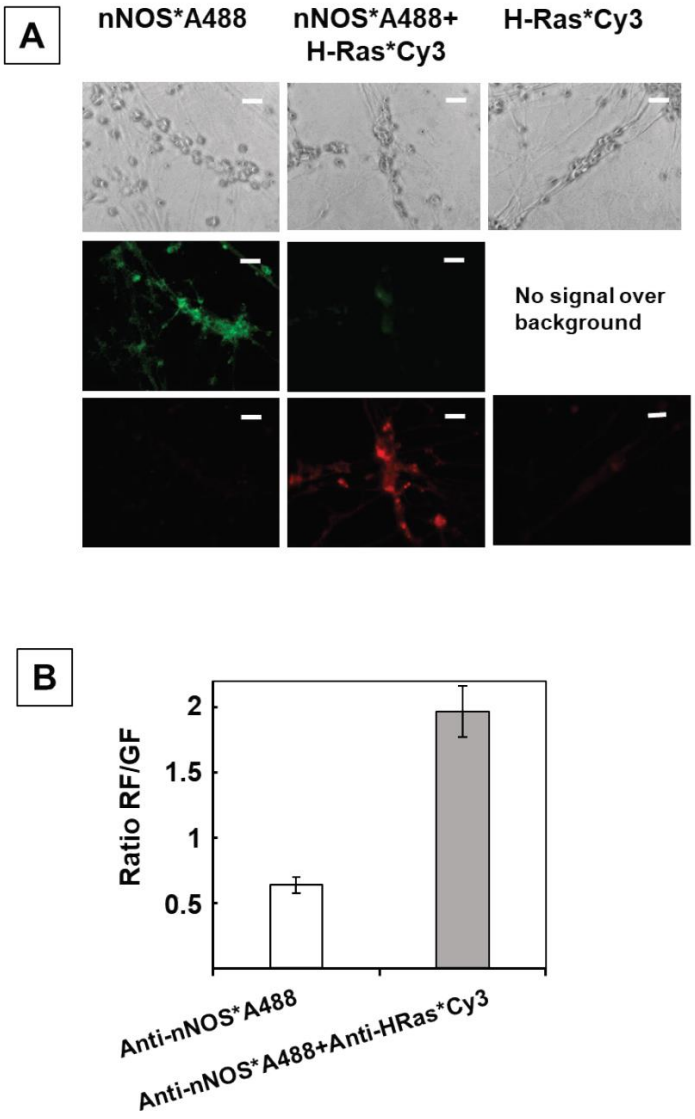

Figure 30: Extensive FRET in CGN from nNOS tagged with IgG-Alexa488 (as FRET donor) to H-Ras tagged with IgG-Cy3 (as FRET acceptor). (A) Representative quantitative fluorescence microscopy images of CGN stained with anti-nNOS (sc-5302)/IgG-Alexa488 (nNOS*A488), with anti-nNOS/IgG-Alexa488 and anti-H-Ras (sc-32026)/IgG-Cy3 (nNOS*A488/H-Ras*Cy3) and only with anti-HRas/IgG-Cy3 (H-Ras*Cy3). Bright field (BF), green fluorescence (GF) and red fluorescence (RF) images are shown for each one of the

selected fields. Green and red frames display the donor and acceptor fluorescence, respectively. The exposure time for acquisition of all fluorescence images was 0.3 s. Scale bar inserted in fluorescence microscopy images = 10 μm. **(B)** Ratio of Red/Green fluorescence intensity per pixel (RF/GF) obtained from the analysis of fluorescence intensity data of CGN somas stained with anti-nNOS/IgG Alexa488 only (nNOS*A488) and double stained with anti-nNOS/IgG Alexa488//anti-H-Ras/IgG-Cy3 (nNOS*A488/H-Ras*Cy3). The average intensity of fluorescence per pixel within CGN somas were taken using the ROI tool of the Hamamatsu HCImage software to select somas as areas of interest in experiments performed by triplicate (n>200 CGN somas in each case). Images of CGN stained only with anti-H-Ras/IgG-Cy3 (H-Ras*Cy3) were acquired to subtract the direct excitation component of the red fluorescence intensity per pixel. The results shown in this panel B are the mean ± s.e. (*) $p<0.05$, i.e. statistically significant with respect to the control (CGN labeled with the Alexa488 FRET donor only).

3.4.2. The production of ROS that is inhibited by MβCD decreased during CGN maturation and this is reverted by C*b*$_5$R3 silencing.

The production of ROS monitored by H_2DCF-DA decreased between 3 and 4-fold from inmature CGN at 5 DIV to mature CGN at 9-10 DIV, and this decrease largely accounts for the ROS production in CGN that is sensitive to MβCD (Figure 31A). This result suggested that inmature CGN should be more vulnerable to extracellular oxidative neurotoxic insults than mature CGN. We have experimentally assessed this point using SIN-1, a superoxide anion and nitric oxide donor that can trigger oxidative CGN death under controlled exposure conditions [190]. Noteworthy, cell death induced by exposure to the ROS/RNS releasing agent SIN-1 is higher for CGN at 5 DIV than at 9-10 DIV (Figure 31B).

We have studied the effect of C*b*$_5$R3 silencing on ROS production by mature CGN, because we have shown in previous works that C*b*$_5$R3 affords a major contribution to ROS production at the neuronal plasma membrane of CGN [113-116], and also of rat brain synaptic plasma membranes [136]. Western blotting showed that we have achieved approximately 50% C*b*$_5$R3 silencing at the protein expression level with respect to control CGN, with a statistically non-significant 10-15% decrease of C*b*$_5$R3 induced by treatment with control-siRNA (Figure 31C). This partial C*b*$_5$R3 silencing produced between 3.5 and 4.5-fold increase of ROS production relative to control and control-siRNA CGN, respectively, when monitored by H_2DCF-DA (Figure 31D).

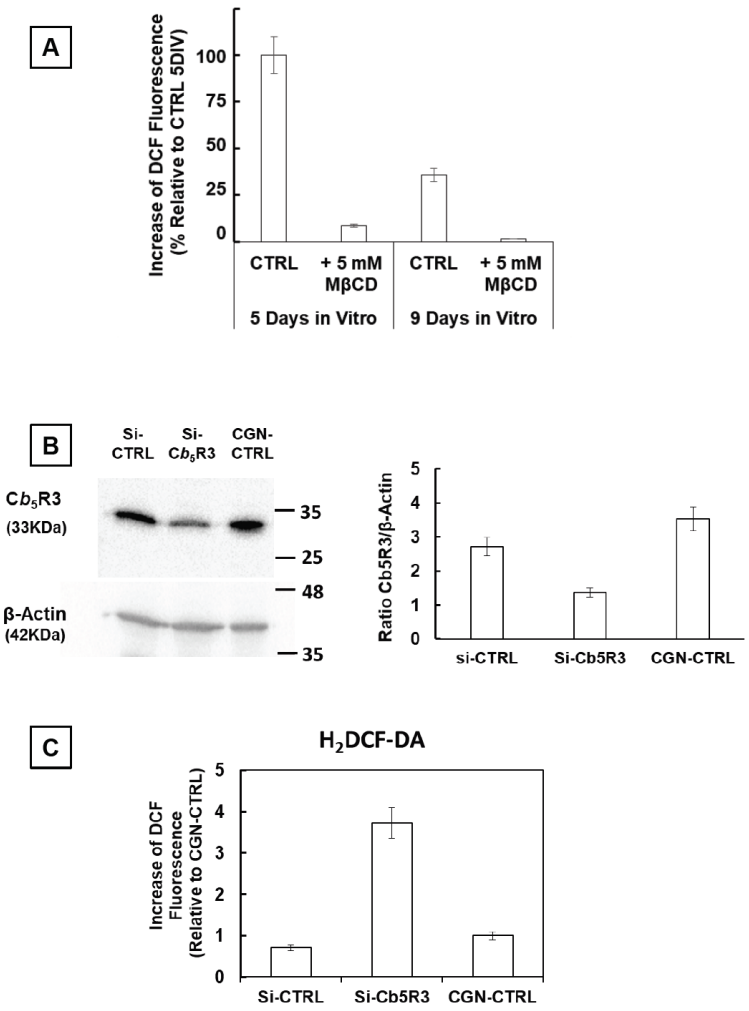

Figure 31: CGN maturation in vitro elicits an attenuation of the production of ROS detected by H_2DCF-DA that is impaired by C*b*$_5$R3 silencing. (A) CGN production of ROS detected by H_2DCF-DA decay more than 50% from 5 to 9 DIV, and either at 5 and 9 DIV is more than 90% inhibited by 5 min preincubation with 5 mM MβCD. These measurements were performed with 10 µM H2DCF-DA as indicated in the legend of the Figure 11. **(B)** Treatment of CGN at 4 DIV with si-Cb_5R3 RNA during 90 hours (si-Cb5R3) resulted in ~50% and ~60% decrease of Cb_5R3 expression with respect to CGN treated with si-Control RNA (si-CTRL) or with respect to untreated CGN (CGN-CTRL), respectively. Western blotting of Cb5R3 in CGN lysates were performed and after immunodetection of Cb_5R3 with rabbit anti-Cb_5R3 (ProteinTech 10894-1-AP, 1:200 dilution), the PVDF membrane was washed, stripped and used for immunodetection of β-actin as indicated in the legend of the Figure 15. The images shown in this panel are representative of the results obtained with three different CGN preparations. The results have been analyzed with Bio Rad ChemiDocTM XRS+ software and plotted as the averages of the ratio of intensities (Cb5R3/ β-actin). **(C)** CGN production of ROS detected by H_2DCF-DA increases between 3.5 and 4 fold in CGN treated with si-Cb_5R3 RNA (si-Cb_5R3) with respect to untreated CGN (CGN-CTRL) and with respect to CGN treated with si-Control RNA (si CTRL). (*) $p<0.05$, i.e. statistically significant with respect to CGN-CTRL or si CTRL. The difference between si-CTRL and CGN-CTRL is not statistically significant. The results shown in panels A, B and C are the means of experiments performed by triplicate ± s.e.

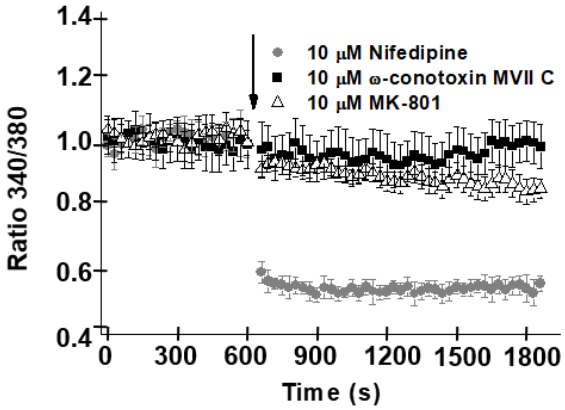

Figure 32: Cytosolic calcium concentration is not affected by ω-conotoxin MVII C neither by MK-801. Mature CGNs in culture were loaded with Fura-2, by the addition of 5 µM Fura-2 acetoxymethyl ester (Fura-2 AM) and 0.025% Pluronic-F127 at 37 °C during 60 min h in a 5% CO2 culture chamber, and then changed to MLocke's K25 buffer (37 °C) and plate in the fluorescence microscope. Time dependence of population averages of the 340/380 ratio in neuronal somas is showed in the figure; After 600s of image acquisition was added 10 µM ω-conotoxin MVII C (dark solid squares) and 10 µM MK-801 (white triangles) as Q-type voltage sensitive calcium channels and NMDAr inhibitors respectively; and also for the positive control nifedipine (grey solid circles) at the point indicated by the arrow. Each inhibitor was added to a different culture plate. Data acquisition and analysis were done after the selection of neuronal somas using the region of interest (ROI) tool of the HCImage software, with exposure times lower than 0.4 s at time intervals of 30 s. The 340/380 ratio values shown are the average ± S.E. of experiments done with three different preparations of CGNs (n > 300 neuronal somas of fields taken from six plates for each experimental condition).

4. Discussion

The results of this work show that lipid rafts allow for more efficient control of the LTCC phosphorylation level in mature CGNs in vitro. Here, it is shown that PKA and CaMK-II also associate with caveolin-1-rich lipid rafts in the plasma membrane of CGN and that treatment with the lipid raft-disrupting agent MβCD largely decreases the phosphorylation level of the β2 subunit of LTCCs to levels observed in the presence of inhibitors of PKA and CaMK-II, and also to those observed in the proapoptotic conditions attained by low potassium (5 mM) in the extracellular medium, an experimental condition that inactivates LTCCs [2]. These effects of MβCD are observed at concentrations that induce a large depletion of cholesterol in CGNs before a significant loss of cell viability. Consistently, the pretreatment of CGNs with MβCD and the removal of MβCD–cholesterol complexes formed produced a large decrease in the steady state cytosolic $[Ca^{2+}]_i$ in the neuronal somas; the decrease is close to that induced by the LTCC blocker nifedipine, highlighting that MβCD treatment leads to a large functional inactivation of LTCCs, even in the partial depolarizing conditions elicited by 25 mM KCl in the extracellular medium. Taken together, our results strongly support the notion that the disruption of lipid rafts impairs the activation of LTCCs by partial depolarizing conditions by decreasing the phosphorylation of their β2 subunit by PKA and CaMK-II. Indeed, it is to be noted that the initial rate and kinetic half-time of the decrease in $[Ca^{2+}]_i$ produced by the CaMK-II inhibitor KN-93 are about 3-fold higher than those obtained for the noninhibitor analogue KN-92 (Figure 7C), despite both displaying a potency similar as inhibitors of LTCC [193]. Moreover, a difference of ~2 min between the half-time values of the kinetics of the decrease in $[Ca^{2+}]_i$ by KN-92 and KN-93 can be accounted for by the well-known slow kinetics of the loss of calcium-independent CaMK-II activity, which has been reported to take place at a timescale of minutes in neurons [209]. As has been showed in a previous work that functional lipid rafts define the high-calcium sub-microcompartments near the plasma membrane of mature CGNs [151], these results are also consistent with a stringent requirement for local Ca^{2+}-dependent activation of CaMK-II in the channel vicinity, as suggested by the blockade of CaMK-II-dependent LTCC facilitation by the "fast" Ca^{2+} chelator 1,2-bis(2-aminophenoxy)ethane-N,N,N0,N0-tetraacetic acid (BAPTA) but not by the slow chelator ethylene glycol-bis(β-aminoethyl ether) N,N,N0,N0-tetraacetic acid (EGTA) [210]. In addition, our results are in accordance with a previous work reporting the modulation of the structural coupling between LTCCs and regulatory proteins by cholesterol in cardiomyocytes [96], where the authors concluded that alterations in the current of LTCCs are mediated by MβCD.
The relevance of the sustained increase in $[Ca^{2+}]_i$ produced by 25 mM KCl plasma membrane depolarization to CGN survival is highlighted by the fact that, within the first 3 h after inducing apoptosis in 5 mM KCl medium, cell death can be largely blocked by simply increasing the KCl concentration of the extracellular medium to 25 mM [113, 211], which promotes neuronal survival. The results of this work show that in mature CGN cultures, the level of phosphorylation of the β2 subunit of LTCCs in a survival medium containing 25 mM KCl is significantly higher than that in proapoptotic 5 mM KCl medium, thus uncovering a major role for the phosphorylation of the LTCC β2 subunit in the activity of these calcium channels. Indeed, our results show that LTCC activity accounts for nearly 85% of the steady-state increase in cytosolic calcium concentration in the CGN somas that is observed with the partial depolarization of the plasma membrane when extracellular potassium rises from 5 mM (proapoptotic condition) to 25 mM (neuron survival condition) (see Figure 32). This agrees with the major relevance

of LTCC activity to the survival of these neurons in culture which was noticed earlier [2, 190, 212], and it is also consistent with the low level of L-glutamate detected in the extracellular medium when CGNs are in 25 mM KCl MLocke's medium [191]. Treatment of CGNs in 25 mM KCl MLocke's medium with the PKA inhibitor H-89 decreases the steady-state cytosolic $[Ca^{2+}]_i$ down to the values measured in the proapoptotic 5 mM KCl MLocke's medium in less than 15 min. Moreover, the effects of H-89 on the steady-state $[Ca^{2+}]_I$ in the somas of CGNs in MLocke's K25 are largely dominated by the inhibition of calcium entry through LTCCs. Noteworthy is that the sum of the decreases in the phosphorylation level of the LTCC β2 subunit elicited by CaMK-II and PKA inhibitors correlates with the large decrease in the phosphorylation level of the LTCC β2 subunit resulting from the proapoptotic conditioning of CGNs. Thus, the phosphorylation of the β2 subunit can largely account for the activation of LTCCs by partial plasma membrane depolarization induced by the presence of 25 mM KCl in the extracellular medium.

In contrast, we found that the steady-state cytosolic $[Ca^{2+}]_i$ is not significantly altered by calphostin C, an inhibitor of PKC, excluding a major role for this protein kinase in the control of cytosolic calcium homeostasis in mature CGNs in culture. These results also indicate that the activity of the mentioned calcium channels plays the leading role in modulating the excitability threshold of CGNs. Under our experimental conditions in culture and in the absence of neurotrophic factors, the contribution of other calcium channels and of NMDAr to maintain a sustained level of cytosolic $[Ca^{2+}]_i$ and thus promoting neuronal survival is only very minor for mature CGNs [190, 191] (see also Figure 32). In the brain, nearly 80% of the β-subunits of LTCCs belong to the $Ca_V1.2$ (α1C) subtype, and 10–25% are the subtype $Ca_V1.3$ (α1D) [19], while in CGN, $Ca_V1.2$ accounts for 89% and $Ca_V1.3$ for 11% of LTCC transcripts [213]. Interestingly, the hyperactivation of $Ca_V1.2$ LTCCs by CaMK-II is implicated in Timothy Syndrome, a multiorgan human genetic disorder whose symptoms include mental retardation and cardiac disease [214, 215], and the excessive activation of $Ca_V1.3$ LTCCs is implicated in the loss of dendritic spines following dopamine depletion in animal models of parkinsonism [216]. Thus, the activity of LTCCs plays a major role in the fine-tuning of CGN excitability, as cytosolic $[Ca^{2+}]_i$ plays a major role in neuronal secretory activity—both the basal secretory activity and the minimum stimuli needed to elicit a neuronal response. Indeed, it has been shown that LTCCs play a relevant role in NMDAr-independent long-term potentiation [217]. Therefore, the impairment of LTCC activity by MβCD is likely to be a molecular mechanism underlying the neurological disorders induced by this compound. The altered LTCC response to a partial depolarization of the plasma membrane in CGNs upon inhibition of PKA, as reported in this work, lends support to a major role for this protein kinase in the normal functioning of granule neurons in the cerebellar cortex. Several β subunits of LTCCs are expressed in rat brain cerebellum [128], namely, β2, β3, and β4, but not the isoform β1, with the β4 isoform of the β subunit showing higher levels of expression. However, it has been shown that activated/autophosphorylated CaMK-II binds to the β2 isoform, but it does not bind to β3 or to β4 [31]. Also, CaMK-II coimmunoprecipitates with forebrain LTCCs that contain $Ca_V1.2α1$ and β1 or β2 subunits, but CAMK-II is not detected in LTCC complexes containing β4 subunits [219. In addition, it has been demonstrated that LTCC modulation by PKA is due to β2 and $α1_c$ subunit phosphorylation [20, 26]. Mutations of serine 478 (Ser478) and serine 479 (Ser479) from the β2 subunit resulted in the complete inhibition of the PKA-induced increase in calcium currents through LTCCs [26]. On these grounds, we selected for this

study an antibody produced by FabGennix Inc. (PCCb2-140AP), using as the immunogen a synthetic peptide with the amino acid sequence “ecs kqr s(p)rh kskdry c” which is located near the C-terminal end of the rat β2 subunit of LTCCs and which is absent in β3 and β4 isoforms. This amino acid sequence is also very close to other phosphorylation sites reported for PKA and CaMK-II in the β2 subunit of LTCCs, namely, Ser478, Ser479, and Thr498 [26, 30, 31]. Moreover, the two serines present in this sequence, which correspond to Ser566 and Ser570 in rat’s β2 subunit (Uniprot: Q8VGC3), are also potential sites for phosphorylation by both kinases, particularly Ser570, which fulfills the criteria for a consensus phosphorylation site of CaMK-II. Indeed, Grueter *et* al. [31] reported a stoichiometry of 6 phosphorylation sites targeted by CaMK-II per mol of β2 subunits. Thus, our results can be rationalized in terms of phosphorylation of the β2 subunit of LTCCs at the serines present in the amino acid sequence “ecs kqr s(p)rh kskdry c” or in terms of immunoreactivity of the PCCb2-140AP antibody with the vicinal phosphorylation sites, i.e., Ser478(P) and/or Ser479(P) and/or Thr498(P). It is to be noted that both CaMK-II and PKA have been reported to act synergistically to increase the calcium current intensity through LTCCs in cardiac myocytes [220].

Concerning to the rate of ROS production the results showed that a short-time treatment of CGN with the cholesterol-trapping agent MβCD strongly inhibits this rate in a culture of mature CGN. The total duration of the exposure of CGN to MβCD in our experiments has been 15-20 min, because fluorescence microscopy images were acquired for 5-10 min after 5 min pre incubation of CGN with MβCD before placing the cell culture plates in the fluorescence microscope and handlings to focus the selected field for images. As have been shown before (table II), this treatment with MβCD efficiently extracts cholesterol without producing a significant loss of cell viability in our CGN cultures up to concentrations of MβCD ≥ 20 mM.

Furthermore, is show that three different ROS-sensitive dyes, i.e. H_2DCF-DA, DHE and DAF2-DA, monitors a similar and large decrease of ROS production by upon treatment of CGN with MβCD. As shown with H_2DCF-DA this decrease is significantly attenuated by CGN treatment with MβCD-cholesterol complexes, which prevent cholesterol depletion. Moreover, MβCD-induced decrease of ROS production is widespread in the CGN in culture and well seen both in neuronal somas and extensions. Although DHE is a fluorescence probe that monitors mainly superoxide anion [195, 196], H_2DCF-DA is a ROS probe that monitors a broad range of ROS [196] and DAF2-DA monitors not only nitric oxide but also the production of other ROS, like those generated upon the rapid reaction of nitric oxide with superoxide anion and ascorbate free radicals [221]. Noteworthy, the inhibition of ROS/RNS production monitored by H_2DCF-DA and DAF2-DA is more sensitive to lower concentrations of MβCD than the inhibition of superoxide anion production monitored by DHE. H_2DCFDA and DHE have been used to show the oxidative stress of CGN during early stages of apoptosis [113, 114, 116, 145], in L-glutamate-induced excitotoxic death [125, 222, 223] and in other oxidative stress-mediated neuronal death [196]. Furthermore, both dyes have been widely used to monitor oxidative-induced cell death in other neuronal cultures. On these grounds, we can conclude that this treatment elicits a generalized and strong impairment of the production of the most relevant ROS involved in oxidative stress-inducing conditions that are neurotoxic for these neurons in culture. Cholesterol extraction by MβCD has been shown to induce lipid rafts disruption in different cell cultures [224, 225].

Therefore, these results suggested a major contribution of lipid rafts to overall ROS/RNS production in our mature CGN cultures. The rapid and nearly complete inhibition of the ROS production monitored by DHE and H_2DCF-DA by extracellularly added SOD strongly support this hypothesis, because SOD does not permeate across the plasma membrane. Furthermore, this result indicates a major role of superoxide anion in the generation of another ROS produced in CGN and detected by H_2DCF-DA. Indeed, the lag phase in the production of ROS detected by H_2DCF-DA, in contrast with the absence of lag phase in the production of superoxide anion monitored with DHE, also give additional experimental support to this conclusion. A major role of extramitochondrial production of superoxide anion and of ROS detected by H_2DCF-DA is supported also by the fact that the mitochondrial uncoupling protonophores FCCP and DNP produced less than 50% inhibition of the production of these ROS in mature CGN. Previous works have shown that deregulation of several redox systems associated with neuronal lipid rafts can produce overshots of ROS and/or RNS, namely, of superoxide anion by Cb_5R3 [226], nitric oxide by nNOS [8, 103, 151], and hydrogen peroxide and superoxide anion by cytochromes P450 [227]. All these redox systems are flavoproteins, and DPI, a broad spectrum flavoprotein inhibitor, produced more than 90% inhibition of ROS/RNS production monitored by the dyes used in this work.

In previous works, our group showed that both Cb_5R3 and nNOS are present in caveolin-1/cholesterol-rich lipid rafts of mature CGN [93, 103, 116, 151]. However, the expression of many cytochromes P450 is strongly downregulated in primary neuronal cultures maturated *in vitro* [228], as well as in other growth-stimulated mammalian cell cultures [229]. To experimentally assess this point in our CGN culture we selected the CYP46 isoform of cytochrome P450, which has 24S-cholesterol hydroxylase activity and is a cytochrome P450 isoform that should be expected to be associated with neuronal lipid rafts owing to its important role in brain cholesterol homeostasis [230]. As shown by Western blotting, during CGN maturation in culture there is a strong downregulation of the expression of CYP46 (Figure 33), and as a result its expression level in mature CGN is negligible. Noteworthy, as we have shown earlier (Figure 5) and in previous works [151] there are large differences between the MβCD concentrations needed to inhibit two major calcium systems involved in the control of cytosolic calcium homeostasis of CGN, e.g. LTCCs and NMDAr. Therefore, the differences between the potency of inhibition by MβCD of the ROS/RNS production monitored by the different dyes used in this work are likely to be due to the different sensitivity of the redox systems mentioned above and of their regulatory proteins to the extent of lipid rafts disruption by different concentrations of MβCD.

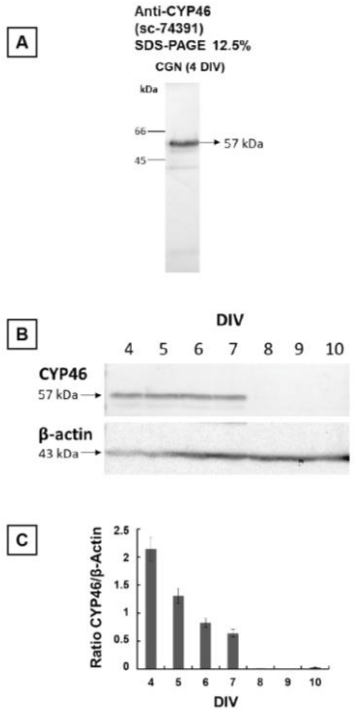

Figure 33: Downregulation of CYP46 expression during CGN maturation *in vitro*. A: Western blotting showing the specific immunodetection of CYP46 in CGN lysates (4 DIV) with goat anti-CYP46 (Santa Cruz Biotechnology sc-74391, 1:100 dilution). **B:** Immunodetection of CYP46 in CGN lysates as a function of days in vitro (DIV). After immunodetection of CYP46 with goat anti-CYP46 (Santa Cruz Biotechnology sc-74 391, 1:100 dilution), the PVDF membrane was washed and stripped and used for immunodetection of β-actin with monoclonal mouse anti-β-actin (Sigma- Aldrich A1978, 1:200 dilution). The images shown are representative of the results obtained with three different CGN preparations. The results have been plotted in Panel C as the means ±s.e. of the ratio of intensities (CYP46/β-actin) versus days in vitro.

Fluorescence microscopy images of CGN stained with fluorescent cholera toxin B and Western blotting of H-Ras content show more than two-fold increase of lipid rafts per neuron during the maturation of CGN cultures *in vitro*. On the other hand, mature CGN at 9-10DIV are more resistant than immature CGN at 5DIV to the oxidative insult produced by extracellular exposure to SIN-1, a ROS/RNS releasing compound [231, 232] that has been shown to mimic the extracellular oxidative stress associated with inflammation and ischemia-reperfusion in mammalian brain [140, 232, 233]. Consistently, we found that CGN maturation leads to a large decrease of the production of ROS detected by H_2DCF-DA. This attenuation of ROS production in mature CGN can be reverted by silencing the expression of Cb_5R3 to approximately 50%. Cb_5R3 is a redox protein associated with lipid rafts, whose expression level increases approximately 2.5-fold from 5DIV to 9-10DIV [115], and whose deregulation leads to an overshot of superoxide anion production by CGN [116]. Therefore, our results show that Cb_5R3 plays a major role in the attenuation of the overall ROS production in mature CGN and reveal a major role of this protein as an antioxidant cellular defense against CGN exposure to extracellular neurotoxic oxidative insults.

A remarkable photoactivation pattern is displayed by CGN stained with DAF2-DA upon irradiation with the fluorescence microscope Xenon lamp 470 nm blue light. The kinetics of ROS production by CGN detected with DAF2-DA is more than 90% inhibited by CGN pre-treatment with MβCD or DPI, as also found for the ROS production monitored with H_2DCF-DA. However, DAF2-DA revealed the occurrence of a clear space-temporal pattern of the increase of fluorescence within the CGN culture. Sequential images showed that a flash-like peak of fluorescence initiates at the center of the field irradiated with the light beam and rapidly spread away across neighbor neurons and through the dendritic extensions. This is a spreading fluorescent wave induced by ROS/RNS because it is approximately 70% attenuated by the peroxynitrite scavenger MnTBAP, and it is completely blocked by addition of SOD plus catalase to the extracellular medium. In addition, the latter result points out that it is largely due to ROS produced at or near the neuronal plasma membrane.

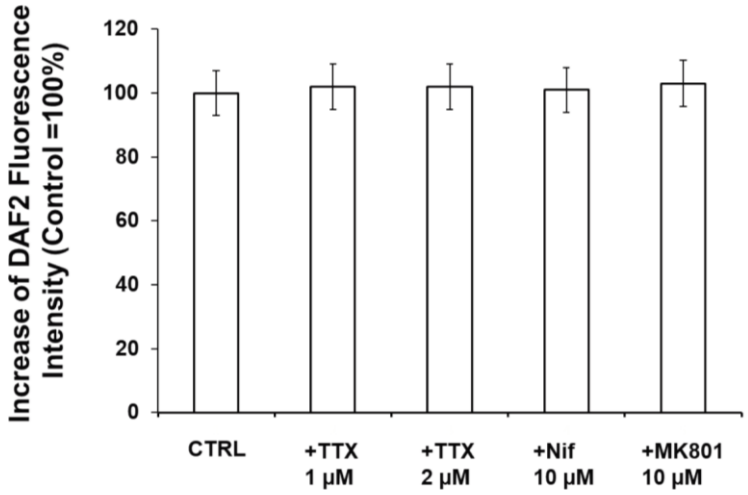

Figure 34: The flash-like increase of DAF2 loaded CGN is not altered by tetrodotoxin, nifedipine or MK801. The increase of fluorescence of mature CGN (9-10 DIV) loaded with DAF2-DA at 1200 s after addition of 5 µM DAF2- DA was not significantly altered with respect to control (CTRL) in the presence of 1 and 2 µM tetrodotoxin (TTX) nor in the presence of 10 µM nifedipine (Nif) or 10 µM MK801. The results shown are means ±s.e. of triplicate experiments.

Thus, ROS propagation in the culture is not isotropic, and the images sequences strongly suggest that ROS propagates along the neuronal plasma membrane. Considering that images were acquired every 5 s and the fluorescence propagation distance observed between sequential images in dendritic extensions, we can calculate a ROS propagation rate higher than 10 µm/s. The possibility that this was reflecting a depolarizing wave can be excluded because it is not affected by preincubation of the CGN with 1 µM tetrodotoxin (Figure 34). DAF2 complexation with calcium may also enhance the fluorescence of this dye [201]. However, the flash-like peak of DAF2-DA fluorescence was not affected by preincubation of CGN with 10 µM nifedipine nor by 10 µM MK-801, i.e. by inhibitors of LTCCs and NMDAr which are the two major calcium entry systems present in the plasma membrane of these neurons (Figure 34). Therefore,

these results reveal for the first time to the best of our knowledge a rapid ROS wiring phenomenon along the dendritic extensions of mature CGN in culture.

The results obtained also showed that the cytotoxicity of exposure to nanomolar concentrations of rotenone for mature CGN in culture in serum-free medium is not mediated by glial contamination. Indeed, a concentration as low as 5.65 ± 0.51 nM of rotenone was enough to trigger 50% cell death of primary CGN maturated in culture 12 h after addition of this neurotoxin, measured with culture plates containing 2.5×10^6 neurons. The addition of serum proteins to the culture medium was found to attenuate rotenone neurotoxicity, and this is likely to underlie the large differences in the neurotoxic concentration range reported for rotenone by different laboratories using culture media supplemented with different types and percentage of serum. Taking into account previous studies showing also glial activation by nanomolar concentrations of rotenone [159], it is likely that the neurotoxicity of rotenone reported from *in vivo* experiments [234. 235] is the sum of direct neurotoxic and microglial activation processes. In previous studies with different neuronal cultures, direct neurotoxicity of rotenone has been suggested to arise from impairment of neuronal bioenergetics [202, 203]. The attained results revealed a strong protection by creatine against CGN death promoted by rotenone, supporting an energetic failure mediated by rotenone in these neurons, since creatine have been reported to attenuate neuronal bioenergetics failure [181, 183, 204, 236]. Moreover, this result is in good agreement with the protection of creatine against cell death in human neuroblastoma SH-SY5Y elicited by 6-hydroxydopamine [237], another Parkinsonism-inducing neurotoxin. The mentioned energetic failure was further supported by the ability of creatine to protect against the mitochondrial depolarization triggered by 5 nM rotenone, a target event of a cellular energetic imbalance. As the results clearly pointed out that a bioenergetics crisis is at the onset of the CGN death induced by rotenone, and this is on line with the major role of impaired bioenergetics in PD suggested by other authors (see above), we experimentally assessed whether the functional state of one of the main bioenergetics compensatory systems CK, is preserved or altered. As observed in Figure 22, the protein levels of CK were unchanged, as well as its activity (Figure 23). Moreover, it has been shown that CK is highly sensitive to an increase of nitroxidative stress in the brain and heart, which leads to a significant inhibition of this enzyme [179, 205]. Therefore, the maintenance of the activity of CK is fully consistent with other experimental observation of this work, namely, that rotenone induced at most a weak nitroxidative stress in CGN. Furthermore, this latter result is also consistent with the beneficial effect of creatine supplementation to revert the neurotoxicity promoted by rotenone, as it would be expected to be ineffective in case of irreversible peroxynitrite-induced oxidative damage of CK. In this scenario of energetic failure, we look forward to understand the effect of rotenone in Ca^{2+} homeostasis, since cytosolic Ca^{2+} concentration can be regarded as a major bioenergetics marker for neuronal activity and survival [8]. Indeed, while shorter (30– 60 min) exposure of CGN to 15 nM rotenone did not lead to mitochondrial membrane depolarization, our results revealed a sustained and early increase in cytosolic Ca^{2+} concentration after acute rotenone treatment, observed within 30 min, which should lead to an increase of neuronal activity. This conclusion is in good agreement with the results of non-invasive brain studies, which indicate a correlation between PD and increased functional connectivity/activity in cerebellum [166].

Noteworthy, creatine largely attenuated the Ca^{2+} homeostasis alteration promoted by rotenone and, thus, this action of creatine may have a special relevance for the neuroprotection against rotenone neurotoxicity, both *in vitro* and *in vivo* studies. In addition, a sustained increase of cytosolic Ca^{2+} concentration contributes to the development of glutamate-induced excitotoxicity that in turn induces neurodegeneration, reviewed in [8]. The results obtained in this work unravel that rotenone induced a sustained stimulation of Ca^{2+} entry through NMDA receptors in CGN in culture. In addition, the results obtained in this work have shown that acute rotenone treatment stimulated also Ca^{2+} entry through LTCCs. Noteworthy, LTCCs and NMDA receptors are vicinal proteins in the plasma membrane of mature CGN [103]; thus, activation of LTCC elicits L-glutamate release near the NMDA receptors. It is worthy to recall here that one of the most relevant Ca^{2+} channels involved in the pace making activity of dopaminergic neurons is the LTCC subtype $Ca_v1.3$ [238]. Moreover, it has been proposed that Ca^{2+} entry through plasma membrane $Ca_v1.3$ Ca^{2+} channels during an excessive activity could play a significant role in the early stages of PD pathology [239]. Thus, our results suggest the development of combination therapies with creatine plus NMDA receptors and/or LTCCs inhibitors to slow down Parkinsonism neurodegeneration. The increase of ROS production monitored by H_2DCFDA reached a maximum after 2 h with rotenone incubation and was only weakly significant after 30-min exposure to rotenone. Although H_2DCF-DA is known to react with many ROS and intracellular oxidants, this probe cannot be reliably used to measure H_2O_2 (see, e.g. [240]). Therefore, the increase of the rate of oxidation of H_2DCF-DA to DCF cannot be taken as a proper measurement of the intracellular oxidative stress. On these grounds, aiming for a better evaluation of the putative increase of intracellular stress induced by rotenone, we measured intracellular GSH and protein 3- nitrotyrosines levels. Our results showed no GSH depletion after 12-h exposure to rotenone, nor a significant increase of protein 3-nitrotyrosines, pointing out that the rotenone-induced cellular oxidative stress is moderate and a delayed or later event with respect to a sustained cytosolic calcium raise in CGN death induced by rotenone. This result is in good agreement with our conclusion that the cytotoxicity of exposure to nanomolar concentrations of rotenone in the CGN death reported in this work is not mediated by glial contamination (see above), since the increase of 3-nitrotyrosines shown in rotenone-treated animal models of Parkinsonism have been rationalized in terms of iNOS upregulation following microglia activation [241, 242]. In addition, creatine had a very strong effect against the intracellular oxidative stress induced by the treatment of CGN with rotenone. This latter result is in good agreement with results reported by others showing that creatine has direct chemical antioxidant properties as it can act as a scavenger of free radical species [243] and also indirect antioxidant capacities in cells and tissues [244, 245].

5. Materials and Methods

5.1. Preparation of rat cerebellar granule neurons (CGN)

CGN have been prepared from Wistar rats as described previously [103, 113-115, 151, 190]. Animal handlings were performed in accordance with Spanish regulations and were approved by the Ethical Committee of the University of Extremadura. CGN cultures were kept at 37 °C in a humidified atmosphere of 95% air/5% CO_2. Cytosine arabinofuranoside (10 µM) was added to fresh culture medium 48 h after plating to prevent replication of non-neuronal cells. Seven days after plating, the culture medium was replaced with the following serum-free Dulbecco's modified Eagle's medium (DMEM):F12 medium (1:1) supplemented with 12.5 mM glucose, 20.82 mM KCl, 5 µg/mL insulin,0.1 mg/mL apo-transferrin, 20 nM progesterone, 50 U/mL penicillin, 25 U/mL streptomycin, 1.1 mM pyruvate and 2 mM L-glutamine. The extracellular medium was changed 30 minutes before running fluorescence microscopy and cell viability experiments to MLocke's K25 buffer (pH 7.4 at 37 ºC): 4 mM NaHCO3, 10 mM Tricine, 5 mM glucose, 2.3 mM $CaCl_2$, 1 mM $MgCl_2$and 134 mM NaCl/25 mM KCl.

Cell viability was experimentally assessed measuring the amount of colored formazan by the reduction of 3-(4,5-dimethylthiazol-2-yl)-2,5-diphenyltetrazolium bromide (MTT) as in previous works [113, 114, 151, 190].

5.2. SPMV preparation

Rat brain SPMV were prepared using a standard procedure as described in [114, 115].

5.3. Lipid Raft Preparation

CGN lipid rafts were isolated as indicated in previous works [93, 103, 151], except that all the buffers were supplemented with the phosphatase inhibitors NaF and $NaVO_3$.

5.4. Contribution of Microglia Contamination to Rotenone-Mediated CGN Death

The contribution of the phagocytic activity of microglia contamination to rotenone-induced CGN death has been experimentally assessed using three different treatments before addition of rotenone: (1) 4-h pre-incubation of neurons at 9 DIV with 5 mM of L-leucine methyl ester (LME) to selectively eliminate the microglia and replacing the medium after this treatment (as in [159]); (2) 1-h incubation with 50 µM cyclo(Arg-Gly-Asp-D-Phe-Val) to block the microglial vitronectin receptor [159]; and (3) 1-h incubation with 5 µM MRS2578 to block the microglial P2Y6 receptor [159]. Afterwards, rotenone was added to the medium, and 12 h later, the viability was assessed by the MTT assay.

5.5. Measurements of Mitochondrial Complex I and Creatine Kinase Activities

Complex I activity of sub-mitochondrial particles was measured as in a previous work [246]. Activity measurements were carried out in Tris–HCl 10 mM, KCl 50 mM, EDTA 1 mM and KCN 2 mM (pH 7.4), plus 50 µM CoQ1 with 75 µg of CGN lysate. The reaction was initiated by the addition of 75 µM NADH and monitored from the linear decrease of absorbance at 340 nm at 37 °C up to 10 min. After 10 min, 6 µg of rotenone/mL was added and the absorbance was recorded during another 10 min to evaluate the activity independent of rotenone. Creatine kinase (CK) activity in lysates has been measured as described earlier in [247]. CK activity was calculated from the rate of formation of reduced nicotinamide adenine dinucleotide phosphate (NADPH) at 37°C, monitored spectrophotometrically at 340 nm. CK activity was later converted to in µmoles of phosphocreatine hydrolyzed per minute per milligram of protein.

5.6. Hoechst 33258 and Propidium Iodide Staining

A direct estimation of CGN with disrupted plasma membrane was obtained through a modified double-staining technique, as described in [248].

5.7. Fluorescence microscopy

CGN in Petri plates were kept at 37°C in MLocke's K25 in the thermostated plate holder of the epifluorescence microscope for image acquisition. Fluorescence microscopy images of CGN have been acquired with a Hamamatsu Orca-R2 CCD camera (binning mode 2 x 2) attached to a Nikon Diaphot 300 epifluorescence microscope (Tokyo, Japan) with an NCF Plan ELWD 40× objective. Quantitative analysis of the average fluorescence intensity per pixel of selected neuronal soma was done with the HCImage software using the region of interest (ROI) tool of this software, as in previous work [151]. 2',7'-dihydrodichloro fluorescein diacetate (H_2DCF-DA), a broad-range ROS indicator [196], has been used as an indicator of the overall oxidative stress. Dihydroethidium (DHE) has been used as an indicator of superoxide anion production [195, 197]. 4,5-diaminofluorescein diacetate (DAF2-DA) has been used to monitor nitric oxide and ROS production upon the rapid reaction of nitric oxide with superoxide anion and ascorbate free radicals [221]. Glutathione (GSH) measurements were determined using the compound monochlorobimane (MCB) (as described in [249]). For image acquisition these dyes were added at the following concentrations: 10 µM (H_2DCF-DA, DHE and MCB) and 5 µM (DAF2-DA).

Mitochondrial depolarization was monitored in CGN with tetramethylrhodamine ethyl ester (TMRE), a fluorescence dye widely used to measure mitochondrial membrane potential [230] by incubation for 15 min with TMRE (0.1 µM) and 0.01% pluronic-F127 at 37 °C. And the reference depolarized state was acquired by addition of 5 µM carbonyl cyanide- 4-(trifluoromethoxy)phenylhydrazone (FCCP) at the end of each experimental assay.

The mitochondrial contribution to the production of ROS by CGN in MLocke's K25 has been evaluated using the uncoupling agent FCCP and 2,4-dinitrophenol (DNP) added to the extracellular medium 10 minutes before the addition of H_2DCF- DA or DHE.

Images of CGN stained with H_2DCF-DA, cholera toxin B-Alexa 488 and DAF2-DA have been acquired with an excitation filter of 470 nm, and 510 nm dichroic mirror/520 nm emission filter (green fluorescence), using an exposure time of 0.5 s for H_2DCF-DA, 0.1 s for cholera toxin B-Alexa 488 and 0.05 s for DAF2-DA. Images of CGN stained with DHE and TMRE have been acquired with an excitation filter of 470 nm, and 580 nm dichroic mirror/590 nm emission filter (red fluorescence), using an exposure time of 0.05 s.

5.8. CGN Treatments

In all experiments with proapoptotic low-potassium conditions, CGN plates were treated with MLocke's K5 buffer for 1 h at 37 °C, 5% CO_2. In experiments performed in low potassium, CGN plates loaded with Fura-2 AM were incubated for 15 min with H-89 (PKA inhibitor) at 37 °C, 5% CO_2, before image acquisition for $[Ca^{2+}]_i$ measurements. To study the phosphorylation levels of the β2 subunits of LTCC after protein kinase inhibition, we treated CGN plates for 15 min at 37 °C and 5% CO2 with 20 μM H-89 to inhibit PKA and 30 μM KN-93 to inhibit CaMK-II. To study the effect of cholesterol extraction on the phosphorylation levels of LTCCs, CGNs were treated for 15 min with 1 mM and 5 mM methyl-β-cyclodextrin (MβCD), a well-known cell-cholesterol sequestering compound, in MLocke's K25 buffer. Finally, to study the effect of cholesterol extraction on $[Ca^{2+}]_i$, CGNs were treated with 5 mM MβCD in serum-free DMEM:F12 medium (1:1), supplemented as indicated before, and, after 1 h treatment, CGNs were washed and loaded with Fura-2 AM for measurements of $[Ca^{2+}]_i$.

5.9. Cell lysates and Western blotting

CGN have been lysed in buffer 25 mM tris-(hydroxymethyl) aminomethane (Tris)–HCl, pH 7.4, 150 mM NaCl, 5 mM ethylenediaminetetraacetic acid, 50 mM NaF, 5 mM $NaVO_3$ and 0.25 % 4-(1,1,3,3-tetramethyl butyl)phenyl- polyethylene glycol (Triton X-100), supplemented with 1x SIGMAFASTTM protease inhibitor cocktail (Sigma-Aldrich). Lysates were collected and supplemented with 50% glycerol and stored at -80 °C until use. The protein concentration of cell lysates was measured with Bradford's method, using bovine serum albumin as standard.

In an SDS-PAGE gel at a concentration of 7.5, 10.4, or 12% acrylamide, for the same protein of interest, a certain amount of CGN lysate or lipid raft fraction was loaded per lane, ranging between 5 and 20 μg of protein in different gels; then, we transferred the gel to PVDF or nitrocellulose membranes with a 0.2 and 0.45 μm average pore size, respectively (Trans-BloT TransferMedium, BioRad, Hercules, CA, USA). Depending on the protein of interest, membrane blocking was carried out with 5% (w/v) non-fat dry milk or 5% bovine serum albumin, both in phosphate-buffered saline (PBS) supplemented with 0.05% polyoxyethylenesorbitan monolaurate (PBST). Before incubation with the primary antibody, membranes were washed three times with PBST. After incubation with the first antibody overnight, membranes were washed six times with PBST and incubated for 1 h at room temperature with the secondary IgG antibody conjugated with horseradish peroxidase. Again, we washed the membrane six times with PBST followed by incubation for 3 min with Super-SignalWest Dura Substrate (Pierce). Western blots

were revealed by exposure to an Amersham Hyperfilm MP autoradiography film (GE Healthcare, UK) or with Bio-Rad ChemiDocTM XRS+. Then, membranes were treated under continuous stirring at room temperature, blocked and treated as indicated above to quantify β-actin to monitor protein load, using mouse anti-β-actin (Sigma-Aldrich-A1978) or rabbit anti-β-actin (Sigma-Aldrich- A5060) as primary antibody and anti-mouse IgG Horseradish peroxidase or anti-rabbit IgG-Horseradish peroxidase as secondary antibody.

Primary antibodies used for Western blotting: mouse anti-3-nitrotyrosine antibody (Calbiochem CC22.8C7.3, Calbiochem-Merck KGaA), goat anti-creatine kinase brain isoform CK-B (Santa Cruz Biotechnology sc-15157), goat anti-H-Ras (Santa Cruz Biotechnology, sc-32026), rabbit anti-caveolin-1 (Santa Cruz Biotechnology, sc-894), mouse anti-nNOS (Santa Cruz Biotechnology, sc-5302), and rabbit anti-Cb_5R3 (ProteinTech 10894-1-AP), rabbit anti-LTCC β1C subunit (sc-25686), rabbit anti-PKA (sc-28892), rabbit anti-CaMK-II (sc-9035), rabbit anti-p-β2 subunit of LTCCs (PCCb2-140AP). All these antibodies were used in the dilution range recommended in their technical sheets and tested for the detection of molecular weight bands expected for their corresponding proteins with whole CGN lysates before use in the experiments of this work.

5.10. Immunoprecipitation

Immunoprecipitation was carried out using the ImmunoCruzTM IP/WB Optima system of Santa Cruz Biotechnology Inc. (Santa Cruz, CA, USA) following the instructions given in their technical data sheets. Samples were analyzed by SDS-PAGE followed by Western blotting as indicated above.

5.11. Measurement of Cholesterol Content in Cell Lysates

To quantify the extent of cholesterol removal by treatment with MβCD, we treated CGNs with 0, 5, 10, and 20 mM MβCD for 15 min in MLocke's K25 buffer. After the treatment, the supernatant was removed, and CGNs were carefully lysed, as indicated above. Cell lysates were homogenized by 50–60 passages through hypodermic needles, stainless steel gauge 26 of ½ inch length. The protein content of these cell lysates was measured using the Bradford assay, and their cholesterol content was measured using a standard assay with Amplex RedTM (Invitrogen Life Sciences Technologies–Thermo Fisher Scientific). The fluorescent product of oxidation of Amplex RedTM, resorufin, was measured with a Perkin-Elmer 650–40 fluorimeter operated in ratio mode, with a fixed excitation wavelength at 530 nm and emission wavelength at 590 nm, with 10/10 excitation/emission slits. Amplex Red 50 µM was added to the assay buffer (pH 7.0): 2-{[2-hydroxy-1,1-bis(hydroxymethyl) ethyl]amino} ethanesulfonic acid (TES) 50 mM, NaCl 100 mM, EDTA 0.1 mM in the presence of horseradish peroxidase 0.2 U/mL. Cholesterol oxidase 1 U/mL was added, and fluorescence was recorded for 20 min at 25 °C until the intensity reached a plateau.

5.12. Fluorescence measurements of cholera toxin B-Alexa 488 bound to resuspended CGN.

Measurements of cholera toxin B-Alexa 488 bound to CGN have been performed by fluorimetry as in [115].

5.13. Fluorescence Resonance Energy Transfer (FRET) imaging

FRET imaging has been performed as in previous works [93, 103, 116, 151], with CGN at the indicated days *in vitro* (DIV) in 24-well plates with 600,000 cells per well or in 35 mm diameter Petri plates with $2.5x10^6$ cells per plate. The plates were washed twice with 1 mL MLocke's K25 buffer to wash the phenol red remaining in the plates. Then CGN were fixed with 2.5% paraformaldehyde, 3 mM $MgCl_2$, 2 mM ethylene glycol-bis (2-aminoethyl ether)-N,N,N',N'-tetraacetic acid and 0.32 M sucrose in PBS's buffer (5 mM sodium phosphate, 137 mM NaCl and 27 mM KCl, pH 7).

5.14. Measurement of the intracellular free Ca^{2+} concentration ($[Ca^{2+}]_i$)

$[Ca^{2+}]_i$ was measured as in previous works [114, 151, 190]. Briefly, CGN were loaded with Fura2 by incubation in DMEM-F12 for 60 min with 5 µM Fura-2-acetoxymethyl ester (Fura2-AM) and 0.025% Pluronic-F127 at 37°C. Then CGN were washed and the culture dish placed in the thermostatic controlled plate (Warner Instrument Co., Hamden, CT) of the Nikon Diaphot 300 inverted epifluorescence microscope. Digital images were taken with a Hamamatsu Orca-R2 CCD camera (binning mode 2 x 2) and Lamdba 10–2 filter wheel controller and subsequently analyzed with HCImage software.

5.15. Cb5R3 silencing in CGN

For siRNA knockdown studies Accell™ siRNA delivery system was used (DharmaconTM). To knockdown C*b*5R3 we used the E-089102-00-0005 Accell Rat Cyb5r3 (25035) siRNA SMART pool and as control was used the D-001910-10-05 Accell Non-targeting pool. siRNAs were prepared following the instructions of the manufacturer. Briefly, 5x siRNA Buffer was diluted to 1x siRNA Buffer using sterile RNase-free water; a 100 µM siRNA solution was prepared in 1x siRNA buffer and up and down 3-5 times while avoiding introduction of bubbles; the solution was placed on an orbital mixer/shaker for 90 minutes at 37 °C and briefly centrifuged to collect solution from the bottom of the tube. In separate tubes the 100 µM siRNA was mixed with Accell Delivery Media 1:100 (delivery mix). CGN were prepared as previously described and at DIV 4 the growth medium was replaced by 500 µL of the appropriate delivery mix to each well (12 wells plate). Cells were incubated at 37 °C with 5% CO2 for 90 hours for Western blotting analysis, or by 72 hours for fluorescence microscopy measurements. Thereafter, cell lysates for Western Blotting or fluorescence microscopy measurements of ROS production with H_2DCF-DA were performed as described above.

5.16. Chemicals and reagents

H_2DCF-DA was purchased from Molecular Probes (Life Sciences Technologies, Carlsbad, CA, USA). DHE and DAF2-DA were obtained from the Spain office of Sigma (St. Louis, MO, USA). Cholera toxin B-Alexa 488 (cat. number C22841) and Mn (III) tetrakis (4-benzoic acid) porphyrin chloride (MnTBAP) were obtained from Invitrogen (Molecular Probes, Eugene, OR, USA). KB-7943 and ω-conotoxin MVIIC were purchased from Tocris Bioscience (Bristol, UK). MβCD, MK-801, nifedipine, nimodipine, and the specific protein kinase inhibitors H-89 (B1427), KN-93 (K1385), and calphostin C (C6303) were supplied by Sigma-Aldrich (Spain office). The ImmunoCruzTM IP/WB Optima B system (sc-45039) and KN-92 (sc-311369) were purchased from Santa Cruz Biotechnology (Santa Cruz, CA, USA). Fura2-AM from Invitrogen (Life Sciences Technologies) was supplied by Thermo Fisher Scientific (Spain office).

Primary antibodies: goat anti-H-Ras (sc-32026), rabbitanti-caveolin-1 (sc-894), mouse anti-nNOS (sc-5302), goat anti-CYP46 (sc-74391) rabbit anti-LTCC β1C subunit (sc-25686), rabbit anti-PKA (sc-28892), rabbit anti-CaMK-II (sc-9035) and goat anti-creatine kinase brain isoform CK-B (sc-15157), were supplied by Santa Cruz Biotechnology (Santa Cruz, CA, USA); rabbit anti-C*b*5R3 (ProteinTech 10894-1-AP); mouse anti-β-actin (A1978) and rabbit anti-β- actin (A5060) were supplied by Sigma-Aldrich (Spain office). Mouse anti-3-nitrotyrosine antibody (CC22.8C7.3) was supplied by Calbiochem-Merck KGaA. rabbit anti-p-β2 subunit of LTCCs (PCCb2-140AP) was supplied by FabGennix Inc. (Frisco, TX, USA) Fluorescent secondary antibodies: anti-rabbit IgG-Alexa488 (cat.number A11008) and anti-mouse IgG- Alexa488 (cat. number A11001) from Invitrogen (Molecular Probes, Eugene, OR, USA), and anti-goat IgG-Cy3 (cat. number C2821) from the Spain office of Sigma (St. Louis, MO, USA). All these antibodies were used in the dilution range recommended in their technical sheets. Anti-rabbit IgG-Horseradish peroxidase and anti-mouse IgG- Horseradish peroxidase were supplied by Sigma-Aldrich. Anti-goat IgG-Horseradish peroxidase was supplied by Pierce (Rockford, IL, USA). Bio-Rad Clarity Western ECL substrate was purchased to Bio-Rad (Spain office). Accell™ siRNA delivery system was supplied from Dharmacon (Lafayette, Colorado, USA), with the E-089102-00-0005 Accell Rat Cyb5r3 (25035) siRNA SMART pool to knockdown C*b*5R3, and the D-001910-10-05 Accell Non-targeting pool as control. Tetrodotoxin was obtained from Sankyo Co. (Tokyo, Japan).

All other reagents and chemicals used were of analytical grade from Sigma-Aldrich (Spain office) or Roche-Merck (Darmstadt, Germany).

5.17. Statistical analysis

Results are expressed as mean ± standard error (s.e.). Statistical analysis was carried out by Mann–Whitney non-parametric test. A significant difference was accepted at the $p < 0.05$ level. All the results were confirmed with at least triplicate measurements with different CGN preparations.

For more detailed explanations please consult the respective publication.

6. Conclusions

In summary, the main conclusions of this work are:

(1) Phosphorylation of the β2 subunit of LTCC by the CaMK-II and PKA associated with caveolin-1-rich lipid rafts plays a critical role to maintain LTCC activity in CGNs grown in culture.
(2) Cholesterol depletion of CGN by MβCD decreases the steady-state $[Ca^{2+}]_i$ down to the sustained proapoptotic low $[Ca^{2+}]_i$ range.
(3) Lipid rafts of the plasma membrane affords a major contribution to the overall ROS/RNS production by CGN in culture under partially depolarizing conditions that promote neuronal survival, and the lipid raft associated Cb_5R3 has an important modulatory role of this biological function.
(4) The levels of biomarkers of lipid rafts and of lipid rafts associated redox proteins nNOS and Cb_5R3 increases between 2 and 3-fold during CGN maturation *in vitro*.
(5) Lipid rafts of the plasma membrane also provides key structural elements to speed up ROS/RNS signaling propagation between neurons in mature CGN in culture.
(6) Concentrations of creatine that protect against rotenone-induced loss of cell viability of mature CGN *in vitro* attenuate rotenone-induced cytosolic calcium dysregulation, increase of ROS production and mitochondrial depolarization.
(7) Rotenone enhances the calcium entry through NMDA receptors and LTCC in CGN.
(8) Rotenone-induced alteration of CGN calcium homeostasis precedes mitochondrial depolarization and the generalized intracellular oxidative stress induced by this neurotoxin.

7. Conclusiones

(1) La fosforilación de la subunidad β2 de LTCC por CaMK-II y PKA asociadas a las balsas lipídicas ricas en caveolina-1 desempeña un papel crítico para mantener la actividad de los LTCC en cultivos de neuronas granulares del cerebelo.
(2) La depleción celular del colesterol por MβCD disminuye la concentración de estado estacionario del calcio citosólico de la neuronas granulares del cerebelo hasta concentraciones que promueven la muerte neuronal apoptótica.
(3) Los nanodominios asociados a los "rafts" o balsas lipídicas de la membrana plasmática tienen una contribución relevante en la producción de especies reactivas del oxígeno y del nitrógeno de las neuronas granules de cerebelo en cultivo bajo condiciones de despolarización parcial que promueven la supervivencia neuronal, y la Cb_5R3 asociada a estos nanodominios tiene un papel modulador de esta función biológica.
(4) Los niveles de biomarcadores de "rafts" lipídicos y de las proteínas redox nNOS y Cb_5R3 asociadas a estas balsas lipídicas se incrementan entre 2 y 3-veces durante la maduración de las neuronas granulares del cerebelo *in vitro*.
(5) Las balsas lipídicas de la membrana plasmática también proporcionan elementos estructurales clave para acelerar la propagación de la señalización de especies reactivas del oxígeno y del nitrógeno entre neuronas en cultivos maduros de neuronas granulares del cerebelo.
(6) Concentraciones de la creatina que protegen contra la disminución de viabilidad celular de las neuronas granulares del cerebelo inducida por la rotenona *in vitro* atenúan la desregulación del calcio citosólico, el aumento de la producción de especies reactivas del oxígeno y la despolarización mitocondrial inducidas por esta neurotoxina.
(7) La rotenona estimula la entrada de calcio a través de los receptores NMDA y de los LTCC en las neuronas granulares del cerebelo.
(8) La alteración inducida por rotenona de la homeostasis de calcio en neuronas granulares del cerebelo precede a la despolarización mitocondrial y al estrés oxidativo intracelular generalizado inducido por esta neurotoxina.

8. Publications

Journal of
Neurophysiology and Neurological Disorders

JScholar
Fostering Scholarly Communication

Research Open Access

Cholesterol-Rich Plasma Membrane Submicrodomains Can Be a Major Extramitochondrial Source of Reactive Oxygen Species in Partially Depolarized Mature Cerebellar Granule Neurons in Culture

Sofia Fortalezas[1], Joana Poejo[1], Alejandro K Samhan-Arias[2] and Carlos Gutierrez-Merino[1*]

[1]Department of Biochemistry and Molecular Biology, Faculty of Sciences, and Institute of Molecular Pathology Biomarkers, University of Extremadura, 06006- Badajoz, Spain
[2]Department of Biochemistry, Autonomous University of Madrid (UAM), and 'Alberto Sols' Biomedical Research Institute (CSIC-UAM), c / Arturo Duperier 4, 28029-Madrid, Spain

***Corresponding author:** Carlos Gutierrez-Merino, Dept. Biochemistry and Molecular Biology, Faculty of Sciences, and Institute on Molecular Pathology Biomarkers, University of Extremadura, 06006-Badajoz, Tel: 606953213, E-mail: carlosgm@unex.es

Received Date: October 24, 2019 **Accepted Date:** December 04, 2019 **Published Date:** December 06, 2019

Citation: Sofia Fortalezas (2019) Cholesterol-Rich Plasma Membrane Submicrodomains Can Be a Major Extramitochondrial Source of Reactive Oxygen Species in Partially Depolarized Mature Cerebellar Granule Neurons in Culture. J Neurophysiol Neurol Disord 5: 1-22.

Abstract

Excessive production of reactive oxygen and nitrogen species can elicit neuronal cell death and brain neurodegeneration. In previous studies, we have shown that lipid rafts nanodomains of mature cerebellar granule neurons (CGN) contain most of the neuronal nitric oxide synthase and also of cytochrome b_5 reductase isoform 3 (C*b*5R3), which is the component of neuronal synaptic plasma membrane vesicles that generates superoxide anion upon stimulation by cytochrome *c*. In this work, we show that CGN maturation in vitro elicits between two- and three-fold increase of the overall lipid rafts, and a similar increase of the expression of neuronal nitric oxide synthase and C*b*5R3. Only 5-15 min incubation of CGN with millimolar concentrations of methyl-β-cyclodextrin led to more than 90% attenuation of the kinetics of reactive oxygen species (ROS) production monitored by dihydro dichlorofluorescein diacetate (H_2DCF-DA), dihydroethidium (DHE) and 4,5-diaminofluorescein diacetate (DAF2-DA). In contrast, the results obtained using H_2DCF-DA and DHE pointed out that preincubation of CGN with 2,4-dinitrophenol or carbonyl cyanide-4- (trifluoromethoxy) phenylhydrazone (FCCP) only produced a decrease of 38±5% and 42±5% of the rate of ROS production, respectively. In addition, superoxide dismutase added to the extracellular medium of CGN also elicited more than 90% attenuation of the increase of DHE fluorescence that monitors superoxide anion production. CGN maturation leads to a large decrease of the production of ROS detected by H_2DCF-DA, and this attenuation of ROS production in mature CGN can be reverted by silencing the expression of C*b*5R3 to approximately 50%. The kinetics of ROS/reactive nitrogen species (RNS) production by CGN detected with DAF2-DA revealed the occurrence of a spreading ROS/RNS wave rapidly propagating along the neuronal plasma membrane. In conclusion, our results point out that redox systems associated with lipid rafts make a large contribution to total ROS/RNS production in mature CGN cultures under partially depolarizing conditions.

Keywords: Reactive oxygen and nitrogen species; neuronal lipid rafts; cerebellar granule neurons; methyl-β-cyclodextrin; cytochrome b_5 reductase; neuronal nitric oxide synthase.

International Journal of
Molecular Sciences

MDPI

Article

Methyl-β-Cyclodextrin Impairs the Phosphorylation of the β_2 Subunit of L-Type Calcium Channels and Cytosolic Calcium Homeostasis in Mature Cerebellar Granule Neurons

Sofia Fortalezas †, Dorinda Marques-da-Silva † and Carlos Gutierrez-Merino *

Department of Biochemistry and Molecular Biology of the Faculty of Sciences and Institute of Molecular Pathology Biomarkers, University of Extremadura, 06006-Badajoz, Spain; sofia_furta@hotmail.com (S.F.); dorindams@gmail.com (D.M.-d.-S.)

* Correspondence: carlosgm@unex.es

† These authors contributed equally to this paper.

Received: 25 September 2018; Accepted: 12 November 2018; Published: 20 November 2018

Abstract: The activation of L-type calcium channels (LTCCs) prevents cerebellar granule neurons (CGNs) from entering low-K^+-induced apoptosis. In previous works, we showed that LTCCs are largely associated with caveolin-1-rich lipid rafts in the CGN plasma membrane. In this work, we show that protein kinase A (PKA) and calmodulin-dependent protein kinase II (CaMK-II) are associated with caveolin-1-rich lipid rafts of mature CGNs, and we further show that treatment with the cholesterol-trapping and lipid raft-disrupting agent methyl-β-cyclodextrin decreases the phosphorylation level of the LTCC β_2 subunit and the steady-state calcium concentration in neuronal somas ($[Ca^{2+}]_i$) to values close to those measured in 5 mM KCl proapoptotic conditions. These effects correlate with the effects produced by a short (15 min) treatment of CGNs with H-89 and KN-93—inhibitors of PKA and CaMK-II, respectively—in 25 mM KCl medium. Moreover, only a 15 min incubation of CGNs with H-89 produces about a 90% inhibition of the calcium entry that would normally occur through LTCCs to increase $[Ca^{2+}]_i$ upon raising the extracellular K^+ from 5 to 25 mM, i.e., from proapoptotic to survival conditions. In conclusion, the results of this work suggest that caveolin-1-rich lipid rafts play a major role in the control of the PKA- and CaMK-II-induced phosphorylation level of the LTCC β_2 subunit, thus preventing CGNs from entering apoptosis.

Keywords: β_2 subunit of L-type calcium channels; cholesterol depletion; caveolin-1-rich lipid rafts; PKA; CaMK-II; cytosolic calcium homeostasis; cerebellar granule neurons

1. Introduction

Cyclodextrins are used as additives to improve the aqueous solubility of poorly soluble drugs and increase their bioavailability [1], and they are being increasingly used in nanoparticle-based drug delivery [2]. Cyclodextrins are also used as anti-browning agents in different foods and foodstuffs [3]. However, a link between cyclodextrins and iatrogenic hearing loss has been noted in several species, including humans [4]. In particular, methyl-β-cyclodextrin has been widely used for the selective removal of cholesterol and disruption of lipid rafts in different cell lines (see, e.g., [5,6]). The neurological risks of using methyl-β-cyclodextrin are informed by the reported toxicity of this compound to neuronal cell lines [7]. Thus, the molecular mechanism underlying selective neuronal cell death induced by methyl-β-cyclodextrin deserves to be studied.

L-type calcium channels (LTCCs) together with *N*-methyl D-aspartate receptors (NMDAr), plasma membrane Ca^{2+}-ATPase (PMCA), and sodium calcium exchangers are associated with the

Neurotoxicity Research (2018) 34:717–732
https://doi.org/10.1007/s12640-018-9940-0

ORIGINAL ARTICLE

Creatine Protects Against Cytosolic Calcium Dysregulation, Mitochondrial Depolarization and Increase of Reactive Oxygen Species Production in Rotenone-Induced Cell Death of Cerebellar Granule Neurons

Sofia Fortalezas[1] · Dorinda Marques-da-Silva[1] · Carlos Gutierrez-Merino[1]

Received: 15 December 2017 / Revised: 9 July 2018 / Accepted: 31 July 2018 / Published online: 9 August 2018

Abstract

Rotenone is a neurotoxin that is an active component of many pesticides which has been shown to induce Parkinsonism in animal models. We show that the cytotoxicity of exposure to nanomolar concentrations of rotenone in cultures of mature cerebellar granule neurons (CGN) in serum-free medium is not due to phagocytosis by glial contamination. A concentration as low as 5.65 ± 0.51 nM of rotenone was enough to trigger 50% cell death of mature CGN in culture after 12 h. The addition of serum proteins to the culture medium attenuated rotenone neurotoxicity, and this can account at least in part for the requirement of higher rotenone concentrations to elicit neuronal cytotoxicity reported in previous works. Creatine partial protection against CGN death promoted by 5 nM rotenone correlated with creatine protection against rotenone-induced mitochondrial depolarization and oxidative stress. Furthermore, creatine largely attenuated the early dysregulation of cytosolic Ca^{2+} concentration after acute rotenone treatment. Noteworthy, our results also revealed that the sustained alteration of Ca^{2+} homeostasis induced by rotenone takes place at the onset of the enhancement of intracellular oxidative stress and before mitochondrial depolarization, pointing out that cytosolic Ca^{2+} dysregulation is a very early event in the rotenone toxicity to CGN.

Keywords Creatine · Rotenone · Cerebellar granule neurons · Oxidative stress · Mitochondrial depolarization · Intracellular calcium homeostasis

Abbreviations

$[Ca^{2+}]_i$	intracellular calcium concentration
CGN	cerebellar granule neurons
CK	creatine kinase
CPA	cyclopiazonic acid
DCF	2′,7′-dichlorofluorescein
DIV	days in vitro
DMEM	Dulbecco's modified Eagle's medium
DMSO	dimethyl sulfoxide
FBS	fetal bovine serum
FCCP	carbonyl cyanide-4-(trifluoromethoxy) phenylhydrazone
Fura-2 AM	fura-2-acetoxymethyl ester
H2DCF-DA	2′,7′-dichlorodihydrofluorescein diacetate
LME	L-leucine methyl ester
LTCC	L-type calcium channel
MCB	Monochlorobimane
MTT	3-(4,5-dimethylthiazolyl-2)-2,5-diphenyltetrazolium bromide
NMDA	N-methyl-D-aspartate
PBS	phosphate-buffered saline
PBST	PBS supplemented with 0.05% polyoxyethylenesorbitanmonolaurate
PD	Parkinson's disease
PI	propidium iodide
ROS	Reactive oxygen species
SERCA	Ca^{2+}-ATPase of sarco-endoplasmic reticulum

Electronic supplementary material The online version of this article (https://doi.org/10.1007/s12640-018-9940-0) contains supplementary material, which is available to authorized users.

✉ Carlos Gutierrez-Merino
carlosgm@unex.es

[1] Department of Biochemistry and Molecular Biology, Faculty of Sciences, and Institute of Molecular Pathology Biomarkers, University of Extremadura, Avenida de Elvas s/n, 06006 Badajoz, Spain

Redox Biology 15 (2018) 109–114

Contents lists available at ScienceDirect

Redox Biology

journal homepage: www.elsevier.com/locate/redox

Short communication

Cytochrome b_5 reductase is the component from neuronal synaptic plasma membrane vesicles that generates superoxide anion upon stimulation by cytochrome *c*

Alejandro K. Samhan-Arias[a,*], Sofia Fortalezas[b], Cristina M. Cordas[a], Isabel Moura[a], José J.G. Moura[a], Carlos Gutierrez-Merino[b,*]

[a] UCIBIO, REQUIMTE, Departamento de Química, Faculdade de Ciências e Tecnologia, Universidade Nova de Lisboa, 2829-516 Caparica, Portugal
[b] Department of Biochemistry and Molecular Biology, Faculty of Sciences, and Institute of Molecular Pathology Biomarkers, University of Extremadura, 06006 Badajoz, Spain

ARTICLE INFO

Abbreviations:
Cb_5R, Cytochrome b_5 reductase
DTPA, Diethylenetriaminepentaacetic acid
DHE, Dihydroethidium
E^+, Ethidium
FAD, Flavin adenine dinucleotide
NADH, Reduced nicotinamide adenine dinucleotide
NBT, Nitroblue tetrazolium nitroblue tetrazolium
SPMV, Synaptic plasma membrane vesicles
TB, Terrific Broth terrific Broth
SOD, Superoxide dismutase
XA, Xanthine xanthine
XO, Xanthine oxidase

Keywords:
Cytochrome *c*
Superoxide anion
NADH oxidase
Cytochrome b_5 reductase
Neurons

ABSTRACT

In this work, we measured the effect of cytochrome *c* on the NADH-dependent superoxide anion production by synaptic plasma membrane vesicles from rat brain. In these membranes, the cytochrome *c* stimulated NADH-dependent superoxide anion production was inhibited by antibodies against cytochrome b_5 reductase linking the production to this enzyme. Measurement of the superoxide anion radical generated by purified recombinant soluble and membrane cytochrome b_5 reductase corroborates the production of the radical by different enzyme isoforms. In the presence of cytochrome *c*, a burst of superoxide anion as well as the reduction of cytochrome *c* by cytochrome b_5 reductase was measured. Complex formation between both proteins suggests that cytochrome b_5 reductase is one of the major partners of cytochrome *c* upon its release from mitochondria to the cytosol during apoptosis. Superoxide anion production and cytochrome *c* reduction are the consequences of the stimulated NADH consumption by cytochrome b_5 reductase upon complex formation with cytochrome *c* and suggest a major role of this enzyme as an anti-apoptotic protein during cell death.

1. Introduction

The plasma membrane NADH oxidase activity of cerebellar granule neurons represents a disguisable activity producing superoxide anion ($O_2^{\cdot-}$) as a collateral product of NADH consumption [1–4]. The plasma membrane constituents associated to this activity are not well defined although it is known that cytochrome b_5 reductase (Cb_5R) is one of its major components present at the plasma membrane of rat cerebellar granule neurons in culture and of synaptic plasma membrane vesicles (SPMV) from rat brain [1]. This protein increases its association to lipids rafts in apoptosis [2]. In addition, 1–3 h after apoptosis induction an increment of $O_2^{\cdot-}$ has been detected at the peripheral neuronal plasma membrane [2]. This event correlates with the observed times for cytochrome *c* (Cyt *c*) release from mitochondria to the cytosol, as soon as 1 h after apoptosis induction, although the maximum peak for its release was found at 3 h [2].

In this work, we described the function of Cyt *c* as activator of the $O_2^{\cdot-}$ production by Cb_5R, as a component of SPMV, and results were experimentally confirmed with two isoforms of human Cb_5R. Due to the important role of Cyt *c* redox state in apoptosis and its reduction by Cb_5R, we propose a function of Cb_5R, as one the main defensive components during apoptosis after Cyt *c* release from mitochondria to the cytosol.

* Corresponding authors.
E-mail addresses: alejandro.samhan@fct.unl.pt (A.K. Samhan-Arias), carlosgm@unex.es (C. Gutierrez-Merino).

https://doi.org/10.1016/j.redox.2017.11.021
Received 19 October 2017; Received in revised form 23 November 2017; Accepted 24 November 2017
Available online 27 November 2017

Molecular Science

AIMS Molecular Science, 3(1): 12-29.
DOI: 10.3934/molsci.2016.1.12
Received 6 December 2015,
Accepted 17 January 2016,
Published 21 January 2016

http://www.aimspress.com/journal/Molecular

Review

The critical role of lipid rafts nanodomains in the cross-talk between calcium and reactive oxygen and nitrogen species in cerebellar granule neurons apoptosis by extracellular potassium deprivation

Carlos Gutierrez-Merino*, Dorinda Marques-da-Silva, Sofia Fortalezas and Alejandro K. Samhan-Arias

Dept. Biochemistry and Molecular Biology, Faculty of Sciences, University of Extremadura, 06006-Badajoz, Spain

* **Correspondence:** Email: carlosgm@unex.es; Tel: 34 924 289419.

Abstract: The apoptosis of cerebellar granule neurons (CGN) induced by low-potassium in serum free medium *in vitro* has become a widely used model for neuronal apoptosis during *in vivo* brain development. In this review we shall summarize first the basic features of this model for neuronal apoptosis. Next, we shall focus on the L-type calcium channels (LTCC) inactivation as the primary pro-apoptotic signal in low K^+-induced CGN death. This apoptotic process can be split into two major and sequential cellular signaling phases: one reversible phase that offers a temporal window for therapeutic interventions to prevent neuronal death, and an irreversible later phase. Therefore, we shall comment next the critical role of reactive oxygen species (ROS) production and major ROS sources triggering the entry of CGN in the irreversible stages of low K^+-induced apoptosis. Then, we shall present the experimental evidences showing clustering of LTCC and ROS producing enzymes in plasma membrane lipid rafts of CGN matured *in vitro*, which have opened new perspectives for cell signaling in the early and reversible phase of this apoptosis. The role of lipid rafts nanodomains as fast response calcium/nitric oxide transducers of the switch of CGN to low K^+ medium will be discussed next. The two major conclusions drawn from this review are: (1) deregulation of the pool of cytochrome b_5 reductase associated to plasma membrane-lipid rafts, at least in part due to overexpression of cytochrome b_5, can account for the critical superoxide anion overshot which triggers the entry in the irreversible phase of low K^+ apoptosis of CGN, and (2) LTCC inactivation is rapidly transduced by lipid rafts nanodomains into a large drop of cytosolic calcium, a switch-off of nitric oxide production and subsequent inactivation of survival signaling pathways dependent on the activity of CaMKII, PKA and Akt/PKB kinases.

Book: Neurochimestry, IntechOpen; edited by Thomas Heinbockel.

ISBN: 978-953-51-123

Chapter 3

Cytosolic Calcium Homeostasis in Neurons — Control Systems, Modulation by Reactive Oxygen and Nitrogen Species, and Space and Time Fluctuations

Carlos Gutierrez-Merino, Dorinda Marques-da-Silva, Sofia Fortalezas and Alejandro K. Samhan-Arias

Additional information is available at the end of the chapter

http://dx.doi.org/10.5772/57576

1. Introduction

Cytosolic calcium plays a major and central role in neuronal activity and functions both in brain and in peripheral nervous systems, and its sustained alteration is a critical event that leads to neuronal death. On these grounds, it is not surprising that a sustained alteration of intracellular calcium homeostasis in neurons is a point of convergence of the cellular mechanisms underlying many neurodegenerative processes in the brain. Indeed, this has been shown to be the case for the brain's neurodegenerative diseases of higher incidence to humans, like Alzheimer's and Parkinson's, or in the acute neurodegeneration observed in amyotrophic lateral sclerosis, and also for major brain insults, such as excitotoxicity in trauma and ischemia-reperfusion, inflammation and neurotoxicity by drugs and environmental chemicals.

Sustained deregulation of cytosolic calcium concentration have been reported in neuronal apoptosis and necrosis, the two major cellular death pathways involved in brain neurodegeneration. It has been experimentally demonstrated and confirmed by many investigations using cell cultures that a sustained rise of cytosolic calcium concentration in the neuronal soma within the range 0.5-1 μM elicits a rapid necrotic neuronal death, mediated by calcium-dependent proteases activation, like calpains. On the other hand, long-term sustained cytosolic calcium concentrations below 60-70 nM in the neuronal soma promote the slow development of apoptotic neuronal death of neurons in culture [1,2]. Since the central role of calcium in neurotransmitter secretion and neuronal plasticity is also well known, the basal steady state cytosolic calcium concentration in the neuronal soma can be considered as a bioenergetics marker of neuronal activity and survival. We shall then present the major calcium transport

9. References

[1] Orrenius S, Zhivotovsky B and Nicotera P. Regulation of cell death: the calcium–apoptosis link. Nat. Rev. Mol. Cell Biol 2003;4: 552–565.
[2] Franklin JL, Johnson EMJr. Suppression of programmed neuronal death by sustained elevation of cytoplasmic calcium. Trends Neurosci 1992;15: 501-508.
[3] Franklin JL, Johnson EMJr. Block of neuronal apoptosis by a sustained increase of steady-state free Ca2+ concentration. Philos Trans R Soc Lond B Biol Sci 1994;345: 251-256.
[4] Berridge MJ. Neuronal calcium signaling. Neuron 1998;21: 13-26.
[5] Berridge MJ, Lipp P, Bootman MD. The versatility and universality of calcium signalling. Nat Rev Mol Cell Biol 2000;1: 11-21.
[6] Carafoli E, Santella L, Branca D, Brini M. Generation, control, and processing of cellular calcium signals. Crit Rev Biochem Mol Biol 2001;36: 107-260.
[7] Carafoli E. Calcium signaling: a tale for all seasons. Proc Natl Acad Sci USA 2002;99: 1115-1122.
[8] Gutierrez-Merino C, Marques-da-Silva D, Fortalezas S, Samhan-Arias AK. Cytosolic calcium homeostasis in neurons: Control systems, modulation by reactive oxygen and nitrogen species, and space and time fluctuations. In Heinbockel T (Ed), Neurochemistry (ISBN 980-953-307-1129-7), InTech, Rijeka (Croatia), 2014; Chapter 3: pp. 59-110.
[9] Baimbridge KG, Celio MR, Rogers JH. Calcium-binding proteins in the nervous system. Trends Neurosci 1992;15: 303-308.
[10] Tsien RW, Lipscombe D, Madison DV, Bley KR, Fox AP. Multiple types of neuronal calcium channels and their selective modulation. Trends Neurosci 1988;11: 431-438.
[11] Forti L, Tottene A, Moretti A, Pietrobon D. Three novel types of voltage-dependent calcium channels in rat cerebellar neurons. J Neurosci 1994;14: 5243-5256.
[12] Olivera BM, Miljanich GP, Ramachandran J, Adams ME. Calcium channel diversity and neurotransmitter release: the omega-conotoxins and omega-agatoxins. Annu Rev Biochem 1994;63: 823-867.
[13] Catterall WA. Structure and function of voltage-gated ion channels. Annu Rev Biochem 1995;64: 493-531.
[14] Hammond C., editor. Cellular and Molecular Neurobiology. San Diego: Academic Press; 1996.
[15] Tottene A, Moretti A, Pietrobon D. Functional diversity of P-type and R-type calcium channels in rat cerebellar neurons. J Neurosci 1996;16: 6353-6363.
[16] Schild D, Geiling H, Bischofberger J. Imaging of L-type Ca2+ channels in olfactory bulb neurones using fluorescent dihydropyridine and a styryl dye. J Neurosci Methods 1995;59: 183-190.
[17] Ertel EA, Campbell KP, Harpold MM, Hofmann F, Mori Y, Perez-Reyes E, Schwartz A, Snutch TP, Tanabe T, Birnbaumer L, Tsien RW, Catterall WA. Nomenclature of voltage-gated calcium channels. Neuron 2000;25: 533–535.
[18] Catterall WA. Structure and regulation of voltage-gated Ca2+ Channels. Annu Rev Cell Dev Biol 2000;16: 521–555.
[19] Clark NC, Nagano N, Kuenzi FM, Jarolimek W, Huber I, Walter D, Wietzorrek G, Boyce S, Kullmann DM, Striessnig J, Seabrook GR. Neurological phenotypeand

synaptic function in mice lacking the CaV1.3 alpha subunit of neuronal L-type voltage-dependent Ca2+ channels. Neuroscience 2003;120: 435 – 442.
[20] Kamp TJ, Hell JW. Regulation of Cardiac L-Type Calcium Channels by Protein Kinase A and Protein Kinase C. Circ Res 2000;87: 1095-1102.
[21] Davare MA, Dong F, Rubin CS, Hell JW. The A-kinase anchor protein MAP2B and cAMP-dependent protein kinase are associated with class C L-type calcium channels in neurons. J Biol Chem 1999;274: 30280–30287.
[22] De Jongh KS, Murphy BJ, Colvin AA, Hell JW, Takahashi M, Catterall WA. Specific phosphorylation of a site in the full-length form of the alpha 1 subunit of the cardiac L-type calcium channel by adenosine 3',5'-cyclic monophosphate-dependent protein kinase. Biochemistry 1996;35: 10392–10340.
[23] Mitterdorfer J, Froschmayr M, Grabner M, Moebius FF, Glossmann H, Striessnig J. Identification of PK-A phosphorylation sites in the carboxyl terminus of L-type calcium channel alpha 1 subunits. Biochemistry 1996;35: 9400–9406.
[24] Gao T, Yatani A, Dell'Acqua ML, Sako H, Green SA, Dascal N, Scott JD, Hosey MM. cAMP-dependent regulation of cardiac L-type Ca2+ channels requires membrane targeting of PKA and phosphorylation of channel subunits. Neuron 1997;19: 185–196.
[25] Puri TS, Gerhardstein BL, Zhao XL, Ladner MB, Hosey MM. Differential effects of subunit interactions on protein kinase A- and C-mediated phosphorylation of L-type calcium channels. Biochemistry 1997;36: 9605–9615.
[26] Bünemann M, Gerhardstein BL, Gao T, Hosey MM. Functional Regulation of L-type Calcium Channels via Protein Kinase A-mediated Phosphorylation of the β2 Subunit. J Biol Chem 1999;274: 33851–33854.
[27] Grueter CE, Abiria SA, Dzhura I, Wu Y, Ham AJL, Mohler PJ, Anderson ME, Colbran RJ. L-Type Ca2+ Channel Facilitation Mediated by Phosphorylation of the β Subunit by CaMKII. Mol Cell 2006;23: 641–650.
[28] Pinard CR, Mascagni F, βonald AJ. Neuronal localization of Cav1.2 L-type calcium channels in the rat basolateral amygdala. Brain Res 2005;1064: 52 – 55.
[29] Hudmon A, Schulman H, Kim J, Maltez JM, Tsien RW, Pitt GS. CaMKII tethers to L-type Ca2+ channels, establishing a local and dedicated integrator of Ca2+ signals for facilitation. J Cell Biol 2005;171: 537–547.
[30] Lee TS, Karl R, Moosmang S, Lenhardt P, Klugbauer N, Hofmann F, Kleppisch T, Welling A. Calmodulin kinase II is involved in voltage-dependent facilitation of the L-type Cav1.2 calcium channel: Identification of the phosphorylation sites. J Biol Chem 2006;281: 25560–25567.
[31] Grueter CE, Abiria SA, Wu Y, Anderson ME, Colbran RJ. Differential regulated interactions of calcium/calmodulin-dependent protein kinase II with isoforms of voltage-gated calcium channel beta subunits. Biochemistry 2008;47: 1760-1767.
[32] O-Uchi J, Komukai K, Kusakari Y, Obata T, Hongo K, Sasaki H, Kurihara S. Alpha1-adrenoceptor stimulation potentiates L-type Ca2+ current through Ca2+/calmodulin-dependent PK II (CaMKII) activation in rat ventricular myocytes. Proc Natl Acad Sci USA 2005;102: 9400–9405.
[33] Gao L, Blair LA, Salinas GD, Needleman LA, Marshall J. Insulin-like growth factor-1 modulation of CaV1.3 calcium channels depends on Ca2+ release from IP3-sensitive stores and calcium/calmodulin kinase II phosphorylation of the alpha1 subunit EF hand. J Neurosci 2006;26: 6259–6268.

[34] Brown AM, Deutch AY, Colbran RJ. Dopamine depletion alters phosphorylation of striatal proteins in a model of Parkinsonism. Eur J Neurosci 2005;22: 247–256.
[35] Robertson SJ, Ennion SJ, Evans RJ, Edwards FA. Synaptic P2X receptors. Curr Opin Neurobiol 2001;11: 378-386.
[36] Dingledine R., McBain C.J. Glutamate and aspartate. In: Siegel G.J., Agranoff B.W., Albers R.W., Fisher S.K., Uhler M.D. (eds.). Basic Neurochemistry. Molecular, Cellular and Medical Aspects (6th ed.). Philadelphia: Lippincott Williams & Wilkins; 1998. p. 315-333.
[37] Contestabile A. Roles of NMDA receptor activity and nitric oxide production in brain development. Brain Res Brain Res Rev 2000;32: 476-509.
[38] Choi DW, Rothman SM. The role of glutamate neurotoxicity in hypoxic-ischemic neuronal death. Annu Rev Neurosci 1990;13: 171-182.
[39] Choi DW. Glutamate neurotoxicity and diseases of the nervous system. Neuron 1998;1: 623–634.
[40] Mothet JP, Parent AT, Wolosker H, Brady ROJr, Linden DJ, Ferris CD, Rogawski MA, Snyder SH. D-serine is an endogenous ligand for the glycine site of the N-methyl-D-aspartate receptor. Proc Natl Acad Sci USA 2000;97: 4926-4931.
[41] Derkach V, Barria A, Soderling TR. Ca2+/calmodulin-kinase II enhances channel conductance of alpha-amino-3-hydroxy-5-methyl-4-isoxazolepropionate type glutamate receptors. Proc Natl Acad Sci USA 1999;96: 3269–3274.
[42] Hayashi Y, Shi SH, Esteban JA, Piccini A, Poncer JC, Malinow R. Driving AMPA receptors into synapses by LTP and CaMKII: requirement for GluR1 and PDZ domain interaction.Science 2000;287: 2262–2267.
[43] Boehm J, Kang MG, Johnson RC, Esteban J, Huganir RL, Malinow R. Synaptic incorporation of AMPA receptors during LTP is controlled by a PKC phosphorylation site on GluR1. Neuron 2006;51: 213–225.
[44] Kohr G, Eckardt S, Luddens H, Monyer H, Seeburg PH. NMDA receptor channels: subunit-specific potentiation by reducing agents. Neuron 1994;12: 1031-1040.
[45] Rumbaugh G, Vicini S. Distinct synaptic and extrasynaptic NMDA receptors in developing cerebellar granule neurons. J Neurosci 1999;19: 10603-10610.
[46] Petralia RS, Wang YX, Hua F, Yi Z, Zhou A, Ge L, Stephenson FA, Wenthold RJ. Organization of NMDA receptors at extrasynaptic locations. Neuroscience 2010;167: 68-87.
[47] Li ST, Ju JG. Functional roles of synaptic and extrasynaptic NMDA receptors in physiological and pathological neuronal activities. Curr Drug Targets 2012;13: 207-221.
[48] Leonard AS, Hell JW. Cyclic AMP-dependent Protein Kinase and Protein Kinase C Phosphorylate N-Methyl-D-aspartate Receptors at Different Sites. J Biol Chem 1997;272: 12107–12115.
[49] Tingley WG, Ehlers MD, Kameyama K, Doherty C, Ptak JB, Riley CT, Huganir RL. Characterization of Protein Kinase A and Protein Kinase C Phosphorylation of the N-Methyl-D-aspartate Receptor NR1 Subunit Using Phosphorylation Site-specific Antibodies. J Biol Chem 1997;272: 5157–5166.
[50] Fill M, Copello JA. Ryanodine receptor calcium release channels. Physiol Rev 2002;82: 893-922.
[51] Hamilton SL. Ryanodine receptors. Cell Calcium 2005;38: 253-260.

[52] Mikoshiba K. Inositol 1,4,5-trisphosphate IP(3) receptors and their role in neuronal cell function. J Neurochem 2006;97: 1627-1633.
[53] Hidalgo C. Cross talk between Ca2+ and redox signalling cascades in muscle and neurons through the combined activation of ryanodine receptors/Ca2+ release channels. Philos Trans R Soc Lond B Biol Sci 2005;360: 2237-2246.
[54] Paschen W, Frandsen A. Endoplasmic reticulum dysfunction--a common denominator for cell injury in acute and degenerative diseases of the brain? J Neurochem 2001;79: 719-725.
[55] Montero M, Alvarez J, Garcia-Sancho J. Agonist-induced Ca2+ influx in human neutrophils is secondary to the emptying of intracellular calcium stores. Biochem J 1991;277: 73-79.
[56] Parekh AB, Putney JWJr. Store-operated calcium channels. Physiol Rev 2005;85: 757-810.
[57] Arakawa N, Sakaue M, Yokoyama I, Hashimoto H, Koyama Y, Baba A, Matsuda T. KB-R7943 inhibits store-operated Ca(2+) entry in cultured neurons and astrocytes. Biochem Biophys Res Commun 2000;279: 354-357.
[58] Jia Y, Zhou J, Tai Y, Wang Y. TRPC channels promote cerebellar granule neuron survival. Nat Neurosci 2007 ;10 : 559-567.
[59] Selvaraj S, Sun Y, Watt JA, Wang S, Lei S, Birnbaumer L, Singh BB. Neurotoxin-induced ER stress in mouse dopaminergic neurons involves downregulation of TRPC1 and inhibition of AKT/mTOR signaling. J Clin Invest 2012;122: 1354-1367.
[60] Smaili SS, Hsu YT, Youle RJ, Russell JT. Mitochondria in Ca2+ signaling and apoptosis. J Bioenerg Biomembr 2000;32: 35-46.
[61] Simpson PB. The local control of cytosolic Ca2+ as a propagator of CNS communication--integration of mitochondrial transport mechanisms and cellular responses. J Bioenerg Biomembr 2000;32: 5-13.
[62] Crompton M. The mitochondrial permeability transition pore and its role in cell death. Biochem J. 1999;341: 233-249.
[63] Garcia-Martin E, Gutierrez-Merino C. Rate of Na+/Ca2+ exchange across the plasma membrane of synaptosomes measured using the fluorescence of chlorotetracycline. Implications to calcium homeostasis in synaptic terminals. Biochim Biophys Acta 1996;1280: 257-264.
[64] Garcia ML, Strehler EE. Plasma membrane calcium ATPases as critical regulators of calcium homeostasis during neuronal cell function. Front Biosci 1999;4: D869–D882.
[65] Gill DL, Chueh SH, Whitlow LC. Functional importance of the synaptic plasma membrane calcium pump and sodium-calcium exchanger. J Biol Chem 1984;259: 10807-10813.
[66] Guerini D, García-Martín E, Gerber A, Volbracht C, Leist M, Gutierrez-Merino C, Carafoli E. The expression of plasma membrane Ca2+ pump isoforms in cerebellar granule neurons is modulated by cytosolic free Ca2+. J Biol Chem 1999;274: 1667-1676.
[67] Kip SN, Gray NW, Burette A, Canbay A, Weinberg RJ, Strehler EE. Changes in the expression of plasma membrane calcium extrusion systems during the maturation of hippocampal neurons. Hippocampus 2006;16: 20-34.

[68] Hilfiker H, Guerini D, Carafoli E. Cloning and expression of isoform 2 of the human plasma membrane Ca2+ ATPase. Functional properties of the enzyme and its splicing products. J Biol Chem 1994;269: 26178-26183.
[69] Condrescu M, Reeves JP. Actin-dependent regulation of the cardiac Na+/Ca2+ exchanger. Am J Physiol Cell Physiol 2006;290: C691-C701.
[70] O´ Connell KMM, Martens JR, Tamkun MM. Localization of ion channels to lipid raft domains within the cardiovascular system. Trends Cardiovasc Med 2004;14: 37–42.
[71] Gunter TE, Yule DI, Gunter KK, Eliseev RA, Salter JD. Calcium and mitochondria. FEBS Lett 2004;567: 96-102.
[72] Pike LJ. Rafts defined: a report on the keystone symposium on lipid rafts and cell function. J Lipid Res 2006;47: 1597–1598.
[73] Anderson RG. The caveolae membrane system. Annu Rev Biochem 1998;67: 199–225.
[74] Parton RG and Collins BM. Unraveling the architecture of caveolae. PNAS 2016;113: 14170-14172;
[75] Razani B, Woodman SE, Lisanti MP. Caveolae: From Cell Biology to Animal Physiology. Pharmacological Reviews 2002;54: 431-467.
[76] Anderson RG, Jacobson K. A role for lipid shells in targeting proteins to caveolae, rafts, and other lipid domains. Science 2002;296: 1821–1825.
[77] Pike LJ. Growth factor receptors, lipid rafts and caveolae: an evolving story. Biochim. Biophys. Acta 2005;1746: 260–273.
[78] Simons K, Ikonen E. Functional rafts in cell membranes. Nature 1997;387: 569–572.
[79] Thomas CM, E.J. Smart EJ. Caveolae structure and function, J. Cell Mol. Med. 2008;12: 796–809.
[80] Simons K, Toomre D. Lipid rafts and signal transduction. Nat. Rev. Mol. Cell Biol. 2000;1: 31–39.
[81] Patel HH, Murray F, Insel PA. Caveolae as organizers of pharmacologically relevant signal transduction molecules. Annu. Rev. Pharmacol. Toxicol. 2008;48: 359–391.
[82] Brown DA, London E. Functions of lipid rafts in biological membranes. Annu. Rev. Cell Dev. Biol. 1998; 14: 111–136.
[83] Gabella G. Caveolae intracellulares and sarcoplasmic reticulum in smooth muscle. J Cell Sci 1971;8: 601–609.
[84] Popescu LM, Diculescu I, Zelck U, Ionescu N. Ultrastructural distribution of calcium in smooth muscle cells of guinea-pig taenia coli. A correlated electron microscopic and quantitative study. Cell Tissue Res 1974;154: 357–378.
[85] Brazer SC, Singh BB, Liu X, Swaim W, Ambudkar IS. Caveolin-1 contributes to assembly of store-operated Ca2+ influx channels by regulating plasma membrane localization of TRPC1. J Biol Chem 2003;278: 27208–27215.
[86] Murata T, Lin MI, Stan RV, Bauer PM, Yu J, Sessa WC. Genetic evidence supporting caveolae microdomain regulation of calcium entry in endothelial cells. J Biol Chem 2007;282: 16631–16643.
[87] Head BP, Insel PA. Do caveolins regulate cells by actions outside of caveolae? Trends Cell Biol 2007;17: 51–57.
[88] Palade, G. Fine structure of blood capillaries. J. Appl. Phys. 1953;24: 1424.
[89] Patrick Lajoie P, Nabi IR. Lipid Rafts, Caveolae, and Their Endocytosis. Int Rev Cel Mol Bio. 2010;282: 135-167

[90] Duchen MR, Verkhratsky A, Muallem S. Mitochondria and calcium in health and disease, Cell Calcium. 2008;44: 1–5

[91] Rothberg, KG, Heuser, JE, Donzell, WC, Ying, YS, Glenney, JR, Anderson, RG. Caveolin, a protein component of caveolae membrane coats. Cell 1992;68: 673–682.

[92] Balijepalli RC, Foell JD, Hall DD, Hell JW, Kamp TJ. Localization of cardiac L-type Ca2+ channels to a caveolar macromolecular signaling complex is required for b2-adrenergic regulation. Proc Natl Acad Sci USA 2006;103: 7500–7505.

[93] Marques-da-Silva D, Samhan-Arias AK, Tiago T, Gutierrez-Merino C. L-type calcium channels and cytochrome b5 reductase are components of protein complexes tightly associated with lipid rafts microdomains of the neuronal plasma membrane. J Proteomics 2010;73: 1502-1510.

[94] Razani B, Rubin CS, Lisanti MP. Regulation of cAMP-mediated Signal Transduction via Interaction of Caveolins with the Catalytic Subunit of Protein Kinase A. J Biol Chem 1999;274: 26353–26360.

[95] Suzuki T, Du F, Tian Q-B, Zhang J, Endo S. Ca2+/calmodulin-dependent protein kinase IIα clusters are associated with stable lipid rafts and their formation traps PSD-95. J Neurochem 2008;104: 596–610.

[96] Tsujikawa H, Song Y, Watanabe M, Masumiya H, Gupte SA, Ochi R, Okada T. Cholesterol depletion modulates basal L-type Ca2+ current and abolishes its β-adrenergic enhancement in ventricular myocytes. Am J Physiol Heart Circ Physiol 2008;294: H285–H292.

[97] Prybylowski K, Chang K, Sans N, Kan L, Vicini S, Wenthold RJ. The synaptic localization of NR2B-containing NMDA receptors is controlled by interactions with PDZ proteins and AP-2. Neuron 2005;47: 845-857.

[98] Weick JP, Groth RD, Isaksen AL, Mermelstein PG. Interactions with PDZ proteins are required for L-type calcium channels to activate cAMP response element-binding protein-dependent gene expression. J Neurosci 2003;23: 3446–3456.

[99] Zhang H, Maximov A, Fu Y, Xu F, Tang TS, Tkatch T, Surmeier DJ, Bezprozvanny I. Association of CaV1.3 L-type calcium channels with Shank. J Neurosci 2005;25: 1037-1049.

[100] Hering H, Lin C-C, Sheng M. Lipid Rafts in the Maintenance of Synapses, Dendritic Spines, and Surface AMPA Receptor Stability. J Neurosci 2003;23: 3262–3271.

[101] Besshoh S, Chen S, Brown IR, Gurd JW. Developmental Changes in the Association of NMDA Receptors With Lipid Rafts. J Neurosci Res 2007;85: 1876–1883.

[102] Delínte-Ramirez I, Salcedo-Tello P, Bermudez-Rattoni F. Spatial memory formation induces recruitment of NMDA receptor and PSD-95 to synaptic lípid rafts. J Neurochem 2008;106: 1658–1668.

[103] Marques-da-Silva D, Gutierrez-Merino C. L-type voltage-operated calcium channels, N-methyl-D-aspartate receptors and neuronal nitric-oxide synthase form a calcium/redox nano-transducer within lipid rafts. Biochem Biophys Res Commun 2012;420: 257-262.

[104] Hou Q, Huang Y, Amato S, Snyder SH, Huganir RL, Man HY. Regulation of AMPA receptor localization in lipid rafts. Mol Cell Neurosci 2008;38: 213-223.

[105] Keith DJ, Sanderson JL, Gibson ES, Woolfrey KM, Robertson HR, Olszewski K, Kang R, El-Husseini A , Dell'acqua ML. Palmitoylation of A-kinase anchoring protein

79/150 regulates dendritic endosomal targeting and synaptic plasticity mechanisms. J Neurosci 2012;32: 7119-7136.
[106] Sepúlveda MR, Berrocal-Carrillo M, Gasset M, Mata AM. The plasma membrane Ca2+-ATPase isoform 4 is localized in lipid rafts of cerebellum synaptic plasma membranes. J Biol Chem 2006;281: 447-453.
[107] Jiang L, Fernandes D, Mehta N, Bean JL, Michaelis ML, Zaidi A. Partitioning of the plasma membrane Ca2+-ATPase into lipid rafts in primary neurons: effects of cholesterol depletion. J Neurochem 2007;102: 378–388.
[108] Kuszczak I, Samson SE, Pande J, Shen DQ, Grover AK. Sodium–calcium exchanger and lipid rafts in pig coronary artery smooth muscle. Biochim Biophys Acta 2011;1808: 589–596.
[109] Teubl M, Groschner K, Kohlwein SD, Mayer B, Schmidt K. Na+/Ca2+ exchange facilitates Ca2+-dependent activation of endothelial nitric-oxide synthase. J Biol Chem 1999;274: 29529-29535.
[110] Bossuyt J, Taylor BE, James-Kracke M, Hale CC. Evidence for cardiac sodium-calcium exchanger association with caveolin-3. FEBS Lett 2002;511: 113-117.
[111] Sato Y, Sagami I, Shimizu T. Identification of Caveolin-1-interacting Sites in Neuronal Nitric-oxide Synthase. J Biol Chem 2004;279: 8827–8836.
[112] Venema VJ, Ju H, Zou R, Venema RC. Interaction of neuronal nitric-oxide synthase with caveolin-3 in skeletal muscle. Identification of a novel caveolin scaffolding/inhibitory domain. J Biol Chem 1997;272: 28187–28190.
[113] Martin-Romero FJ, Garcia-Martin E, Gutierrez-Merino C. Inhibition of the oxidative stress produced by plasma membrane NADH oxidase delays low-potassium induced apoptosis of cerebellar granule cells. J Neurochem 2002;82: 705–715.
[114] Samhan-Arias AK, Martin-Romero FJ, Gutierrez-Merino C. Kaempferol blocks oxidative stress in cerebellar granule cells and reveals a key role for the plasma membrane NADH oxidase activity in the commitment of apoptosis. Free Radic Biol Med 2004;37: 48-61.
[115] Samhan-Arias AK, Garcia-Bereguiain MA, Martin-Romero FJ, Gutierrez-Merino C. Clustering of plasma membrane-bound cytochrome b5 reductase within 'lipid rafts' microdomains of the neuronal plasma membrane. Mol Cell Neurosci 2009;40: 14–26.
[116] Samhan-Arias AK, Marques-da-Silva D, Yanamala N, Gutierrez-Merino C. Stimulation and clustering of cytochrome b(5) reductase in caveolin-rich lipid microdomains is an early event in oxidative stress-mediated apoptosis of cerebellar granule neurons. J Proteomics 2012;75: 2934-2949.
[117] Sakai J, Li J, Subramanian KK, Mondal S, Bajrami B, Hattori H, Jia Y, Dickinson BC, Zhong J, Ye K, Chang CJ, Ho Y, Zhou J, and Luo HR. Reactive oxygen species (ROS)-induced actin glutathionylation controls actin dynamics in neutrophils. Immunity 2012; 37: 1037–1049.
[118] Brenman JE, Bredt DS. Synaptic signalling by nitric-oxide. Curr Opin Neurobiol 1997;7: 374–378.
[119] Bonfoco E, Leist M, Zhivotovsky B, Orrenius S, Lipton SA, Nicotera P. Cytoskeletal breakdown and apoptosis elicited by NO donors in cerebellar granule cells require NMDA receptor activation. J Neurochem 1996;67: 2484–2493.
[120] Leach RN, Desai JC, Orchard CH. Effect of cytoskeleton disruptors on L-type Ca channel distribution in rat ventricular myocytes. Cell Calcium 2005;38: 515-526.

[121] Gutierrez-Merino C. Redox modulation of neuronal calcium homeostasis and its deregulation by reactive oxygen species. In: Gutierrez-Merino C., Leeuwenburgh C. (eds.) Free Radicals in Biology and Medicine. Kerala: Research Signpost; 2008. pp. 67-101.
[122] Hidalgo C, Donoso P. Crosstalk between calcium and redox signalling: from molecular mechanisms to health implications. Antioxid Redox Signal 2008;10: 1275-1312.
[123] Sies H. Oxidative stress: oxidants and antioxidants. Exp Physiol. 1997;82: 291-295.
[124] Beal MF. Energetics in the pathogenesis of neurodegenerative diseases. Trends Neurosci. 2000;23: 298–304.
[125] Atlante A, Calissano P, Bobba A, Giannattasio S, Marra E, Passarella S. Glutamate neurotoxicity, oxidative stress and mitochondria. FEBS Lett. 2001;497: 1-5.
[126] Andrus PK, Fleck TJ, Gurney ME, Hall ED. Protein oxidative damage in a transgenic mouse model of familial amyotrophic lateral sclerosis. J. Neurochem. 1998;71: 2041-2048.
[127] Cicchetti F, Drouin-Ouellett J, Gross RE. Environmental toxins and Parkinson's disease: what have we learned from pesticide-induced animal models? Trends Pharmacol Sci. 2009;30: 475-483.
[128] Sugimoto K, Iadecola C. Delayed effect of administration of COX-2 inhibitor in mice with acute cerebral ischemia. Brain Res. 2003;960: 273-276.
[129] Gutierrez-Merino C, López-Sánchez C, Lagoa R, Samhan-Arias AK, Bueno C, García-Martínez V. Neuroprotective actions of flavonoids. Curr Med Chem. 2011;18: 1195-1212.
[130] Iadecola C. Bright and dark sides of nitric oxide in ischemic brain injury. Trends Neurosci. 1997;20: 132-139.
[131] Beal MF. Oxidatively modified proteins in aging and disease. Free Radic Biol Med 2002;32: 797-803.
[132] Praticò D, Delanty N. Oxidative injury in diseases of the central nervous system: Focus on Alzheimer's disease. Am. J. Med. 2000;109: 577-585.
[133] Blesa J, Trigo-Damas I, Quiroga-Varela A, Jackson-Lewis VR (2015) Oxidative stress and Parkinson's disease. Front Neuroanat 2015; 9:91
[134] Butterfield DA, Halliwell B. Oxidative stress, dysfunctional glucose metabolism and Alzheimer disease. Nat Rev Neurosci 2019;20: 148-160.
[135] Mao GD, Poznansky MJ. Electron spin resonance study on the permeability of superoxide radicals in lipid bilayers and biological membranes. FEBS Lett 1992;305: 233-236.
[136] Martin-Romero FJ, Gutierrez-Martin Y, Henao F, Gutierrez-Merino C. The NADH oxidase activity of the plasma membrane of synaptosomes is a major source of superoxide anion and is inhibited by peroxynitrite. J Neurochem 2002;82: 604–614.
[137] Samhan-Arias AK, Duarte RO, Martin-Romero FJ, Moura JJG, Gutierrez-Merino C. Reduction of ascorbate free radical by the plasma membrane of synaptic terminals from rat brain. Arch Biochem Biophys 2008;469: 243–254.
[138] Herrero A, Barja G. Localization of the site of oxygen radical generation inside the complex I of heart and nonsynaptic brain mammalian mitochondria. J Bioenerg Biomembr 2000;32: 609-615.

[139] Zimmerman BJ, Granger DN. Mechanisms of reperfusion injury. Am J Med Sci 1994;307: 284-292.
[140] Szabo C, Ischiropoulos H, Radi R. Peroxynitrite: biochemistry, pathophysiology and development of therapeutics. Nat Rev Drug Discov 2007;6: 662-680.
[141] van der Veen RC, Hinton DR, Incardonna F, Hofman FM. Extensive peroxynitrite activity during progressive stages of central nervous system inflammation. J Neuroimmunol 1997;77: 1-7.
[142] Liu D, Ling X, Wen J, Liu J. The role of reactive nitrogen species in secondary spinal cord injury: formation of nitric oxide, peroxynitrite, and nitrated protein. J Neurochem 2000;75: 2144-2154.
[143] Bolaños JP, Almeida A, Stewart V, Peuchen S, Land JM, Clark JB, Heales SJ. Nitric oxide-mediated mitochondrial damage in the brain: mechanisms and implications for neurodegenerative diseases. J Neurochem 1997;68: 2227-2240.
[144] Martin-Romero FJ, Garcia-Martin E, Gutierrez-Merino C. Involvement of free radicals in signalling of low-potassium induced apoptosis in cultured cerebellar granule cells. Int J Dev Biol 1996; Suppl.1: 197S-198S.
[145] Valencia A, Morán J. Role of oxidative stress in the apoptotic cell death of cultured cerebellar granule cells. J Neurosci Res 2001;64: 284–297.
[146] Bedard K, Krause KH. The NOX family of ROS-generating NADPH oxidases: physiology and pathophysiology. Physiol. Rev. 2007;87: 245-313.
[147] Samhan-Arias AK, López-Sánchez C, Marques-da-Silva D, Lagoa R, Garcia-Lopez V, García-Martínez V, Gutierrez-Merino C. High expression of cytochrome b5 reductase isoform 3/cytochrome b5 system in the cerebellum and pyramidal neurons of adult rat brain. Brain Struct. Funct. 2016;221: 2147-2162.
[148] Percy MJ, Lappin TR. Recessive congenital methaemoglobinaemia: cytochrome b5 reductase deficiency. Br J Haematol. 2008;141: 298-308.
[149] Ewenczyk C, Leroux A, Roubergue A, Laugel V, Afenjar A, Saudubray JM, Beauvais P, Billette de Villemeur T, Vidailhet M, Roze E. Recessive hereditary methaemoglobinaemia, type II: delineation of the clinical spectrum. Brain 2008;131 :760-761.
[150] Aalfs CM, Salieb-Beugelaar GB, Wanders RJA, Mannens MMAM, Wijburg FA. A case of methemoglobinemia type II due to NADH-cytochrome b5 reductase deficiency: determination of the molecular basis. Hum. Mutat. 2000;16: 18-22.
[151] Marques-da-Silva D, Gutierrez-Merino C. Caveolin-rich lipid rafts of the plasma membrane of mature cerebellar granule neurons are microcompartments for calcium/reactive oxygen and nitrogen species cross-talk signaling. Cell Calcium 2014;56: 108-123.
[152] Testa CM, Sherer TB, Greenamyre JT. Rotenone induces oxidative stress and dopaminergic neuron damage in organotypic substantia nigra cultures. Mol Brain Res 2005;134: 109–118.
[153] Alam M, Schmidt WJ. Rotenone destroys dopaminergic neurons and induces parkinsonian symptoms in rats. Behav Brain Res 2002;136: 317–324
[154] Betarbet R, Sherer TB, MacKenzie G, Garcia-Osuna M, Panov AV, Greenamyre JT. Chronic systemic pesticide exposure reproduces features of Parkinson's disease. Nat Neurosci 2000;3: 1301–1306.
[155] Barrientos A, Moraes CT. Titrating the effects of mitochondrial complex I impairment in the cell physiology. J Biol Chem 1999;274: 16188–16197

[156] Li N, Ragheb K, Lawler G, Sturgis J, Rajwa B, Melendez JA, Robinson JP. Mitochondrial complex I inhibitor rotenone induces apoptosis through enhancing mitochondrial reactive oxygen species production. J Biol Chem 2003;278: 8516–8525.
[157] Sherer TB, Betarbet R, Testa CM, Seo BB, Richardson JR, Kim JH, Miller GW, Yagi T, Matsuno-Yagi A, Greenamyre JT. Mechanism of toxicity in rotenone models of Parkinson's disease. J Neurosci 2003;23: 10756–10764
[158] Xiong N, Long X, Xiong J, Jia M, Chen C, Huang J, Ghoorah D, Kong X, Lin X, Wang T. Mitochondrial complex I inhibitor rotenone-induced toxicity and its potential mechanisms in Parkinson's disease models. Crit Rev Toxicol. 2012;42: 613–632
[159] Emmrich JV, Hornik TC, Neher JJ, Brown GC. Rotenone induces neuronal death by microglial phagocytosis of neurons. FEBS J 2013;280: 5030–5038.
[160] Ahn SM, Byun K, Cho K, Kim JY, Yoo JS, Kim D, Paek SH, Kim SU, Simpson RJ, Lee B. Human microglial cells synthesize albumin in brain PloS one 2008; 3:e2829 doi:10.1371/journal.pone.0002829
[161] Reiber H, Peter JB. Cerebrospinal fluid analysis: disease-related data patterns and evaluation programs Journal of the neurological sciences 2001;184: 101-122
[162] Brockmann K, Reimold M, Globas C, Hauser TK, Walter U, Machulla HJ, Rolfs A, Schöls L. PET and MRI reveal early evidence of neurodegeneration in spinocerebellar ataxia type 17 Journal of nuclear medicine : official publication, Society of Nuclear Medicine 2012;53: 1074-1080
[163] Gao L, Zhang J, Hou Y, Hallett M, Chan P, Wu T. The cerebellum in dual-task performance in Parkinson's disease. Sci Rep. 2017;7: 45662
[164] Ni Z, Pinto AD, Lang AE ,Chen R. Involvement of the cerebellothalamocortical pathway in Parkinson disease. Ann Neurol 2010;68: 816-824
[165] Wu T, Long X, Zang Y, Wang L, Hallett M, Li K ,Chan P. Regional homogeneity changes in patients with Parkinson's disease. Hum. Brain Mapp. 2009;30: 1502-1510
[166] Wu T, Wang L, Chen Y, Zhao C, Li K, Chan P. Changes of functional connectivity of the motor network in the resting state in Parkinson's disease. Neurosci lett 2009;460: 6-10
[167] Hornykiewicz O. Parkinsons disease and its chemotherapy. Biochemical Pharmacology 1975;24: 1061-1065
[168] Braak H, Del Tredici K. Neuropathological Staging of Brain Pathology in Sporadic Parkinson's disease: Separating the Wheat from the Chaff. J Parkinsons Dis. 2017; 7: S71-S85.
[169] Wu T, Hallett M. The cerebellum in Parkinson’s disease. Brain 2013; 136: 696–709
[170] Cannon JR, Greenamyre JT. Neurotoxic in vivo models of Parkinson's disease recent advances. Prog Brain Res. 2010; 184:17-33.
[171] Contestabile A. Cerebellar granule cells as a model to study mechanisms of neuronal apoptosis or survival in vivo and in vitro. Cerebellum. 2002; 1:41-55.
[172] Dexter DT, Holley AE, Flitter WD, Slater TF, Wells FR, Daniel SE, Lees AJ, Jenner P, Marsden CD. Increased levels of lipid hydroperoxides in the parkinsonian substantia nigra: an HPLC and ESR study. Mov Disord. 1994; 9: 92-7.
[173] Jenner P, Olanow CW. Understanding cell death in Parkinson's disease. Ann Neurol. 1998; 44: S72-84.

[174] Olanow CW, Tatton WG. Etiology and pathogenesis of Parkinson's disease. Annu Rev Neurosci. 1999; 22:123-44.
[175] McGeer PL, Itagaki S, Boyes BE, McGeer EG. Reactive microglia are positive for HLA-DR in the substantia nigra of Parkinson's and Alzheimer's disease brains. Neurology. 1988; 38:1285-91.
[176] Schapira AH, Jenner P. Etiology and pathogenesis of Parkinson's disease Movement disorders. Mov Disord 2011;26: 1049-1055
[177] Zeng XS, Geng WS and Jia JJ. Neurotoxin-Induced Animal Models of Parkinson Disease: Pathogenic Mechanism and Assessment. ASN Neuro. 2018; 10: 1759091418777438.
[178] Schlattner U, Tokarska-Schlattner M, Wallimann T. Mitochondrial creatine kinase in human health and disease. Biochim Biophys Acta 2006;1762: 164–180.
[179] Aksenov M, Aksenova M, Butterfield DA, Markesbery WR (2000) Oxidative modification of creatine kinase BB in Alzheimer's disease brain. J Neurochem 2000;74: 2520–2527
[180] Ferrante RJ, Andreassen OA, Jenkins BG, Dedeoglu A, Kuemmerle S, Kubilus JK, Kaddurah-Daouk R, Hersch SM, Beal MF. Neuroprotective effects of creatine in a transgenic mouse model of Huntington's disease. J Neurosci 2000;20: 4389–4397
[181] Andreassen OA, Jenkins BG, Dedeoglu A, Ferrante KL, Bogdanov MB, Kaddurah-Daouk R, Beal MF. Increases in cortical glutamate concentrations in transgenic amyotrophic lateral sclerosis mice are attenuated by creatine supplementation. J Neurochem 2001;77: 383–390
[182] Bender A, Koch W, Elstner M, Schombacher Y, Bender J, Moeschl M, Gekeler F, Muller-Myhsok B, Gasser T, Tatsch K, Klopstock T. Creatine supplementation in Parkinson disease: a placebocontrolled randomized pilot trial. Neurology 2006; 67: 1262–1264.
[183]Bender A, Beckers J, Schneider I, Hölter SM, Haack T, Ruthsatz T, Vogt-WeisenhornDM, Becker L, Genius J, Rujescu D, Irmler M,Mijalski T, Mader M, Quintanilla-Martinez L, Fuchs H, Gailus-Durner V, de Angelis MH, Wurst W, Schmidt J, Klopstock T. Creatine improves health and survival of mice. Neurobiol Aging 2008;29: 1404–1411.
[184] Bender A, Klopstock T. Creatine for neuroprotection in neurodegenerative disease: end of story? Amino Acids. 2016;48: 1929-40
[185] Trifaró JM, Vitale ML. Cytoskeleton dynamics during neurotransmitter release. Trends Neurosci 1993;16: 466-47
[186] Berridge MJ, Lipp P, Bootman MD. The versatility and universality of calcium signalling. Nat Rev Mol Cell Biol. 2000;1: 11-21.
[187] Benowitza LI, Routtenbergb A. GAP-43: an intrinsic determinant of neuronal development and plasticity. Trends Neurosci 1997;20: 84-91.
[188] Schapira AH. Calcium dysregulation in Parkinson's disease. Brain 2013;136: 2015–2016.
[189] Selvaraj S, Sun Y, Watt JA, Wang S, Lei S, Birnbaumer L, Singh BB. Neurotoxin-induced ER stress in mouse dopaminergic neurons involves downregulation of TRPC1 and inhibition of AKT/ mTOR signaling. J Clin Invest 2012;122: 1354–1367.
[190] Gutierrez-Martin Y, Martin-Romero FJ, Henao F, Gutierrez-Merino. C. Alteration of cytosolic free calcium homeostasis by SIN-1: High sensitivity of L-type Ca2+

channels to extracellular oxidative/nitrosative stress in cerebellar granule cells. J. Neurochem. 2005; 92: 973–989.
[191] Garcia-Bereguiain MA, Samhan-Arias AK, Martin-Romero FJ, Gutierrez-Merino C. Hydrogen sulfide raises cytosolic calcium in neurons through activation of L-type Ca2+ channels. Antioxid. Redox Signal. 2008; 10: 31–42.
[192] Gutierrez-Merino C, Marques-da-Silva D, Fortalezas S, Samhan-Arias AK. The critical role of lipid rafts nanodomains in the cross-talk between calcium and reactive oxygen and nitrogen species in cerebellar granule neurons apoptosis by extracellular potassium deprivation. AIMS Mol. Sci. 2016; 3: 12–29.
[193] Anderson ME, Braun AP, Wu Y, Lu T, Wu Y, Schulman H, Sung RJ. KN-93, an Inhibitor of Multifunctional Ca++/Calmodulin-Dependent Protein Kinase, Decreases Early After Depolarizations in Rabbit Heart. J. Pharm. Exp. Ther. 1998;287: 996–1006.
[194] Morgan DML. Tetrazolium (MTT) Assay for Cellular Viability and Activity. In: Morgan D.M.L. (eds) Polyamine Protocols. Methods in Molecular Biology™, 1998; vol 79. Humana Press
[195] Zhao H, Kalivendi S, Zhang H, Joseph J, Nithipatikom K, Vasquez-Vivar J, Kalyanaraman B. Superoxide reacts with hydroethidine but forms a fluorescent product that is distinctly different from ethidium: potential implications in intracellular fluorescence detection of superoxide. Free Radic. Biol. Med. 2003;34: 1359-1368.
[196] Wardman P. Fluorescent and luminescent probes for measurement of oxidative and nitrosative species in cells and tissues: progress, pitfalls, and prospects. Free Radic. Biol. Med. 2007;43: 995-1022.
[197] Zielonka J, Hardy M, Kalyanaraman B. HPLC study of oxidation products of hydroethidine in chemical and biological systems: ramifications in superoxide measurements. Free Radic. Biol. Med. 2009;46: 329-338.
[198] Iyanagi T. Structure and function of NADPH-cytochrome P450 reductase and nitric oxide synthase reductase domain. Biochem. Biophys. Res. Commun. 2005;338: 520-528.
[199] Zhou L, Zhu DY. Neuronal nitric oxide synthase: Structure, subcellular localization, regulation, and clinical implications. Nitric Oxide 2009;20: 223-230.
[200] Kojima H, Nakatsubo N, Kikuchi K, Kawahara S, Kirino Y, Nagoshi H, Hirata Y, Nagano T. Detection and Imaging of Nitric Oxide with Novel Fluorescent Indicators: Diaminofluoresceins. Anal. Chem. 1998;70: 2446-2453.
[201] Broillet MC, Randin O, Chatton JY. Photoactivation and calcium sensitivity of the fluorescent NO indicator 4,5-diaminofluorescein (DAF-2): implications for cellular NO imaging. FEBS Lett 2001;491: 227-232.
[202] Greenamyre JT, MacKenzie G, Peng TI, Stephans SE. Mitochondrial dysfunction in Parkinson's disease. Biochem Soc Symp 1999;66: 85–97
[203] Radad K, Rausch WD, Gille G. Rotenone induces cell death in primary dopaminergic culture by increasing ROS production and inhibiting mitochondrial respiration. Neurochem Int 2006;49: 379–386.
[204] Pan JW, Takahashi K. Cerebral energetic effects of creatine supplementation in humans. Am J Physiol Regul Integr Comp Physiol 2007;292: R1745–R1750.
[205] Mihm MJ, Bauer JA. Peroxynitrite-induced inhibition and nitration of cardiac myofibrillar creatine kinase. Biochimie 2002;84: 1013–1019

[206] Mihm MJ, Yu F, Weinstein DM, Reiser PJ, Bauer JA. Intracellular distribution of peroxynitrite during doxorubicin cardiomyopathy: evidence for selective impairment of myofibrillar creatine kinase. Br J Pharmacol 2002;135: 581–588.
[207] Schilling K, Schmidt HH, Baader SL. Nitric oxide synthase expression reveals compartments of cerebellar granule cells and suggests a role for mossy fibers in their development. Neuroscience 1994;59: 893-903.
[208] Li M, Wang L, Peng Y, Wang JC, Zhou LH. Knockdown of the neuronal nitric oxide synthase gene retard the development of the cerebellar granule neurons in vitro. Dev. Dyn. 2010;239: 474-481.
[209] Coultrap SJ, Bayer KU. CaMKII regulation in information processing and storage. Trends Neurosci. 2012;35: 607–618.
[210] Xiao RP, Cheng H, Lederer WJ, Suzuki T, Lakatta EG. Dual regulation of Ca2+/calmodulin-dependent kinase II activity by membrane voltage and by calcium influx. Proc. Natl. Acad. Sci. 1994;91: 9659–9663.
[211] Gallo V, Kingsbury A, Balázs R, Jørgensen OS. The role of depolarization in the survival and differentiation of cerebellar granule cells in culture. J. Neurosci. 1987;7: 2203–2213.
[212] Toescu EC. Activity of voltage-operated calcium channels in rat cerebellar granule neurons and neuronal survival. Neuroscience 1999;94: 561–570
[213] Koschak A, Obermair GJ, Pivotto F, Sinnegger-Brauns MJ, Striessnig J, Pietrobon D. Molecular nature of anomalous L-type calcium channels in mouse cerebellar granule cells. J. Neurosci. 2007;27: 3855–3863
[214] Splawski I, Timothy KW, Sharpe LM, Decher N, Kumar P, Bloise R, Napolitano C, Schwartz PJ, Joseph RM, Condorius K, et al. Ca(V)1.2 calcium channel dysfunction causes a multisystem disorder including arrhythmia and autism. Cell 2004;119: 19–31
[215] Thiel WH, Chen B, Hund TJ, Koval OM, Purohit A, Song LS, Mohler PJ, Anderson ME. Proarrhythmic defects in Timothy syndrome require calmodulin kinase II. Circulation 2008;118: 2225–2234
[216] Day M, Wang Z, Ding J, An X, Ingham CA, Shering AF, Wokosin D, Ilijic E, Sun Z, Sampson AR, et al. Selective elimination of glutamatergic synapses on striatopallidal neurons in Parkinson disease models. Nat. Neurosci. 2006;9: 251–259
[217] Moosmang S, Haider N, Klugbauer N, Adelsberger H, Langwieser N, Müller J, Stiess M, Marais E, Schulla V, Lacinova L et al. Role of hippocampal Cav1.2 Ca2+ channels in NMDA receptor-independent synaptic plasticity and spatial memory. J. Neurosci. 2005;25: 9883–9892
[218] Ludwig A, Flockerzi V, Hofmann F. Regional Expression and Cellular Localization of the α1 and β Subunit of High Voltage-Activated Calcium Channels in Rat Brain. J. Neurosci. 1997;17: 1339–1349
[219] Abiria SA, Colbran RJ. CaMKII associates with CaV1.2 L-type calcium channels via selected β subunits to enhance regulatory phosphorylation. J. Neurosci. 2010;112: 150–161
[220] Soltis AR, Saucerman JJ. Synergy between CaMKII Substrates and β-Adrenergic Signaling in Regulation of Cardiac Myocyte Ca2+ Handling. Biophys. J. 2010;99: 2038–2047

[221] McQuade LE, Lippard SJ. Fluorescent probes to investigate nitric oxide and other reactive nitrogen species in biology (truncated form: fluorescent probes of reactive nitrogen species). Curr. Opin. Chem. Biol. 2010;14: 43-49
[222] Reynolds IJ, Hastings TG. Glutamate induces the production of reactive oxygen species in cultured forebrain neurons following NMDA receptor activation. J. Neurosci. 1995;15: 3318-3327
[223] Jacobs CM, Aden P, Mathisen GH, Khuong E, Gaarder M, Løberg EM, Lømo J, Maehlen J, Paulsen RE. Chicken cerebellar granule neurons rapidly develop excitotoxicity in culture. J. Neurosci. Methods 2006;156: 129-135
[224] Barman S, Nayak DP. Lipid Raft Disruption by Cholesterol Depletion Enhances Influenza A Virus Budding from MDCK Cells. J. Virol. 2007;81: 12169-12178
[225] Lu JC, Chiang YT, Lin YC, Chang YT, Lu CY, Chen TY, Yeh CS. Disruption of Lipid Raft Function Increases Expression and Secretion of Monocyte Chemoattractant Protein-1 in 3T3-L1 Adipocytes. PLOS One 2016;11: e0169005
[226] Samhan-Arias AK, Gutierrez-Merino C (2014) Purified NADH-Cytochrome b5 Reductase Is a Novel Superoxide Anion Source Inhibited by Apocynin: Sensitivity to nitric oxide and peroxynitrite. Free Radic. Biol. Med. 2014;73: 174-189
[227] Schenkman JB, Jansson I. The many roles of cytochrome b5. J. Pharmacol. Ther. 2003;97: 139-152
[228] Mulero-Navarro S, Santiago-Josefat B, Pozo-Guisado E, Merino JM, Fernandez-Salguero PM. Down-regulation of CYP1A2 induction during the maturation of mouse cerebellar granule cells in culture: role of nitric oxide accumulation. Eur. J. Neurosci. 2003;18: 2265-2272.
[229] Tinel M, Berson A, Elkahwaji J, Cresteil T, Beaune P, Pessayre D. Downregulation of cytochromes P450 in growth-stimulated rat hepatocytes: role of c- Myc induction and impaired C/EBP binding to DNA. J. Hepatol. 2003;39: 171-178
[230] Moutinho M, Nunes MJ, Rodrigues E. Cholesterol 24-hydroxylase: Brain cholesterol metabolism and beyond. Biochem. Biophys. Acta –Molecular and Cell Biology of Lipids 2016;1861: 1911-1920
[231] Kelm M, Dahmann R, Wink D, Feelisch M. The nitric oxide/superoxide assay. Insights into the biological chemistry of the NO/O2·- interaction. J. Biol. Chem. 1997;272: 9922-9932.
[232] Martín-Romero FJ, Gutiérrez-Martín Y, Henao F, Gutierrez-Merino C. Fluorescence measurements of steady state peroxynitrite production upon SIN-1 decomposition: NADH versus dihydrodichlorofluorescein and dihydrorhodamine 123. J. Fluorescence 2004;14: 17-23
[233] Bao F, Liu D. Peroxynitrite generated in the rat spinal cord induces neuron death and neurological deficits. Neuroscience 2002;115: 839-849
[234] Swarnkar S, Singh S, Mathur R, Patro IK, Nath C. A study to correlate rotenone induced biochemical changes and cerebral damage in brain areas with neuromuscular coordination in rats. Toxicology 2010;272: 17–22
[235] Swarnkar S, Singh S, Sharma S, Mathur R, Patro IK, Nath C. Rotenone induced neurotoxicity in rat brain areas: a histopathological study. Neurosci Lett 2011;501: 123–127
[236] Hosamani R, Ramesh SR, Muralidhara. Attenuation of rotenone induced mitochondrial oxidative damage and neurotoxicty in Drosophila melanogaster supplemented with creatine. Neurochem Res 2010;35: 1402–1412

[237] Cunha MP, Martín-de-Saavedra MD, Romero A, Parada E, Egea J, del Barrio L, Rodrigues ALS, López MG. Protective effect of creatine against 6-hydroxydopamine-induced cell death in human neuroblastoma SH-SY5Y cells: involvement of intracellular signaling pathways. Neuroscience 2013;238: 185–194

[238] Chan CS, Guzman JN, Ilijic E, Mercer JN, Rick C, Tkatch T, Meredith GE, Surmeier DJ. Rejuvenation' protects neurons in mouse models of Parkinson's disease. Nature 2007;447: 1081–1086

[239] Surmeier DJ, Guzman JN, Sanchez-Padilla J, Goldberg JA. The origins of oxidant stress in Parkinson's disease and therapeutic strategies. Antioxid Redox Signal 2011;14: 1289–1301

[240] Kalyanaram B, Darley-Usmar V, Davies KJA, Dennery PA, Forman HJ, Grisham MB, Mann GE, Moore K, Roberts LJ II, Ischiropoulos H. Measuring reactive oxygen and nitrogen species with fluorescent probes: challenges and limitations. Free Radic Biol Med 2012;52: 1–6

[241] He Y, Imam SZ, Dong Z, Jankovic J, Ali SF, Appel SH, Le W. Role of nitric oxide in rotenone-induced nigro-striatal injury. J Neurochem 2003;86: 1338–1345

[242] Drechsel DA, Patel M. Role of reactive oxygen species in the neurotoxicity of environmental agents implicated in Parkinson's disease. Free Radic Biol Med 2008;44: 1873–1886

[243] Lawler JM, Barnes WS, Wu G, Song W, Demaree S. Direct antioxidant properties of creatine. Biochem Biophys Res Commun 2002;290: 47–52

[244] Sestili P, Martinelli C, Bravi G, Piccoli G, Curci R, Battistelli M, Falcieri E, Agostini D, Gioacchini AM, Stocchi V. Creatine supplementation affords cytoprotection in oxidatively injured cultured mammalian cells via direct antioxidant activity. Free Radic Biol Med 2006;40: 837–849

[245] Sestili P, Martinelli C, Colombo E, Barbieri E, Potenza L, Sartini S, Fimognari C. Creatine as an antioxidant. Amino Acids 2011;40: 1385–1396

[246] Lagoa R, Graziani I, Lopez-Sanchez C, Garcia-Martinez V, Gutierrez- Merino C. Complex I and cytochrome c are molecular targets of flavonoids that inhibit hydrogen peroxide production by mitochondria. Biochim Biophys Acta 2011;1807: 1562–1572.

[247] Lagoa R, Lopez-Sanchez C, Samhan-Arias AK, Ganan CM, Garcia- Martinez V, Gutierrez-Merino C. Kaempferol protects against rat striatal degeneration induced by 3-nitropropionic acid. J Neurochem 2009;111: 473–487.

[248] Soares SS, Henao F, Aureliano M, Gutierrez-Merino C. Vanadate induces necrotic death in neonatal rat cardiomyocytes through mitochondrial membrane depolarization. Chem Res Toxicol 2008;21: 607–618.

[249] Keelan J, Allen NJ, Antcliffe D, Pal S, Duchen MR. Quantitative imaging of glutathione in hippocampal neurons and glia in culture using monochlorobimane. J Neurosci Res 2001;66: 873–884

[230] Chazotte B. Labeling mitochondria with TMRM or TMRE. Cold Spring Harb Protoc 2011;2011: 895–897.